

**UCSF**

**UC San Francisco Electronic Theses and Dissertations**

**Title**

Oxysterol requirements for positioning naïve and activated dendritic cells

**Permalink**

<https://escholarship.org/uc/item/0ht6s02j>

**Author**

Lu, Erick

**Publication Date**

2018

Peer reviewed|Thesis/dissertation

Oxysterol requirements for positioning naïve and activated  
dendritic cells

by

Erick Lu

DISSERTATION

Submitted in partial satisfaction of the requirements for the degree of

DOCTOR OF PHILOSOPHY

in

Biomedical Sciences

in the

GRADUATE DIVISION

of the

UNIVERSITY OF CALIFORNIA, SAN FRANCISCO

Copyright 2018

by

Erick Lu

This dissertation is dedicated to my parents,

Xiao Ping Wang and Gang Lu

## ACKNOWLEDGEMENTS

I am proud to have been a part of the scientific community at UCSF, which has always been very supportive, helpful, and scientifically engaging. I am grateful to the countless people who have helped me in graduate school, and would like to acknowledge those who have had the greatest impact on me during this time.

I would like to thank Dr. Jason Cyster for being my mentor and taking me into his lab. I first met Jason while I was interviewing for the Biomedical Sciences graduate program at UCSF. He introduced himself to me at one of the evening receptions to tell me about his research. I immediately became interested in the lab. He excited me about learning immunology and performing basic science research. I could feel his passion, and it was contagious. Most importantly for me, he made me feel like I had the potential to become a great scientist like him someday. I knew that he would be a great mentor, and joined his lab.

Over the past years, Jason has always been extremely supportive and engaging. As a scientific mentor, he taught me how to think critically about scientific concepts and experimental design. He dedicated a significant amount of his time to making sure that any questions I had were answered and that I was on track with my research. Even though he was mentoring several graduate students in the lab, he provided each of us with as much support as we needed. He was willing to answer emails and schedule meetings outside of normal working hours, which I was especially grateful for when publishing my first paper. When parts of my project did not work out, Jason worked with me to solve the problems or think of different directions to take, and put a lot of effort into making sure I succeeded. Jason is my role model. I am still amazed by his work ethic and his unwavering passion for science. He inspires me to work hard and become a better scientist and person. I am very grateful and thankful to have had Jason as my mentor.

I would also like to thank Dr. Mark Ansel and Dr. Richard Locksley for providing constructive feedback and support as members of my thesis committee. I appreciate the time they took to ensure that my scientific and career development was on track. I have greatly benefited from their professional advice. I am also grateful to Dr. Mark Ansel, Dr. Michael Rosenblum, Dr. Jeoung-Sook Shin, and Dr. Anthony DeFranco for critically evaluating my scientific thinking as members of my qualifying exam committee. Dr. Clifford Lowell was a great BMS advisor during my first few years in the program. I also thank Dr. Karsten Gronert for taking me into his lab while I was an undergraduate at UC Berkeley, and Dr. Samantha Wang for mentoring me and making my first research experience enjoyable.

I am very fortunate to have worked alongside all the members of the Cyster lab. Although everyone came from drastically different backgrounds, we were able to connect with each other through our desire to improve our abilities as scientists and learn new things. I am most thankful to Eric Dang for mentoring me when I first entered the lab and consistently providing insightful feedback on my projects throughout the course of graduate school. No matter how busy he was, he would always answer my questions and help me troubleshoot techniques. He was also a source of inspiration; I was always amazed at his progress during his lab meeting presentations, and this motivated me to work hard as well. Lauren Rodda and Jagan Muppidi were both the best bay-mates that I could have hoped for. I am grateful to Jagan for teaching me many lab tips and tricks, and for an enriching experience working together on a project. Lauren was an extremely hard worker and inspired me to stay motivated, and I greatly enjoyed the many insightful discussions that we had about our experiences in grad school. Shelly Mintz joined the lab at the same time as I did—she provided thoughtful advice on my research projects and was also a great friend to go through grad school with. Andrea Reboldi had a wealth of knowledge of

immunology and always patiently answered my questions. Jiayi Wu provided thoughtful advice on biochemistry and career goals, and was a friendly face when working late nights in the lab. Michael Barnes was always there for me when I needed expertise on T cell biology, and made the lab a significantly more positive environment. I am very happy to have worked on projects with Hayakazu Sumida and Jianhua Li, both of whom inspired me to work hard and remain persistent. Brian Laidlaw always provided critical scientific feedback and asked me challenging questions. Antonia Gallman, Elise Wolf, Finn Wolfreys, Tamar Ben-shaan, Lihui Duan, Hsin Chen and Dan Liu were all great colleagues to work with and made lab enjoyable. Jinping An saved me a large amount of time by genotyping mice and keeping the lab's mouse colony organized. Ying Xu greatly helped me by teaching me various techniques in molecular biology and cloning many constructs over the years. Claire Chan and Melanie Gordon could always be depended on for administrative tasks and kept the lab running smoothly. Bernarda Lopez increased our lab efficiency by consistently replenishing our reagents, organizing our supplies, and cleaning our equipment. I would also like to thank the BMS office staff, including Demian Sainz and Ned Molyneaux, for their support throughout the years.

Last, I would like to thank my family for always encouraging me to learn more, work hard, and be a better person. They taught me how to stay motivated and persistent, and have provided me with the means to pursue my passions in life. In particular, my partner Jinny Sun has been the most supportive person during this period of my life. She has helped me become a better person both scientifically and emotionally, and is my never-ending source of happiness. I am grateful to have someone by my side who understands the scientific process and who also shares the excitement that comes with it.

## CONTRIBUTIONS TO PRESENTED WORK

All work presented in this dissertation was performed under the direct supervision and guidance of Dr. Jason G. Cyster. Chapter 2 was published in *Science Immunology* as “Distinct oxysterol requirements for positioning naïve and activated dendritic cells in the spleen” (Lu et al., 2017)<sup>1</sup>. The thesis abstract was adapted from this publication. The co-authors for this publication were Eric V. Dang, Jeffrey G. McDonald, and Jason G. Cyster. Dr. Jason G. Cyster and I conceptualized the study and designed the experiments. Eric V. Dang played a critical role in making preliminary observations about the dendritic cell deficiency reported in mice lacking the enzyme Cyp27a1. This initial discovery sparked interest in determining whether multiple oxysterol ligands may play a role in positioning EBI2-expressing cells *in vivo*. Jeffrey G. McDonald and his research team at UTSW provided mass spectrometry measurements on the tissue extract samples in Figure 2E. I conducted all other experiments described in the paper, analyzed the data, and prepared the figures. Dr. Jason G. Cyster and I collaboratively wrote and revised the manuscript.

---

<sup>1</sup> Lu E., Dang E.V., McDonald J.G., and Cyster J.G. Distinct oxysterol requirements for positioning naïve and activated dendritic cells in the spleen. *Science Immunology*. 2017 Apr 7; Vol. 2, Issue 10. doi:10.1126/sciimmunol.aal5237

# **Oxysterol requirements for positioning naïve and activated dendritic cells**

Erick Lu

## **ABSTRACT**

Correct positioning of dendritic cells (DCs) is critical for efficient pathogen encounter and antigen presentation. Epstein-Barr virus–induced gene 2 (EBI2) is a chemoattractant receptor required for naïve CD4<sup>+</sup>DCIR2<sup>+</sup> DC positioning in response to 7 $\alpha$ ,25-hydroxycholesterol (7 $\alpha$ ,25-HC). However, mice lacking Ch25h, an enzyme required for generating 7 $\alpha$ ,25-HC, exhibit an incomplete splenic DCIR2<sup>+</sup> DC defect compared to mice lacking EBI2. We provide evidence that a second EBI2 ligand, 7 $\alpha$ ,27-HC, can function as a guidance cue to support splenic DCIR2<sup>+</sup> DC positioning and homeostasis. Cyp27a1, an enzyme required for 7 $\alpha$ ,27-HC synthesis, is expressed by stromal cells in the region of naïve DC localization. Mice lacking both Cyp27a1 and Ch25h have a similar deficiency in DCIR2<sup>+</sup> DCs compared to mice lacking EBI2.

After activation, DCIR2<sup>+</sup> DCs migrate to the T cell zone. In some contexts, they position at the B-T zone interface, where they interact with activated CD4<sup>+</sup> T cells. The guidance cues that support positioning of activated DCIR2<sup>+</sup> DCs at this interface are undefined. We find that EBI2 is upregulated in DCIR2<sup>+</sup> DCs in response to certain stimuli, and positioning at the B-T zone interface requires EBI2 and Ch25h. Under conditions of type I IFN induction, EBI2 ligand levels are elevated, causing activated DCIR2<sup>+</sup> DCs to disperse throughout the T zone. Last, we provide evidence that oxysterol metabolism by XCR1<sup>+</sup> DCs is important for EBI2-dependent positioning of activated DCIR2<sup>+</sup> DCs. This work reveals a multi-tiered role for EBI2 in DC positioning. Deficiency in this organizing system results in defective CD4<sup>+</sup> T cell responses.

# TABLE OF CONTENTS

<b>CHAPTER ONE: Introduction</b> .....	1
Dendritic cell subsets in lymphoid tissues .....	2
Positioning of dendritic cell subsets in lymphoid organs.....	4
Epstein-Barr virus–induced gene 2 (gpr183) supports cDC2 positioning and homeostasis .....	7
Identification of oxysterols as ligands for EBI2.....	9
Production of oxysterols in lymphoid organs .....	10
Role of oxysterols in bile acid synthesis and cholesterol homeostasis .....	12
Activation of dendritic cells and their migratory responses.....	13
CD4 <sup>+</sup> T cell and cDC2 interactions early after activation.....	14
Questions answered in this dissertation .....	17
<b>CHAPTER TWO: Distinct oxysterol requirements for positioning naïve and activated dendritic cells in the spleen</b> .....	18
Abstract .....	19
Introduction .....	20
Results .....	23
Discussion .....	56
Materials and Methods .....	63
<b>CHAPTER THREE: Conclusions and Discussion</b> .....	74
Distinct oxysterol gradients guide naïve and activated cDC2 positioning.....	75
Oxysterol gradients in peripheral tissues and lymph nodes .....	76
How are EBI2 ligand gradients constructed in vivo?.....	80
Effects of systemic cholesterol dysregulation on EBI2 function .....	81
Dynamics of EBI2-dependent cDC2 and CD4 <sup>+</sup> T cell co-localization.....	82
cDC2 positioning patterns and related T cell response outcomes.....	83
Positioning patterns of cDC1 following activation.....	85
<b>REFERENCES</b> .....	87

# LIST OF FIGURES

## CHAPTER ONE:

- Figure 1:** Gating strategies to identify cDC2 and cDC1 dendritic cell subsets using flow cytometry in spleen and lymph nodes. .... 3
- Figure 2:** Positioning of splenic cDC2s in blood-exposed marginal zone bridging channels. ... 5
- Figure 3:** Positioning pattern of cDC1s in the spleen. .... 6
- Figure 4:** Positioning of cDC2s in mesenteric lymph nodes using the markers CD11b and DCIR2. .... 8
- Figure 5:** Oxysterol ligand structures and pathway of enzymatic generation. .... 11
- Figure 6:** Figure 6. Co-localization of activated CD4<sup>+</sup> T cells and DCIR2<sup>+</sup> DCs in the outer T cell zone early after immunization. .... 15

## CHAPTER TWO:

- Figure 1.** Influences of Ch25h and Cyp27a1 on splenic DCIR2<sup>+</sup> DCs. .... 24
- Supplementary Figure S1.** Combined contribution of Cyp27a1 and Ch25h to DCIR2<sup>+</sup> DC positioning. .... 25
- Supplementary Figure S2.** cDC2 marker expression by DCs in EBI2- and ligand-deficient mice. .... 26
- Supplementary Figure S3.** M12 EBI2 bioassay sensitivity, oxysterol-induced EBI2 internalization and effect of dietary cholic acid on EBI2 ligand activity in Cyp27a1 KO mice. .... 28
- Figure 2.** Cyp27a1 Ch25h DKO mice reveal a role for 7 $\alpha$ ,27-HC in DCIR2<sup>+</sup> DC positioning and maintenance. .... 30
- Supplementary Figure S4.** Mesenteric LN DCIR2<sup>+</sup> DC homeostasis and positioning in Ch25h and Cyp27a1 single- and double-deficient mice. .... 32
- Figure 3.** Expression pattern of Cyp27a1, Ch25h, Cyp7b1, and Hsd3b7 transcripts in the spleen determined using RNAscope. .... 35
- Supplementary Figure S5.** RNAscope analysis of enzyme expression in spleen and liver, and efficiency of DC ablation. .... 36

<b>Figure 4.</b> Activated DCIR2 <sup>+</sup> DCs up-regulate EBI2 and position at the B-T zone interface in an EBI2- and Ch25h-dependent manner. ....	39
<b>Supplementary Figure S6.</b> EBI2 antagonist specificity, method for quantifying DC distribution, and retroviral transduction efficiency of activated T cells. ....	41
<b>Figure 5.</b> EBI2-mediated DCIR2 <sup>+</sup> DC positioning in the outer T cell zone augments induction of Tfh cells. ....	43
<b>Supplementary Figure S7.</b> Characterization of EBI2:zDC-DTR mixed chimeras.....	44
<b>Figure 6.</b> Type I IFN suppresses EBI2 up-regulation and disrupts outer T cell zone positioning of DCIR2 <sup>+</sup> DCs. ....	47
<b>Supplementary Figure S8.</b> Activation marker induction and positioning of DCIR2 <sup>+</sup> DCs, and sites of type I IFN action in regulating EBI2 expression and function. ....	49
<b>Figure 7.</b> Hsd3b7-expressing Batf3-dependent DCs are required for outer T cell zone positioning of activated DCIR2 <sup>+</sup> DCs. ....	53
<b>Supplementary Figure S9.</b> Activation marker induction, positioning, in vivo PE labeling, and enzyme expression on XCR1 <sup>+</sup> DCs.....	54
<b>Supplementary Figure S10.</b> Model for naïve and activated DCIR2 <sup>+</sup> DC positioning. ....	57
<b>Supplementary Figure S11.</b> Model for type I IFN and Batf3 DC effects on outer T-cell zone positioning of activated DCIR2 <sup>+</sup> DCs. ....	58
<b>Supplementary Figure S12.</b> Sort gating strategy and purity of sorted splenic DCs.....	68

**CHAPTER THREE:**

<b>Figure 1:</b> RNAscope detection of Ch25h expression pattern in the mesenteric lymph node. ..	78
--------------------------------------------------------------------------------------------------	----

# **CHAPTER ONE**

## **Introduction**

## Dendritic cell subsets in lymphoid tissues

Dendritic cells (DCs) play many important roles in initiating adaptive immune responses. First discovered by Ralph Steinman and Zanvil Cohn in the 1970s, DCs have the ability to sense pathogens, capture and process antigens, migrate to T lymphocyte-rich areas, and activate antigen-specific naïve T cells. DCs also provide T cells with a milieu of cytokines and co-stimulatory signals that are tailored for the type of pathogen present. Several lineages of DCs have been described, including classical DCs (cDCs), plasmacytoid DCs (pDCs), monocyte-derived DCs (moDCs), and Langerhans Cells (LCs). This dissertation will focus on the guidance cues that promote the survival and function of classical DCs in lymphoid organs.

Classical DCs in lymphoid organs can be divided into two major subsets, named cDC1 and cDC2 (Guilliams et al., 2014). This classification is largely based on the transcription factor requirements for each subset during development from a common precursor, the pre-DC. cDC2s are dependent on IRF4 during development and express markers such as CD4, CD11b, DCIR2, and SIRP $\alpha$ , whereas cDC1s are dependent on Batf3 during development and express markers such as CD8 $\alpha$ , DEC-205, Clec9a, and XCR1 (Merad et al., 2013; Murphy et al., 2015). Both subsets express high levels of CD11c and MHCII. DC populations in lymphoid organs can be readily enumerated by flow cytometry using a combination of fluorescent-labeled antibodies against the markers above.

Under steady-state conditions in C57BL/6 mice, the majority of splenic DCs are naïve and un-activated. Within the spleen, cDC1s and cDC2s can be distinguished using a combination of the markers CD11c, MHCII, CD8 $\alpha$ , and DCIR2 (**Fig. 1A**). In lymph nodes, cDCs can be further split into “resident” CD11c-hi MHCII-int and “migratory” CD11c-int MHCII-hi populations, both of which contain cDC1- and cDC2-type cells (**Fig. 1B**). Although migratory

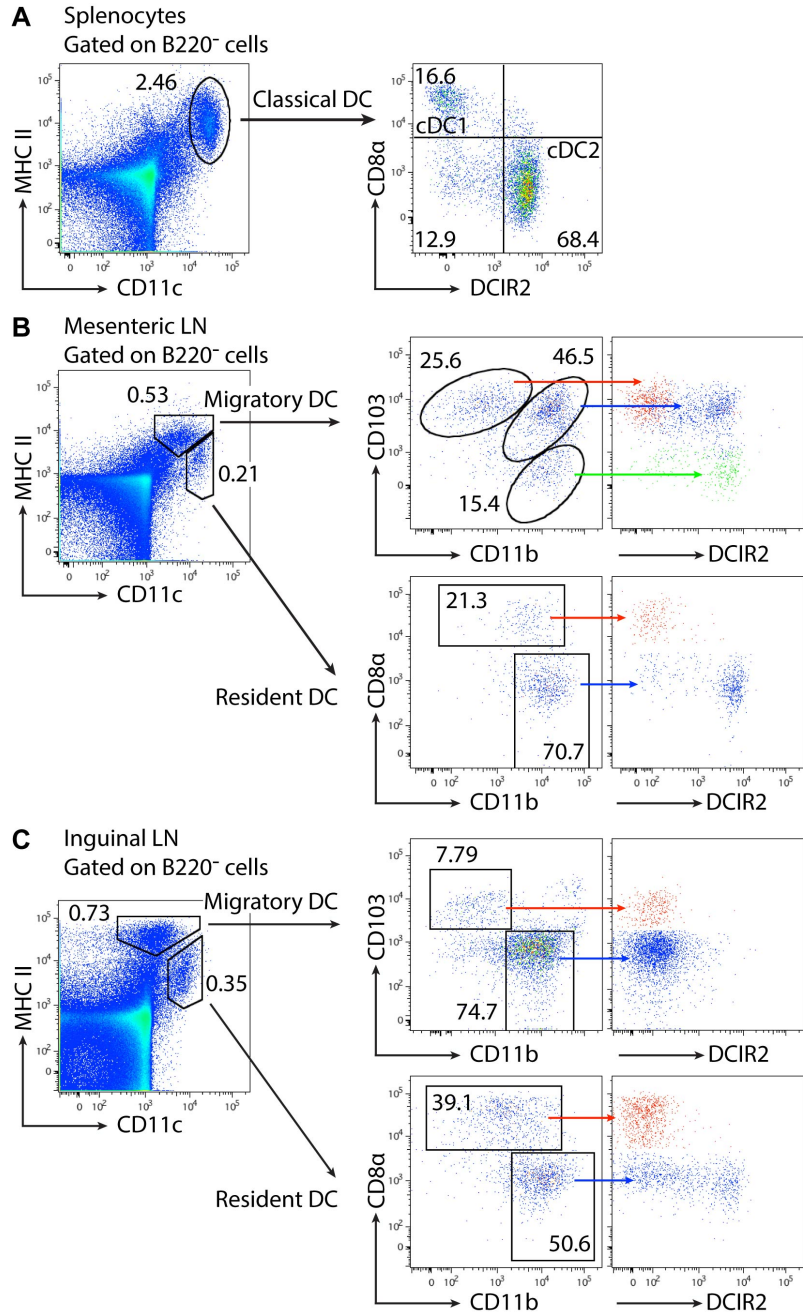


**Figure 1. Gating strategies to identify cDC2 and cDC1 dendritic cell subsets using flow cytometry in spleen and lymph nodes.**

(A) Classical dendritic cells (cDCs) can be identified within splenocytes from C56BL/6 mice by gating on B220<sup>-</sup>, MHC-II<sup>+</sup>, and CD11c<sup>+</sup> cells. This gate can be further split into CD8α<sup>+</sup> cDC1s and DCIR2<sup>+</sup> cDC2s. (B, C) In mesenteric (B) and peripheral (C) LNs, cDCs can be split into migratory or resident cells based on MHC-II and CD11c levels, and these sub-populations can be further categorized using CD103, CD11b, and CD8α. The colored arrows from each gate indicate the same population plotted against DCIR2 on the adjacent plot. Note the differences in DCIR2 expression across CD11b<sup>+</sup> subsets between lymph nodes.

cDCs express higher levels of MHCII and resemble a more activated state, they are present in lymph nodes under homeostatic conditions. Lymph node cDC1 and cDC2 subsets can be distinguished using a combination of CD11b and CD103 for migratory DCs, and CD11b and CD8 $\alpha$  for resident DCs. Further subsetting of cDC2s can be achieved using DCIR2, although expression of this marker varies based on the location of the lymph node. For example, cDC2s in mesenteric lymph nodes are a heterogeneous population comprised of DCIR2<sup>+</sup> CD11b<sup>+</sup> and DCIR2<sup>-</sup> CD11b<sup>+</sup> cells, whereas the majority of cDC2s in the skin-draining inguinal lymph node do not express DCIR2 (**Fig. 1B and C**).

### **Positioning of dendritic cell subsets in lymphoid organs**

In the spleen, cDC1s and cDC2s are positioned strategically in blood-exposed locations in order to facilitate the detection and capture of bloodborne pathogens (Yi and Cyster, 2013). Blood-exposure can be measured through an intravenous injection of a PE-labeled antibody against CD45 or CD11c, which should label any DCs exposed to circulation. A 5-minute injection of anti-CD45-PE labels a majority of both cDC1s and cDC2s (**Fig. 2A**). The positioning of cDC2s can be examined histologically using the marker DCIR2, which is uniquely expressed by this subset of cells in the spleen. cDC2s are concentrated in locations called marginal zone bridging channels, which are defined as areas where the T zone shares a boundary with the red pulp (**Fig. 2B** and (Steinman et al., 1997)). They can also be found in variable numbers in the marginal zone (MZ), and a small number of cDC2s are present in the red pulp (RP). It is unclear whether cDC2s in the RP serve a specific purpose or if they are only transiently positioned there. The positioning of cDC1s can be uniquely examined by staining sections for the marker XCR1. cDC1s are present in the MZ, red pulp, and T zone (**Fig. 3** and

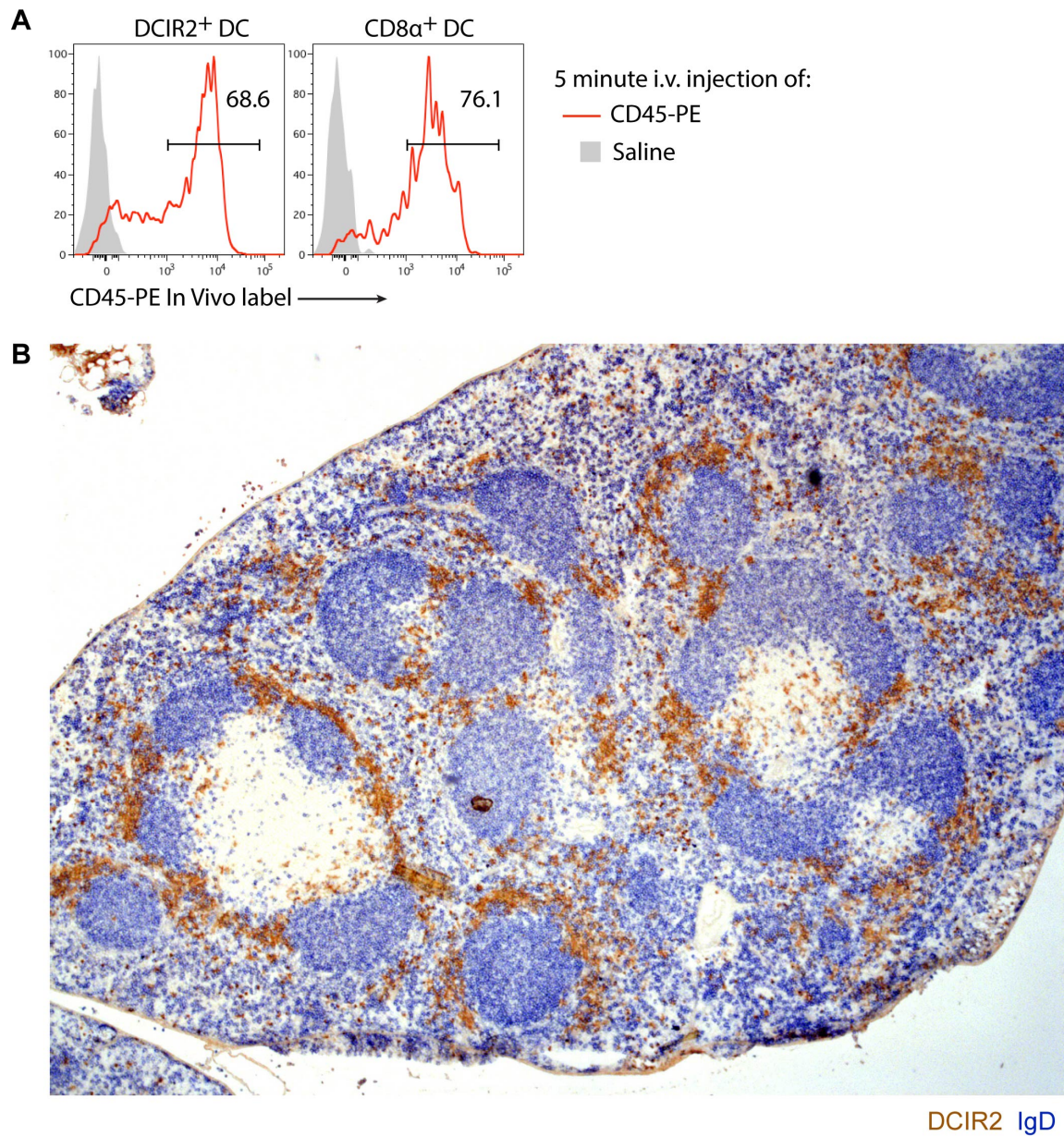
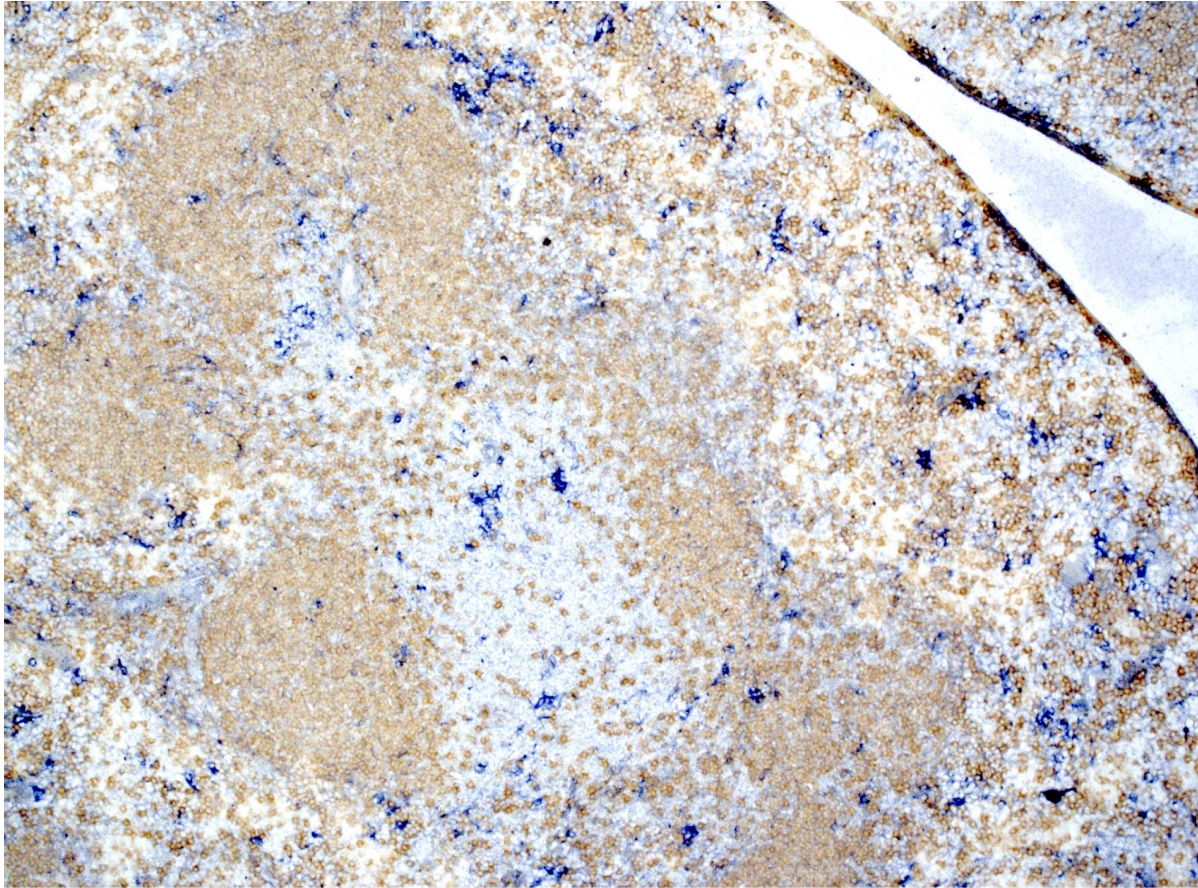


**Figure 2. Positioning of splenic cDC2s in blood-exposed marginal zone bridging channels.**

(A) Histograms showing CD45-PE labeling on DCIR2<sup>+</sup> DC and CD8α<sup>+</sup> DC in the spleen, 5 minutes after intravenous injection of 1μg of anti-CD45-PE antibody. The grey fill indicates background signal from DCs isolated from control mice injected with saline. (B) Immunohistochemistry for cDC2s (DCIR2, brown) and endogenous B cells (IgD, blue) in spleen sections from wild type mice showing localization of DCIR2<sup>+</sup> cDC2 in marginal zone bridging channel, marginal zone, and red pulp locations.



IgD XCR1

**Figure 3. Positioning pattern of cDC1s in the spleen.**

Immunohistochemistry of cDC1s (XCR1, blue) and endogenous B cells (IgD, brown) in spleen sections, showing positioning of XCR1<sup>+</sup> DCs in the red pulp, marginal zone, and T cell zone. The slide was developed extensively, and the strongest dark blue signals are XCR1-specific. The faint blue signals, such as those observed in the marginal zone and T zone, are non-specific.

(Alexandre et al., 2016; Bachem et al., 2012; Calabro et al., 2016; Dorner et al., 2009; Yamazaki et al., 2013)). Although both subsets of DCs are highly exposed to circulation, they each populate specific niches within the spleen.

In lymph nodes, the complex subsetting of cDC1s and cDC2s into both migratory and resident populations and their varied marker expression makes it difficult to track their positioning through conventional histological methods. Histo-cytometry, a technique using multiplexed antibody staining to visualize and quantify complex cell populations, found that cDC1s and cDC2s occupy distinct anatomical locations in lymph nodes (Gerner et al., 2017; 2012; 2015). Lymph node resident  $CD11b^+$  cDC2s were found more proximal to lymphatic sinus locations and in the cortical ridge, whereas resident  $CD8\alpha^+$  cDC1s were present deeper in the T cell-rich paracortex. Migratory  $CD11b^+$  cDC2s were found in inter-follicular regions and also within the cortical ridge, whereas migratory  $CD103^+$  cDC1s were found within the T cell zone. The positioning of the combined migratory and resident cDC2 compartment in inter-follicular and T cell zone locations can be determined by staining for the marker CD11b (**Fig. 4A**).

Although CD11b is expressed by other cell types such as macrophages, the majority of  $CD11b^+$  cells within the inter-follicular and T cell zone locations are composed of cDC2s. In mesenteric lymph nodes, a portion of cDC2s express DCIR2, and their positioning pattern can be uniquely tracked through staining of this marker (**Fig. 4B**).

### **Epstein-Barr virus–induced gene 2 (*gpr183*) supports cDC2 positioning and homeostasis**

The positioning of cDC2s in splenic MZ bridging channel locations is dependent on the G protein-coupled receptor Epstein-Barr virus-induced gene 2 (EBI2) (Gatto et al., 2013; Yi and Cyster, 2013). EBI2 is a G $\alpha$ i-coupled chemoattractant receptor that is highly expressed by many types of immune cells, including B cells, T cells, DCs, and monocytes. As its name suggests,

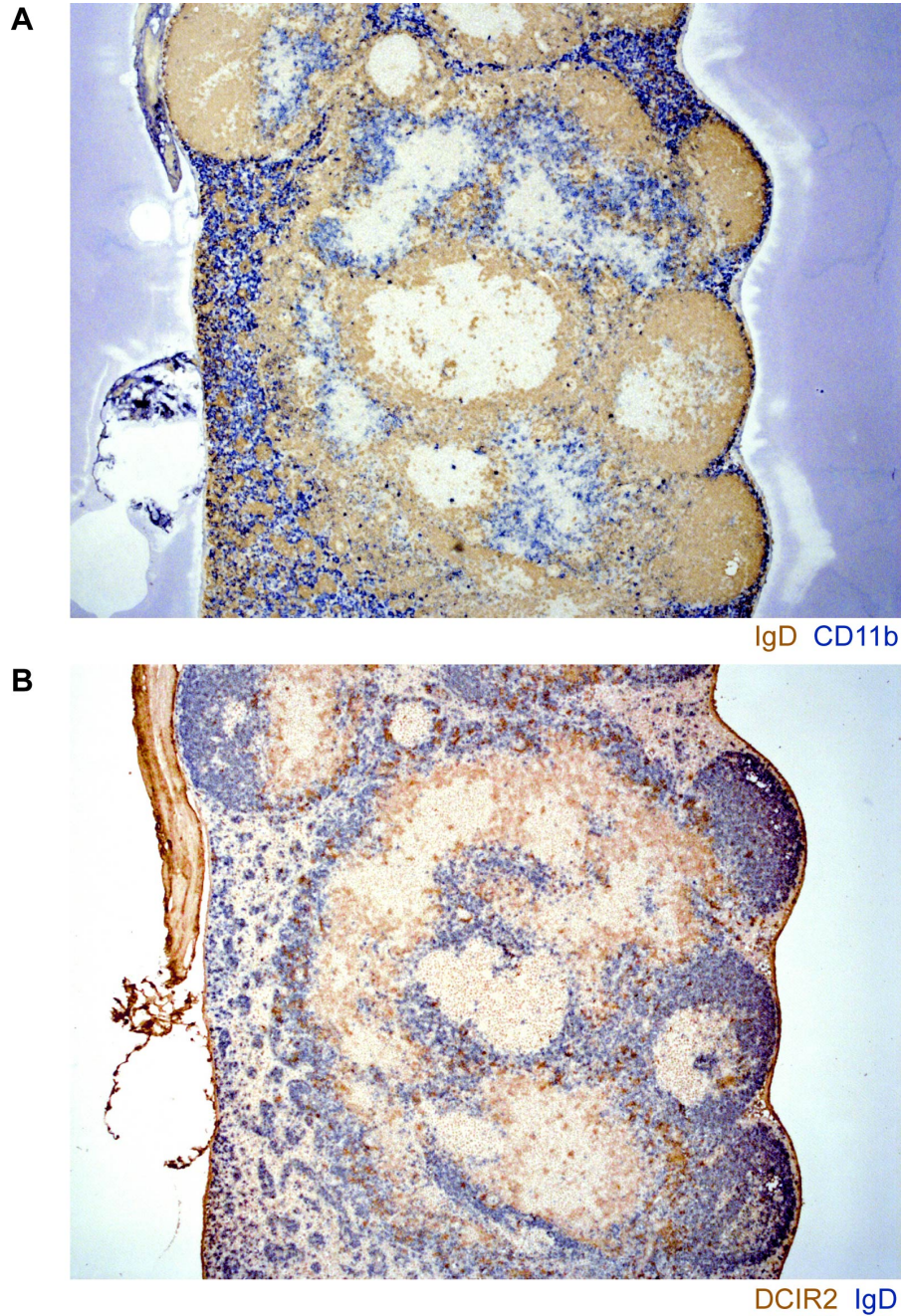


**Figure 4. Positioning of cDC2s in mesenteric lymph nodes using the markers CD11b and DCIR2.**

(A) Immunohistochemistry for CD11b (blue) and IgD (brown) in sections of mesenteric lymph nodes from wild type mice. The CD11b signal in medullary regions comes largely from macrophages, whereas the CD11b signal within the T zone area mostly comes from cDC2s. (B) Immunohistochemistry of mesenteric LN sections cut serially to (A) for DCIR2 (brown) and IgD (blue). Note the similarity in pattern distribution between DCIR2 and CD11b staining within T zone areas.

EBI2 was first discovered as the second most up-regulated gene after Epstein-Barr virus infection of a Burkitt's lymphoma line (Birkenbach et al., 1993). Deficiency of EBI2 resulted in irregular positioning of cDC2s in the red pulp, an overall decrease in cDC2 numbers, diminished T cell responses, and impaired antibody responses (Yi and Cyster, 2013). The decrease in cDC2s was cell intrinsic, since mixed-bone marrow chimeric mice generated using a mixture of EBI2 knockout and wild-type bone marrow resulted a selective deficiency in the knockout cells. The DC deficiency in EBI2 knockout mice could be rescued by injection of an antibody agonist of the lymphotoxin-beta receptor, which was shown to be a crucial survival signal for cDC2s (Kabashima et al., 2005). These results suggested that EBI2-dependent positioning of cDC2 in MZ bridging channels allowed for adequate access to  $LT\alpha 1\beta 2$  signals to promote survival of the cells (Yi and Cyster, 2013).

Prior to the discovery that this receptor was required for maintaining splenic cDC2 positioning, EBI2 was found to be important for guiding B cell positioning early after activation (Gatto et al., 2009; Kelly et al., 2011; Pereira et al., 2009). In antigen-activated B cells, EBI2 worked in conjunction with CCR7 to position the cells at the B-T zone interface to obtain T cell help. This was followed by EBI2-dependent positioning of activated B cells at outer- and inter-follicular regions, after which EBI2 was downregulated by B cells entering the germinal center.

### **Identification of oxysterols as ligands for EBI2**

Through biochemical purification of tissue extracts active on EBI2, two separate research efforts identified di-hydroxylated forms of cholesterol as ligands for the receptor, of which the most potent form was  $7\alpha,25$ -dihydroxycholesterol ( $7\alpha,25$ -HC) (Hannedouche et al., 2011; Liu et al., 2011). The groups identified the ligand from multiple biological sources, including septic

sheep liver, pig liver, and pig spleen. This process involved the homogenization of kilogram amounts of each tissue, preparation of lipid extracts, and multiple rounds of HPLC fractionation, coupled with screening fractions using a secondary messenger bioassay. A highly purified extract active on EBI2 was examined using mass spectrometry, which detected masses corresponding oxidized forms of cholesterol. Testing synthesized forms of hydroxylated and dihydroxylated forms of cholesterol using a radioligand binding assay revealed that the most potent form was  $7\alpha,25$ -HC.  $7\alpha,25$ -HC was able to induce the migration of EBI2-expressing B cells in vitro, and has since been shown to induce migration of other EBI2-expressing cell types, including cDC2s (Gatto et al., 2013; Hannedouche et al., 2011; Li et al., 2016; Nevius et al., 2015; Yi and Cyster, 2013). In addition to  $7\alpha,25$ -HC, the related oxysterol  $7\alpha,27$ -HC also exhibited activity on EBI2 at nanomolar concentrations, at approximately 10-fold less potency.  $7\alpha,27$ -HC differs from  $7\alpha,25$ -HC in the location of the hydroxyl group on the side chain of cholesterol (**Fig. 5A**). It has been unclear whether there is any physiological relevance for the ability of multiple types of oxysterols to activate EBI2.

### **Production of oxysterols in lymphoid organs**

In vivo,  $7\alpha,25$ -HC is produced from cholesterol through the stepwise action of the enzymes Ch25h and Cyp7b1 (**Fig. 5B**). Ch25h adds a hydroxyl group to the 25-position of the side chain of cholesterol, whereas Cyp7b1 adds a hydroxyl group to the  $7\alpha$ -position on the sterol ring.  $7\alpha,25$ -HC can be further metabolized by the enzyme Hsd3b7, which converts the  $3\alpha$ -hydroxyl into a ketone. This form is inactive on EBI2 and does not induce migration of EBI2-expressing cells. Interestingly, Ch25h is expressed at minimal levels in the liver, and is more highly expressed in lymphoid stroma (Hannedouche et al., 2011; Rodda et al., 2018; Yi et al.,

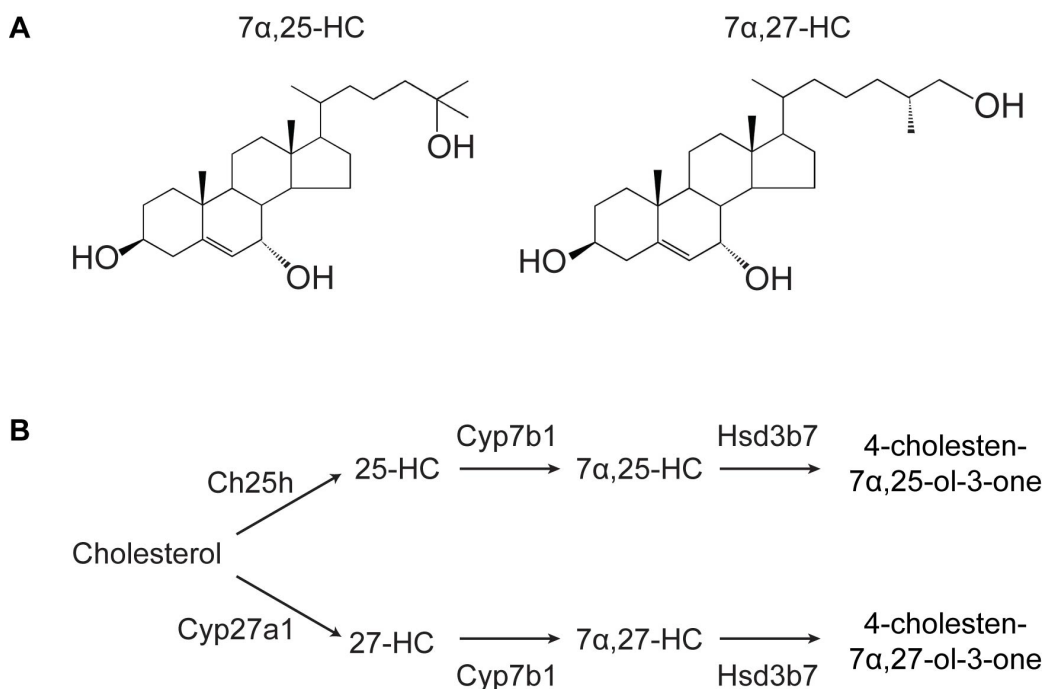


**Figure 5. Oxysterol ligand structures and pathway of enzymatic generation.**

**(A)** Chemical structure of  $7\alpha,25\text{-HC}$  and  $7\alpha,27\text{-HC}$ . Note the difference in the position of the hydroxyl (OH) group on the side chain of the cholesterol backbone. **(B)** Pathway of  $7\alpha,25\text{-HC}$  and  $7\alpha,27\text{-HC}$  generation from cholesterol and metabolism by Hsd3b7. Cyp7b1 can convert both 25-HC and 27-HC into their di-hydroxylated forms, and Hsd3b7 can metabolize both  $7\alpha,25\text{-HC}$  and  $7\alpha,27\text{-HC}$  into forms that are inactive on EBI2.

2012). Ch25h is also rapidly induced under inflammatory conditions, increasing the amount of  $7\alpha,25$ -HC produced (Hannedouche et al., 2011). The approximate expression pattern of Ch25h, Cyp7b1, and Hsd3b7 in the spleen was defined using laser-capture microdissection coupled with qPCR, which provided evidence that Ch25h expression was concentrated in outer follicular regions and near the B-T zone interface (Yi et al., 2012). However, more precise techniques are required to determine the exact pattern of enzyme expression in lymphoid organs. This will be investigated in chapter 2.

Mice lacking the enzyme Cyp7b1 cannot produce  $7\alpha,25$ -HC or  $7\alpha,27$ -HC, and also display a defect in splenic cDC2 positioning and population comparable to EBI2 KO mice (Yi and Cyster, 2013). Surprisingly, we found that mice lacking the enzyme Ch25h displayed a cDC2 defect that was not as severe as in Cyp7b1 KO or EBI2 KO mice, suggesting that a second Cyp7b1-dependent oxysterol may contribute to the homeostasis of these cells, likely  $7\alpha,27$ -HC. Production of  $7\alpha,27$ -HC involves the enzyme Cyp27a1, which adds a hydroxyl group to the 27-position of the side chain of cholesterol to produce 27-HC (Russell, 2003). Cyp7b1 can then convert 27-hydroxycholesterol to  $7\alpha,27$ -HC. How Cyp27a1 and  $7\alpha,27$ -HC contribute to cDC2 positioning and homeostasis will also be investigated in chapter 2.

### **Role of oxysterols in bile acid synthesis and cholesterol homeostasis**

The oxysterol-generating enzymes discussed above were initially characterized in the context of bile acid synthesis and cholesterol regulation. The enzymes Cyp27a1, Cyp7b1 and Hsd3b7 are highly expressed in the liver and their oxysterol products are intermediates in the bile acid synthetic pathway (Russell, 2003). Mice lacking the enzymes Cyp27a1 and Hsd3b7 have diminished bile acid pools and subsequently cannot absorb adequate amounts of dietary

cholesterol (Repa et al., 2000). As a consequence, these mice upregulate endogenous cholesterol and lipid biosynthesis and exhibit accumulation of various lipid and sterol species at abnormal levels in tissues. Similarly, humans deficient in CYP27A1 suffer a neurological disorder due to cholesterol and cholestanol build-up in the brain and tendons (Björkhem and Hansson, 2010). In mice, these effects can largely be rescued by feeding them a diet containing cholic acid, one of the terminal products of the bile acid biosynthesis pathway. In contrast to Cyp27a1, Ch25h is expressed at very low levels in the liver. Although the oxysterol product of Ch25h, 25-HC, has been shown to be a potent negative regulator of cholesterol biosynthesis through the inhibition of SREBP-2, no overt defects in bile acid synthesis or cholesterol homeostasis are observed in mice lacking this enzyme (Radhakrishnan et al., 2007). Chapter 2 will explore whether dysregulated cholesterol biosynthesis through loss of Cyp27a1 can alter levels of di-hydroxylated oxysterols in tissues, and whether this has any impact on EBI2 function in cDC2s.

### **Activation of dendritic cells and their migratory responses**

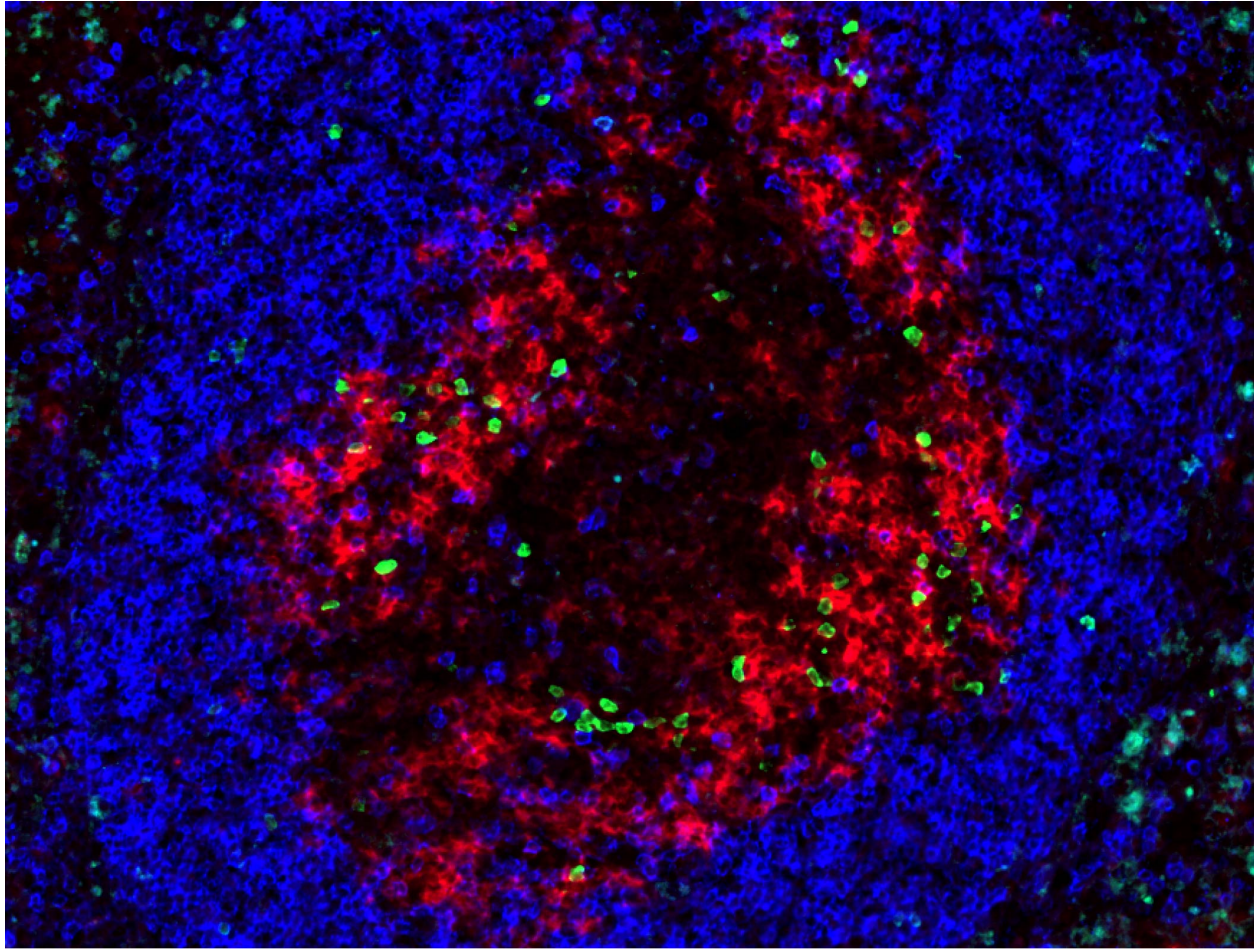
As sentinel cells, DCs express a wide variety of sensors that are able to detect the presence of pathogens or tissue injury. These sensors include the toll-like receptors (TLRs), which induce upregulation of pro-inflammatory pathways in the cell upon binding to pathogen-associated molecular patterns (PAMPs) such as lipopolysaccharide (LPS) or poly I:C (Merad et al., 2013). In addition to sensing pathogens, splenic cDC2s also survey the blood for the presence of xenogenic cells using polymorphic signal regulatory protein  $\alpha$  (SIRP $\alpha$ ), which engages CD47 on host cells (Yi et al., 2015). Injecting xenogenic cells that lack CD47, such as sheep red blood cells (SRBCs), causes splenic cDC2 activation. Canonical activation markers of dendritic cells include the upregulation of CD80, CD86, and MHC-II.

In order to migrate to T cell-rich areas, activated DCs also upregulate the chemokine receptor CCR7 (Calabro et al., 2016; Gunn et al., 1999; Yi and Cyster, 2013). The ligands for CCR7, CCL19 and CCL21, are highly expressed in the T cell zone (Gunn et al., 1999). Within hours, activated splenic DCs migrate from the red pulp and bridging channel locations into the T cell zone (Asselin-Paturel et al., 2005; Czeloth et al., 2007; De Becker et al., 2000; Idoyaga et al., 2009; Sousa and Germain, 1999). Intriguingly, cDC2s are able to discriminate between the inner and outer areas of the T cell zone, and preferentially position along the B-T zone interface if activated by specific stimuli, including SRBCs (Yi and Cyster, 2013). Positioning of activated cDC2s in the outer T cell zone likely facilitates interaction with CD4<sup>+</sup> T cells, which also travel to this area early after activation (Garside et al., 1998; Li et al., 2016). The guidance receptors required for positioning cDC2s in the outer T cell zone will be explored in chapter 2.

### **CD4<sup>+</sup> T cell and cDC2 interactions early after activation**

Direct interactions between antigen-specific CD4<sup>+</sup> T cells and splenic cDC2s occur in the outer T cell zone within hours after immunization with particulate antigen, and both cell types remain co-localized in this location for days afterwards (Li et al., 2016). The kinetics and properties of this interaction can be examined through adoptive transfer of ovalbumin-specific CD4<sup>+</sup> T cells (OT-II) and immunization with ovalbumin conjugated to an adjuvant such as SRBCs (**Fig. 6**). During this time period, cDC2s provide several critical co-stimulatory signals to the T cells that allow for a robust proliferative response and differentiation into effector T cell subsets.

The cocktail of signals provided to T cells by cDC2s are dependent on the type of pathogen or adjuvant administered. In several contexts, cDC2s have been shown to support the



IgD OTII DCIR2

**Figure 6. Co-localization of activated  $CD4^+$  T cells and  $DCIR2^+$  DCs in the outer T cell zone early after immunization.**

WT mice containing adoptively transferred congenic OTII T cells were immunized with ovalbumin conjugated to SRBCs. This is an immunofluorescence image tracking positioning of the  $CD4^+$  OTII T cells (green),  $DCIR2^+$  DCs (red), and endogenous B cells (blue) in spleen sections 12 hours after immunization, showing that the OTII T cells are co-localized with  $DCIR2^+$  DCs in the outer areas of the T cell zone.

induction of robust T follicular helper (Tfh) cell responses, including the splenic response to SRBC-OVA and listeria-OVA (Li et al., 2016) and the mediastinal LN response to nasally administered OVA mixed with LPS (Krishnaswamy et al., 2017). Studies targeting antigen to either cDC1 or cDC2 subsets using anti-DEC-205-OVA or anti-DCIR2-OVA, respectively, showed that antigen presentation by cDC2s supported a greater Tfh cell response (Shin et al., 2015).

There are several mechanisms by which cDC2s are able to promote Tfh cell differentiation. Adjuvants such as poly I:C and LPS have been shown to promote Tfh differentiation by inducing DC production of IL-6, which signals to T cells to upregulate expression of BCL6 (Cucak et al., 2009). BCL6 is a transcriptional repressor important for Tfh cell development (Baumjohann et al., 2011; Crotty, 2014; Liu et al., 2012). cDC2s also upregulate ICOSL after activation, which engages ICOS on the T cell to induce BCL6 expression (Choi et al., 2011; Li et al., 2016). Furthermore, cDC2s have also been shown to upregulate the IL-2 receptor alpha chain (CD25) upon activation and release its soluble form (Li et al., 2016). IL-2 signaling has been shown to suppress the development of Tfh cells, and the quenching of IL-2 by DC-derived CD25 promoted Tfh cell differentiation.

The signals described above require either direct contact or occur most efficiently in a paracrine fashion. Thus, proper co-localization of activated CD4<sup>+</sup> T cells and cDC2s is important. Disruption of early co-localization through the removal of EB12 in CD4<sup>+</sup> T cells has been shown to impair CD4<sup>+</sup> T cell proliferation and differentiation into Tfh cells (Li et al., 2016). How the Tfh cell response is affected through disruption of cDC2 positioning early after activation will be explored in chapter 2.

## Questions answered in this dissertation

1. What oxysterols are required for proper positioning and survival of splenic cDC2s?

- *Do Ch25h-deficient mice produce a second EBI2 ligand?*
- *Does Cyp27a1 generate 7 $\alpha$ ,27-HC in the spleen?*
- *Can Cyp27a1 and its product, 7 $\alpha$ ,27-HC, promote cDC2 survival in the absence of Ch25h?*
- *Does Cyp27a1 contribute to cDC2 homeostasis in lymph nodes?*
- *What is the distribution of oxysterol-generating enzymes in the spleen?*

2. How do activated cDC2s position in the splenic outer T zone?

- *Is there an oxysterol gradient within the T zone that supports EBI2-dependent outer T zone positioning?*
- *Does outer-T zone positioning of cDC2s impact Tfh cell generation and the B cell response?*
- *How do different PAMPs influence EBI2 expression, oxysterol production, and cDC2 positioning in the spleen?*
- *Do cDC1s play a role in positioning activated cDC2s in the spleen?*

## **CHAPTER 2**

### **Distinct oxysterol requirements for positioning naïve and activated dendritic cells in the spleen**

This chapter was originally published as:

Lu E., Dang E.V., McDonald J.G., and Cyster J.G. Distinct oxysterol requirements for positioning naïve and activated dendritic cells in the spleen. *Science Immunology*. 2017 Apr 7;

Vol. 2, Issue 10. doi:10.1126/sciimmunol.aal5237

## Abstract

Correct positioning of dendritic cells (DCs) is critical for efficient pathogen encounter and antigen presentation. Epstein-Barr virus–induced gene 2 (EBI2) has been identified as a chemoattractant receptor required for naïve CD4<sup>+</sup>DCIR2<sup>+</sup> DC positioning in response to 7 $\alpha$ ,25-hydroxycholesterol (7 $\alpha$ ,25-HC). We now provide evidence that a second EBI2 ligand, 7 $\alpha$ ,27-HC, is involved in splenic DCIR2<sup>+</sup> DC positioning and homeostasis. Cyp27a1, the enzyme uniquely required for 7 $\alpha$ ,27-HC synthesis, is expressed by stromal cells in the region of naïve DC localization. After activation, DCIR2<sup>+</sup> DCs move into the T cell zone. We find that EBI2 is rapidly up-regulated in DCIR2<sup>+</sup> DCs under certain activation conditions, and positioning at the B-T zone interface depends on EBI2. Under conditions of type I interferon induction, EBI2 ligand levels are elevated, causing activated DCIR2<sup>+</sup> DCs to disperse throughout the T zone. Last, we provide evidence that oxysterol metabolism by Batf3-dependent DCs is important for EBI2-dependent positioning of activated DCIR2<sup>+</sup>DCs. This work indicates that 7 $\alpha$ ,27-HC functions as a guidance cue in vivo and reveals a multitiered role for EBI2 in DC positioning. Deficiency in this organizing system results in defective CD4<sup>+</sup> T cell responses.

## Introduction

Dendritic cells (DCs) play crucial roles in presenting antigens to T cells within lymphoid organs. In the spleen, classical DCs can be divided into two major subsets: cells that express CD4, CD11b, and DCIR2 and are dependent on interferon (IFN) regulatory factor 4 (IRF4) for their development (cDC2), and cells that express CD8 $\alpha$ , DEC205, and XCR1 and require basic leucine zipper transcription factor activating transcription factor-like 3 (Batf3) for their development (cDC1) (Durai and Murphy, 2016). The former DCs are important for presenting antigens to CD4<sup>+</sup> T cells, whereas the latter are often crucial for cross-presentation of antigens to CD8<sup>+</sup> T cells; however, both types of DCs can contribute to CD4<sup>+</sup> and CD8<sup>+</sup> T cell responses, depending on the type of antigen (Durai and Murphy, 2016).

Within the spleen, DCIR2<sup>+</sup> cDC2s are enriched in the blood-exposed marginal zone (MZ) bridging channels that extend between the T cell zone and the red pulp (RP) (Gatto et al., 2013; Steinman et al., 1997; Yi and Cyster, 2013). XCR1<sup>+</sup>cDC1s are present in the MZ, RP, and T cell zone (Alexandre et al., 2016; Bachem et al., 2012; Calabro et al., 2016; Dorner et al., 2009; Yamazaki et al., 2013). After exposure to activating stimuli such as sheep red blood cells (SRBCs), lipopolysaccharide (LPS), or the double-stranded RNA mimetic polyinosinic:polycytidylic acid (poly I:C), splenic DCs move rapidly into the splenic T cell zone and, in some cases, position preferentially along the B-T zone interface (Asselin-Paturel et al., 2005; Czeloth et al., 2007; De Becker et al., 2000; De Trez et al., 2005; Gunn et al., 1999; Idoyaga et al., 2009; Sousa and Germain, 1999; Yi and Cyster, 2013). Positioning at the B-T zone interface likely increases the amount of encounter with activated CD4<sup>+</sup> T cells because they also favor this location (Garside et al., 1998; Li et al., 2016). DC movement into the T cell zone involves CCR7 up-regulation (Calabro et al., 2016; Gunn et al., 1999; Yi and Cyster, 2013; Yi et

al., 2015). However, the factors that allow activated DCs to distinguish between the outer and the inner T cell zone are not defined.

Epstein-Barr virus–induced gene 2 (EBI2; also known as GPR183) is a  $G\alpha_i$ -coupled chemoattractant receptor that is highly expressed by lymphocytes and DCs (Cyster et al., 2014; Gatto and Brink, 2013). EBI2 in B cells functions together with CCR7 to distribute antigen-activated B cells along the B-T zone interface in lymphoid organs (Gatto et al., 2009; Kelly et al., 2011; Pereira et al., 2009). After B cells have received T cell help and begun down-regulating CCR7, they position to inter- and outer-follicular regions in an EBI2-dependent manner (Gatto et al., 2009; Kelly et al., 2011; Pereira et al., 2009). EBI2 function in B and T cells is important for mounting T cell–dependent antibody responses (Gatto et al., 2009; Li et al., 2016; Pereira et al., 2009).

Using biochemical purification procedures, EBI2 ligands were identified as dihydroxylated forms of cholesterol (Hannedouche et al., 2011; Liu et al., 2011). In vitro studies established that  $7\alpha,25$ -HC was a potent EBI2 ligand.  $7\alpha,27$ -HC also had ligand activity but was about 10-fold less potent, whereas  $25$ -HC and  $27$ -HC had minimal activity (Hannedouche et al., 2011; Liu et al., 2011).  $7\alpha,25$ -HC is synthesized from cholesterol by the stepwise action of the enzymes Ch25h and Cyp7b1, whereas  $7\alpha,27$ -HC synthesis requires Cyp27a1 and Cyp7b1 (Russell, 2003). The enzyme Hsd3b7 metabolizes  $7\alpha,25$ -HC and  $7\alpha,27$ -HC into products that lack EBI2 ligand activity (Yi et al., 2012). In vivo studies established that mice lacking Ch25h suffered from defects in B and T cell positioning and antibody responses similar to mice lacking EBI2 (Li et al., 2016; Yi et al., 2012), suggesting that  $7\alpha,25$ -HC may be the sole ligand acting on EBI2 in lymphoid tissues.

In earlier studies, we and others established that EBI2 was critical for MZ bridging channel positioning of CD4<sup>+</sup>DCIR2<sup>+</sup> DCs and for their homeostasis, with EBI2-deficient mice having about fourfold less of these splenic cells (Gatto et al., 2013; Yi and Cyster, 2013). The defective DC homeostasis reflected a reduced ability of EBI2-deficient cells to access LT $\alpha$ 1 $\beta$ 2 on B cells. Ch25h- and Cyp7b1-deficient mice also showed defects in these DCs, establishing a critical role for 7 $\alpha$ ,25-HC in DC maintenance (Gatto et al., 2013; Yi and Cyster, 2013).

When we further characterized Ch25h-deficient mice, we noted that the defects in their splenic DCIR2<sup>+</sup> cDC2 compartment were less severe than those in EBI2-deficient mice. Specifically, we found that Ch25h-deficient mice retained more CD4<sup>+</sup>DCIR2<sup>+</sup> DCs than EBI2-deficient mice and that the disruption in bridging channel positioning of these DCs was less complete. This led us to find that Cyp27a1 also contributes to the EBI2-dependent maintenance of splenic cDC2s. We show that both Cyp27a1 and Ch25h are expressed in MZ bridging channels, and we propose that these enzymes act cooperatively to control naïve (sentinel) DC positioning. We also found that cDC2s up-regulate EBI2 after activation and establish that their positioning in the splenic outer T cell zone depends on EBI2 and Ch25h. We show that EBI2 function in DCs after activation is suppressed by type I IFN, suggesting a mechanism whereby different innate stimuli lead to different T cell activating roles for DCs. Last, we provide evidence for cross-talk between DC subsets by showing that Batf3-dependent DCs promote outer T cell zone positioning of DCIR2<sup>+</sup> DCs in a manner that depends on their expression of the oxysterol-metabolizing enzyme Hsd3b7.

## Results

### Cyp27a1 functions in positioning and homeostasis of DCIR2<sup>+</sup> DCs

In the course of testing the enzyme requirements for EBI2 ligand production (**Fig. 1A**), we noticed that the defect in splenic DCIR2<sup>+</sup> DC positioning in Ch25h-deficient mice was less severe than that in EBI2-deficient mice. Immunohistochemical staining of tissue sections revealed that Ch25h-deficient mice retained small clusters of DCIR2<sup>+</sup> DCs in MZ bridging channels, whereas these were almost undetectable in EBI2- and Cyp7b1-deficient mice (**Fig. 1B** and fig. S1). Enumeration of splenic DCIR2<sup>+</sup> cDCs by flow cytometry showed that their deficiency was less severe in Ch25h-deficient mice than in EBI2- and Cyp7b1-deficient mice (**Fig. 1C**). We used the DCIR2 marker in these studies because it uniquely allows identification of cDC2s in tissue sections and is expressed by most of the splenic cDC2s. Similar numerical deficiencies were obtained when we examined cDC2 frequencies using CD4, endothelial cell-selective adhesion molecule (ESAM), signal regulatory protein  $\alpha$  (SIRP $\alpha$ ), or CD11b (fig. S2).

A comparison of spleen extracts for EBI2 ligand bioactivity using a subnanomolar-sensitive assay [(Kelly et al., 2011); fig. S3A] revealed that Ch25h-deficient mice retained detectable EBI2 ligand, whereas ligand was almost undetectable in Cyp7b1-deficient mice (**Fig. 1D**). These observations and the in vitro evidence that 7 $\alpha$ ,27-HC has a potency on EBI2 within 10-fold of 7 $\alpha$ ,25-HC [(Hannedouche et al., 2011); fig. S3A] led us to consider the possibility that Cyp27a1 acts as a second enzyme upstream of Cyp7b1 to generate EBI2 ligand activity in the spleen. Quantitative reverse transcription polymerase chain reaction analysis revealed that Cyp27a1 was highly expressed in the spleen and splenic stroma and also within the DCs themselves and was much less expressed in lymphocytes (**Fig. 1E**). In vitro migration analysis

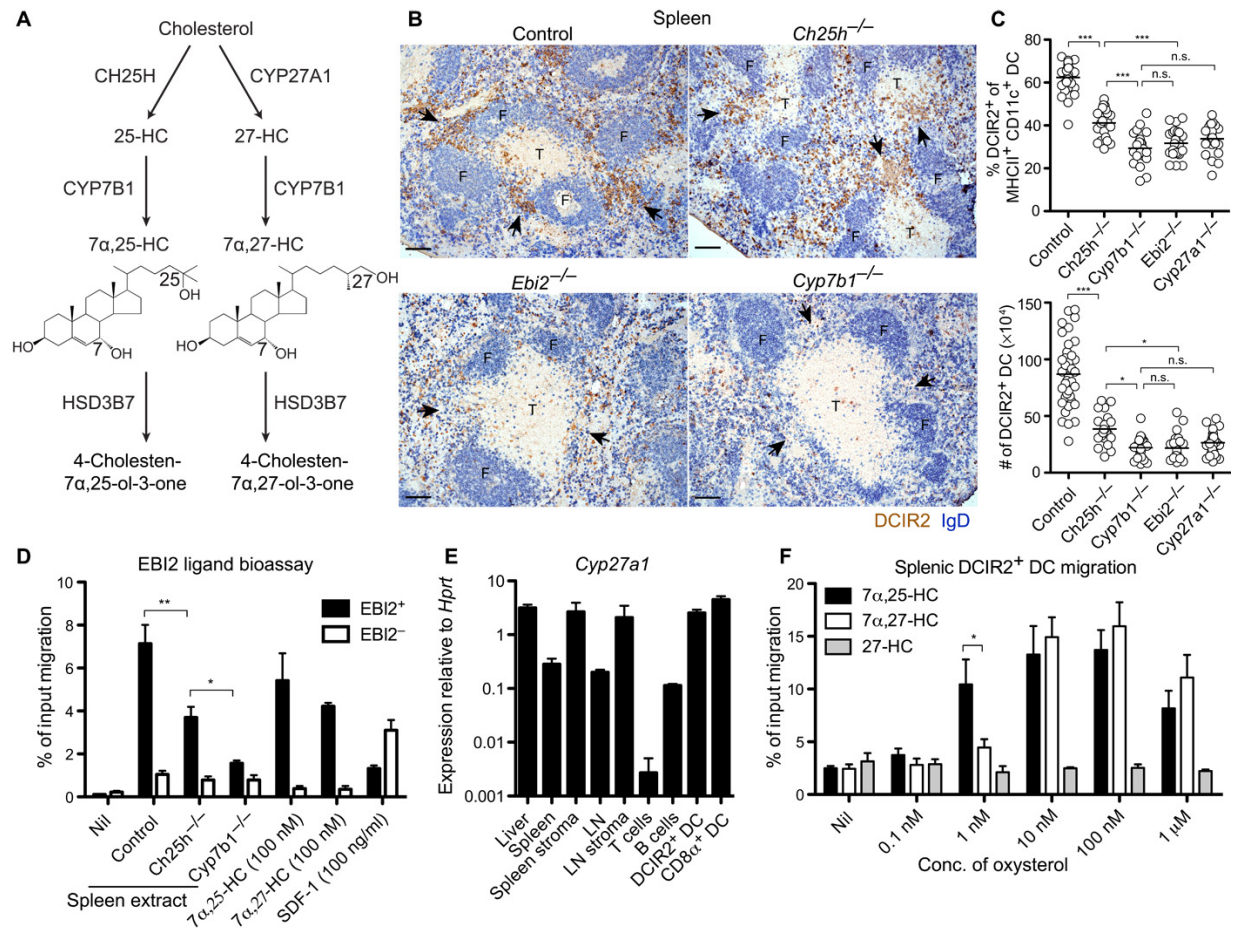


**Figure 1. Influences of Ch25h and Cyp27a1 on splenic DCIR2<sup>+</sup> DCs.**

(A) Pathway of 7 $\alpha$ ,25-HC and 7 $\alpha$ ,27-HC biosynthesis from cholesterol and metabolism by Hsd3b7. (B) Positioning of DCIR2<sup>+</sup> DCs (brown) and B cells [immunoglobulin D (IgD), blue] in spleen sections from mice of the indicated genotype. Control indicates *Ch25h*<sup>+/-</sup>. Arrowheads indicate the location of MZ bridging channels. F, follicle; T, T cell zone. (C) Summary data for DCIR2<sup>+</sup> DC frequencies and numbers in mice of the indicated genotypes. Control indicates pooled data from *Ch25h*<sup>+/-</sup> and *Cyp27a1*<sup>+/-</sup> mice. (D) EBI2 ligand bioassay of spleen extracts from the indicated animals using a reporter cell line (M12) transduced with EBI2. Control indicates *Ch25h*<sup>+/-</sup> and *Cyp27a1*<sup>+/-</sup> mice. SDF-1, stromal cell-derived factor-1. Nil indicates migration media alone. (E) *Cyp27a1* mRNA expression in tissue and cell subsets shown relative to *Hprt*. LN refers to mesenteric LN. (F) Migration of DCIR2<sup>+</sup> DCs toward the indicated oxysterols in Transwell assays. Conc., concentration. Data in (B) to (E) are representative of at least two independent experiments with at least three mice per condition. Migration assay (F) contains data from three independent experiments. Scale bars, 100  $\mu$ m. \**P* < 0.05; \*\**P* < 0.01; \*\*\**P* < 0.001; n.s., not significant (*P* > 0.05) by one-way ANOVA with Bonferroni's post hoc test for indicated comparisons.

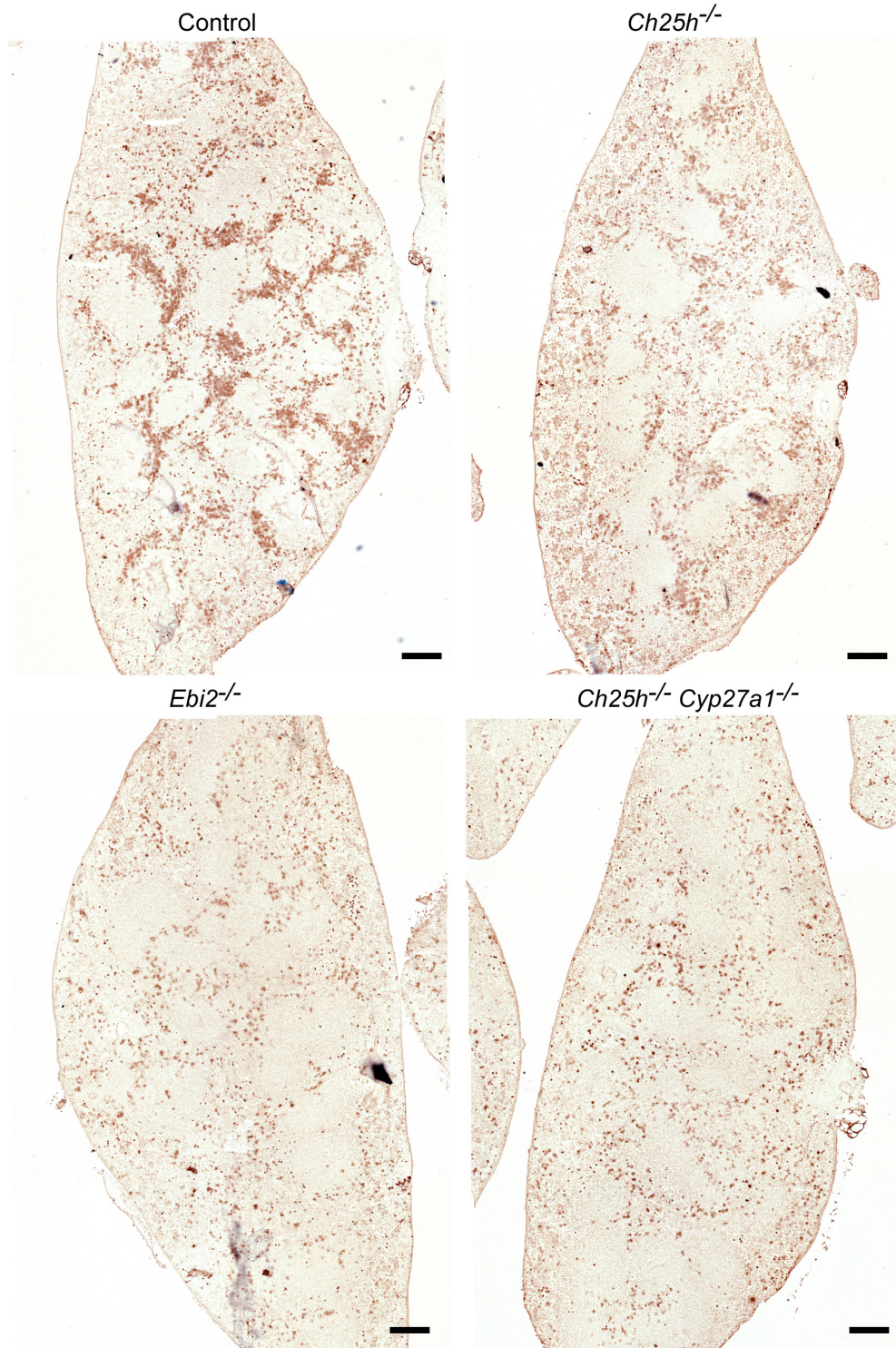


**Figure S1. Combined contribution of Cyp27a1 and Ch25h to DCIR2<sup>+</sup> DC positioning.**

Positioning of DCIR2<sup>+</sup> DCs (brown) in spleen sections from mice of the indicated genotype. In order to better visualize DC clusters, a counterstain was not used. Data are representative of 3 mice per condition. Scale bar, 200 μm.

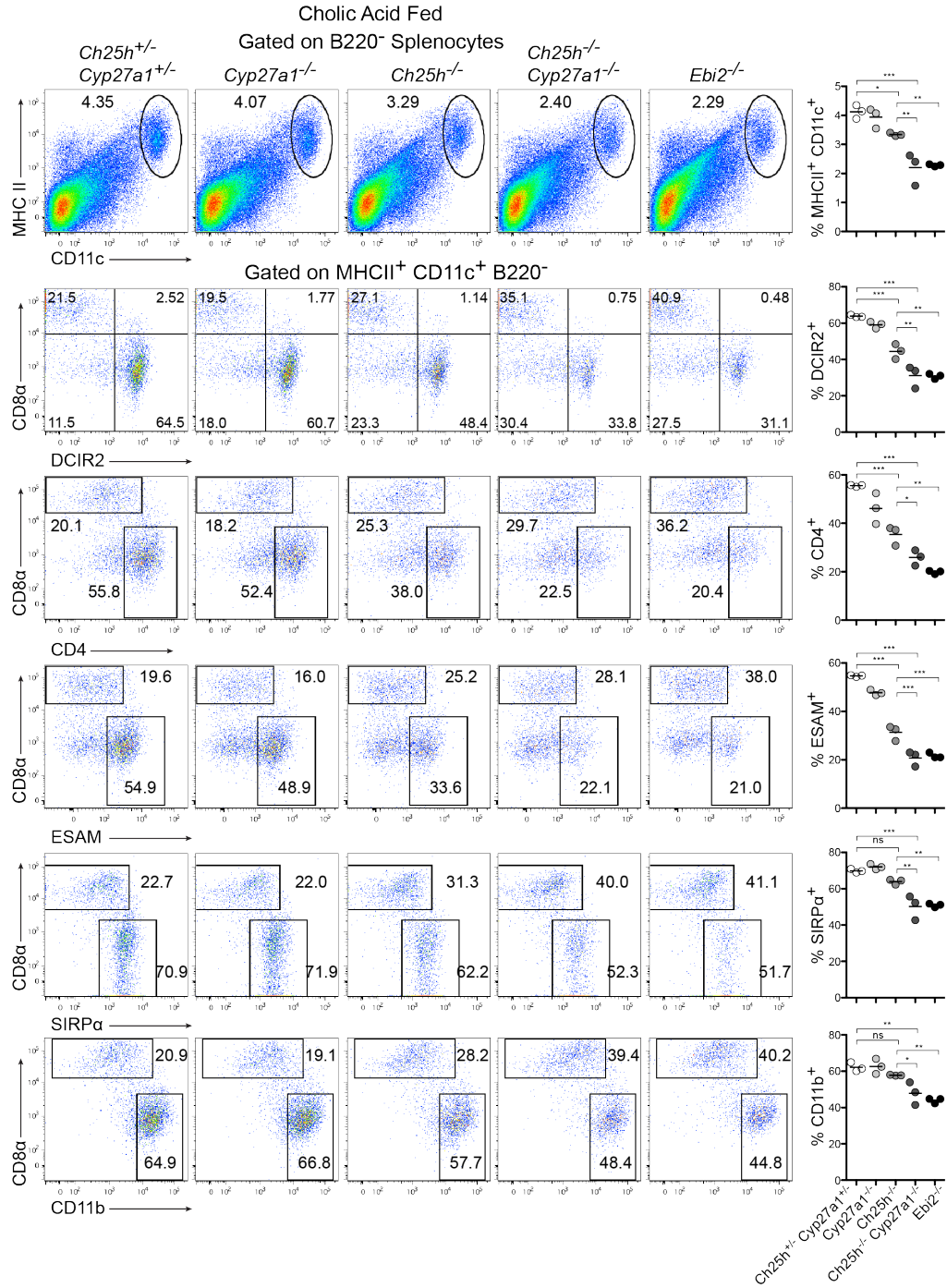


**Figure S2. cDC2 marker expression by DCs in EBI2- and ligand-deficient mice.**

Mice of the indicated genotypes were fed cholic acid-containing diet for 2 weeks and analyzed for splenic DC populations. Summary graphs are shown on the right for each row of flow cytometry plots. Top row shows representative plots for frequency of MHCII<sup>+</sup> CD11c<sup>+</sup> cells, pre-gated on B220<sup>-</sup> cells. Lower rows show representative plots of cDC2 markers plotted against CD8α, pre-gated on the MHCII<sup>+</sup> CD11c<sup>+</sup> population. Data shown here for DCIR2<sup>+</sup> DC frequency is also included in Figure 2B (pooled data). \*p < 0.05, \*\*p < 0.01, \*\*\*p < 0.001, 'ns' p > 0.05 by one-way ANOVA with Bonferroni's post hoc test for the indicated comparisons.

demonstrated that  $7\alpha,27$ -HC, although less potent than  $7\alpha,25$ -HC, was an efficacious attractant of DCs in the low nM range (**Fig. 1F**).  $7\alpha,27$ -HC appeared to retain more activity at high (100 nM) concentrations than that observed for  $7\alpha,25$ -HC. This might reflect differences in the extent of receptor desensitization because 100 nM  $7\alpha,27$ -HC caused less internalization of EB12 than 100 nM  $7\alpha,25$ -HC, although both ligands caused similar down-modulation at micromolar concentrations (fig. S3B).

In initial experiments with Cyp27a1-deficient mice, we observed that they have a marked deficiency of DCIR2<sup>+</sup> DCs (**Fig. 1C**). Unexpectedly, this deficiency exceeded that observed in Ch25h-deficient mice. Cyp27a1 has an important role in bile acid precursor synthesis in the liver, and mice lacking this enzyme have elevated plasma cholesterol and triglyceride concentrations (Russell, 2003). This is a consequence of elevated sterol response element-binding protein (SREBP-1 and SREBP-2) activity and reduced nuclear hormone receptor (farnesoid X receptor) activity in these mice because of their diminished bile acid pool and reduced absorption of dietary cholesterol (Russell, 2003). Previous work has shown that these phenotypes can be corrected by maintaining mice on a cholic acid-containing diet (Repa et al., 2000). When Cyp27a1 knockout (KO) mice were placed on this diet, their DCIR2<sup>+</sup> DC frequencies became similar to those of controls (**Fig. 2, A and B**). One explanation for these observations is that Cyp27a1-deficient mice overproduce  $7\alpha,25$ -HC (Soroosh et al., 2014), and this disrupts the  $7\alpha,25$ -HC gradient needed for DC maintenance. Consistent with this notion, we found that EB12 ligand bioactivity was elevated in spleen extracts from Cyp27a1 KO mice, but bioactivity was normal in spleen extracts from Cyp27a1 KO mice placed on a cholic acid-containing diet (fig. S3C). Similarly, bioactivity was present in plasma of Cyp27a1 KO mice on regular diet but was undetectable in plasma of mice maintained on a cholic acid-containing diet (fig. S3D).

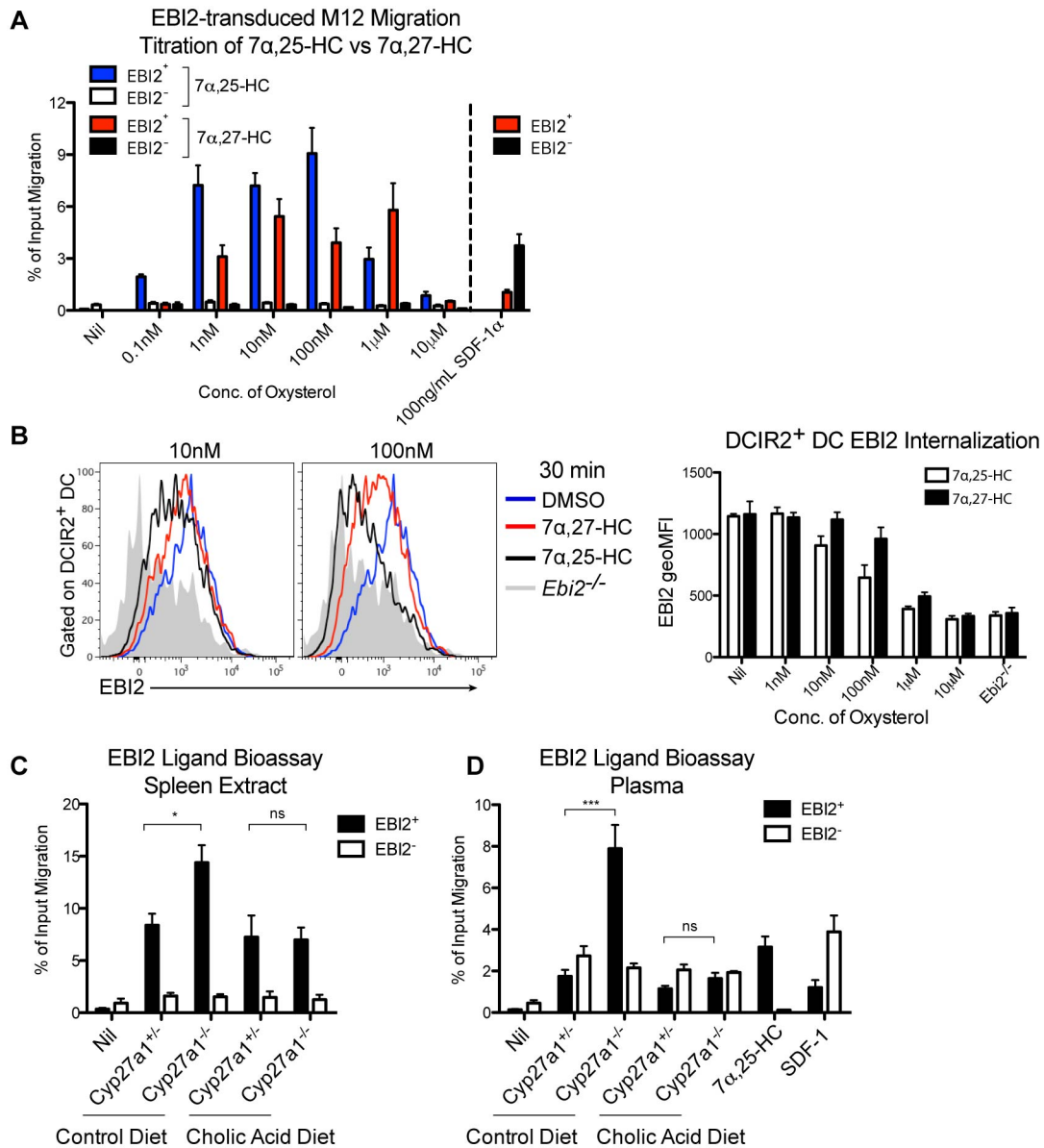


**Figure S3. M12 EBI2 bioassay sensitivity, oxysterol-induced EBI2 internalization and effect of dietary cholic acid on EBI2 ligand activity in *Cyp27a1* KO mice.**

(A) Migration assay of EBI2-transduced M12 cells towards indicated amounts of 7 $\alpha$ ,25-HC, 7 $\alpha$ ,27-HC, or the chemokine SDF-1 (CXCL12). (B) Surface expression of EBI2 on DCIR2<sup>+</sup> DCs incubated with the indicated concentrations of oxysterols for 30 min at 37°C, plotted alongside the same *Ebi2*<sup>-/-</sup> staining control (left panels). Summary data quantitated using geometric MFI in graph on the right. (C, D) EBI2 ligand bioassay of spleen extracts (C) and plasma (D) from mice of the indicated genotype that were maintained on regular diet or cholic acid-containing diet. Data are representative of 2 independent experiments (A, B) or of at least 3 mice per group (C, D). \**p* < 0.05, \*\*\**p* < 0.001, ‘ns’ *p* > 0.05 by one-way ANOVA with Bonferroni’s post hoc test.

With these observations in mind, all further studies with Cyp27a1-deficient mice were performed with animals maintained on a cholic acid-containing diet. We speculated that the contribution of Cyp27a1 to EBI2-mediated DC positioning and homeostasis may normally be subdominant to the contribution of Ch25h. DCIR2<sup>+</sup> DC frequencies in Ch25h and Cyp27a1 double-knockout (DKO) mice were reduced more substantially than in Ch25h-deficient mice and, to a similar extent, in EBI2- and Cyp7b1-deficient mice (**Figs. 2, A and B, and 1C**). This reduction in DCs was not due to selective loss of the DCIR2 marker because analysis of additional markers of splenic cDC2s (CD4, SIRP $\alpha$ , ESAM, and CD11b) revealed a similar deficiency in each case (fig. S2). Analysis of spleen sections revealed that the bridging channel DCIR2<sup>+</sup> DC clusters detectable in Ch25h KO mice were no longer detectable in mice that also lacked Cyp27a1 (**Fig. 2C** and fig. S1). Instead, the remaining DCs were scattered in the RP as observed for EBI2-deficient mice (**Fig. 2C** and fig. S1). Consistent with these observations, spleen extracts from Ch25h and Cyp27a1 DKO mice had minimal EBI2 ligand bioactivity (**Fig. 2D**). Liquid chromatography–tandem mass spectrometry (LC-MS/MS) analysis of pooled soluble spleen extracts from multiple wild-type (WT) mice revealed that 7 $\alpha$ ,27-HC was present at a concentration of ~0.013 ng/mg tissue (~30 nM), whereas it was undetectable in Cyp27a1 KO spleen extracts (**Fig. 2E**). Because the splenocytes were removed without cell lysis during generation of these extracts, this measurement approximates what is found in the interstitial fluid. It is likely that local concentrations in tissue subregions are considerably higher. We also confirmed the importance of Hsd3b7 in metabolizing 7 $\alpha$ ,27-HC by observing that Hsd3b7 deficiency caused a marked increase in this oxysterol in the spleen (**Fig. 2E**).

To test whether the Ch25h and Cyp27a1 DKO mice retained any EBI2-dependent activity in vivo, we reconstituted irradiated DKO and control mice with an equal mixture of WT and

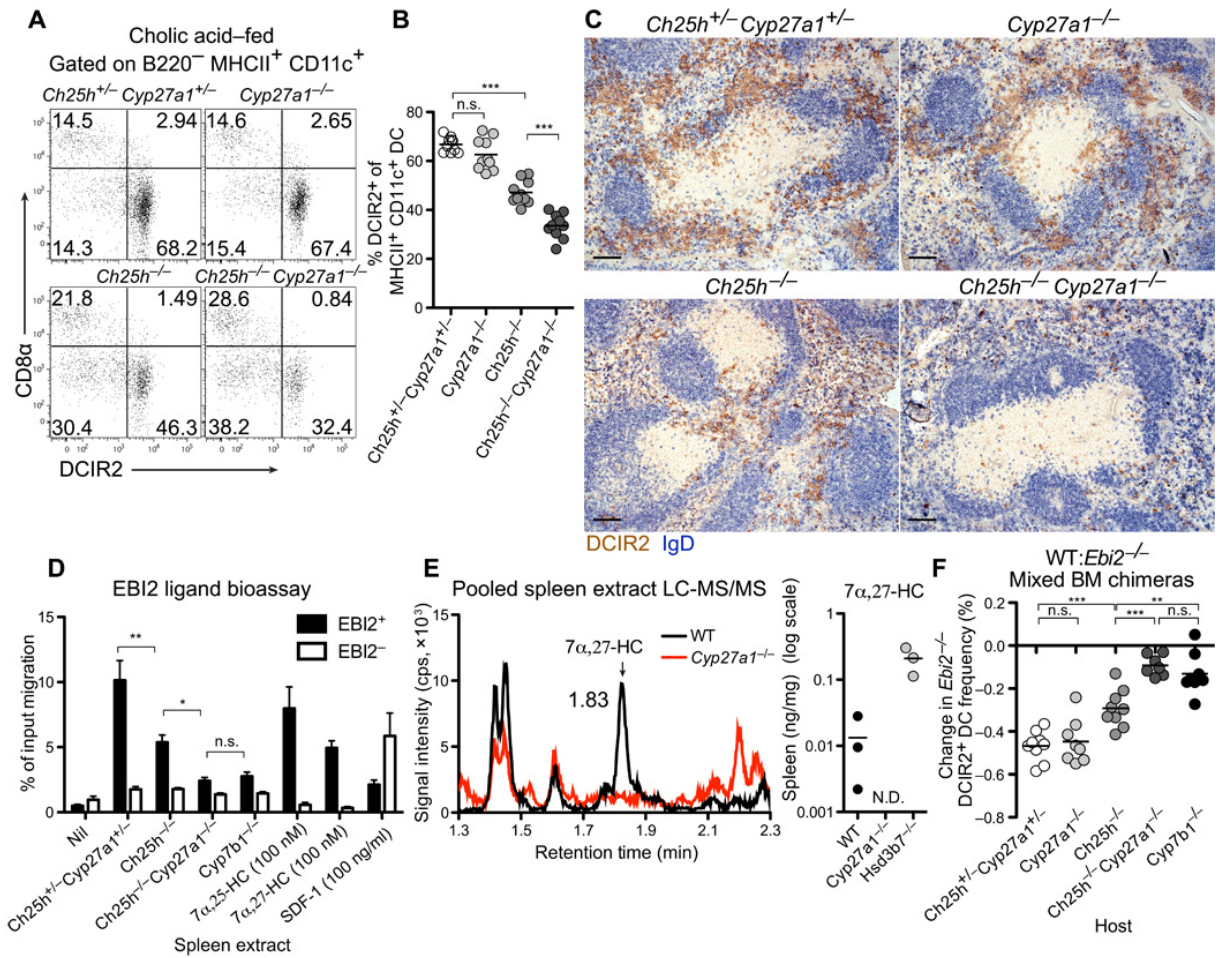


**Figure 2. *Cyp27a1* *Ch25h* DKO mice reveal a role for  $7\alpha,27$ -HC in DCIR2<sup>+</sup> DC positioning and maintenance.**

Adult mice were fed 0.5% cholic acid diet for at least 2 weeks. (A to C) Flow cytometry plot (A), summary DCIR2<sup>+</sup> DC frequency data (B), and positioning of DCIR2<sup>+</sup> DCs (brown) and B cells (IgD, blue) in spleen sections (C) from the indicated mice. (D) EBI2 ligand bioassay of spleen extracts from the indicated mice. (E) LC-MS/MS detection of  $7\alpha,27$ -HC in spleen extracts pooled from 10 to 12 mice for WT and *Cyp27a1*<sup>-/-</sup> or from single *Hsd3b7*<sup>-/-</sup> mice per measurement. Left: Representative chromatogram (N.D., not detected;  $n = 2$  sets of pooled mice for *Cyp27a1*<sup>-/-</sup>). cps, counts per second. (F) Percent change in *Ebi2*<sup>-/-</sup> DCIR2<sup>+</sup> DCs in mice reconstituted with an equal mixture of WT and *Ebi2*<sup>-/-</sup> BM, calculated by comparing the chimerism of DCIR2<sup>+</sup> DCs against CD8 $\alpha$ <sup>+</sup> DCs. Data in (A) to (D) and (F) are representative of at least two independent experiments with at least three mice per group. Scale bars, 100  $\mu$ m. \* $P < 0.05$ ; \*\* $P < 0.01$ ; \*\*\* $P < 0.001$ ; n.s., not significant ( $P > 0.05$ ) by one-way ANOVA with Bonferroni's post hoc test for indicated comparisons.

EBI2-deficient bone marrow (BM). Upon reconstitution, we observed the expected twofold outcompetition of EBI2 KO DCs by WT DCs in control hosts (**Fig. 2F**). In Ch25h-deficient hosts, the WT DCs were deficient but still outcompeted the EBI2 KO DCs (**Fig. 2F**). However, in Ch25h and Cyp27a1 DKO hosts, the WT and EBI2 KO DCs were almost equally compromised, similar to the findings in Cyb7b1-deficient hosts (**Fig. 2F**). These data demonstrate that both Ch25h and Cyp27a1 contribute to the generation of EBI2 ligand activity controlling DCIR2<sup>+</sup> DC homeostasis. These data also show that Cyp27a1 was required in radiation-resistant (stromal) cells and not intrinsically in the DCs to maintain DCIR2<sup>+</sup> DC homeostasis (**Fig. 2F**).

Analysis of mesenteric lymph nodes (LNs) in cholic acid-fed Cyp27a1-deficient mice showed that migratory and resident DCs were present at normal frequencies and that DCIR2<sup>+</sup> DCs were correctly distributed (fig. S4, A and B). Ch25h-deficient mice showed a reduction in DCIR2<sup>+</sup> migratory (MHCII<sup>hi</sup>CD11c<sup>+</sup> CD11b<sup>+</sup>) and resident (MHCII<sup>int</sup>CD11c<sup>hi</sup> CD11b<sup>+</sup>) DCs that was comparable to the deficiency observed in EBI2-deficient mice (fig. S4, A and B). Ch25h and Cyp27a1 DKO mice showed the same deficiency observed in Ch25h KO mice (fig. S4, A and B) suggesting that Cyp27a1 may not be required for DC homeostasis in LNs. This was further established using the mixed BM chimera approach because the EBI2-deficient DCs were underrepresented to the same extent in WT and Cyp27a1 KO hosts (fig. S4C). Moreover, WT and EBI2-deficient cells were equally deficient in Ch25h KO hosts and further removing Cyp27a1 had no additional effect (fig. S4C). In tissue sections, DCIR2<sup>+</sup> DCs were most concentrated in regions of the T cell zone near B cell follicles; this distribution was disrupted in EBI2-deficient and Ch25h-deficient mice but appeared unaffected

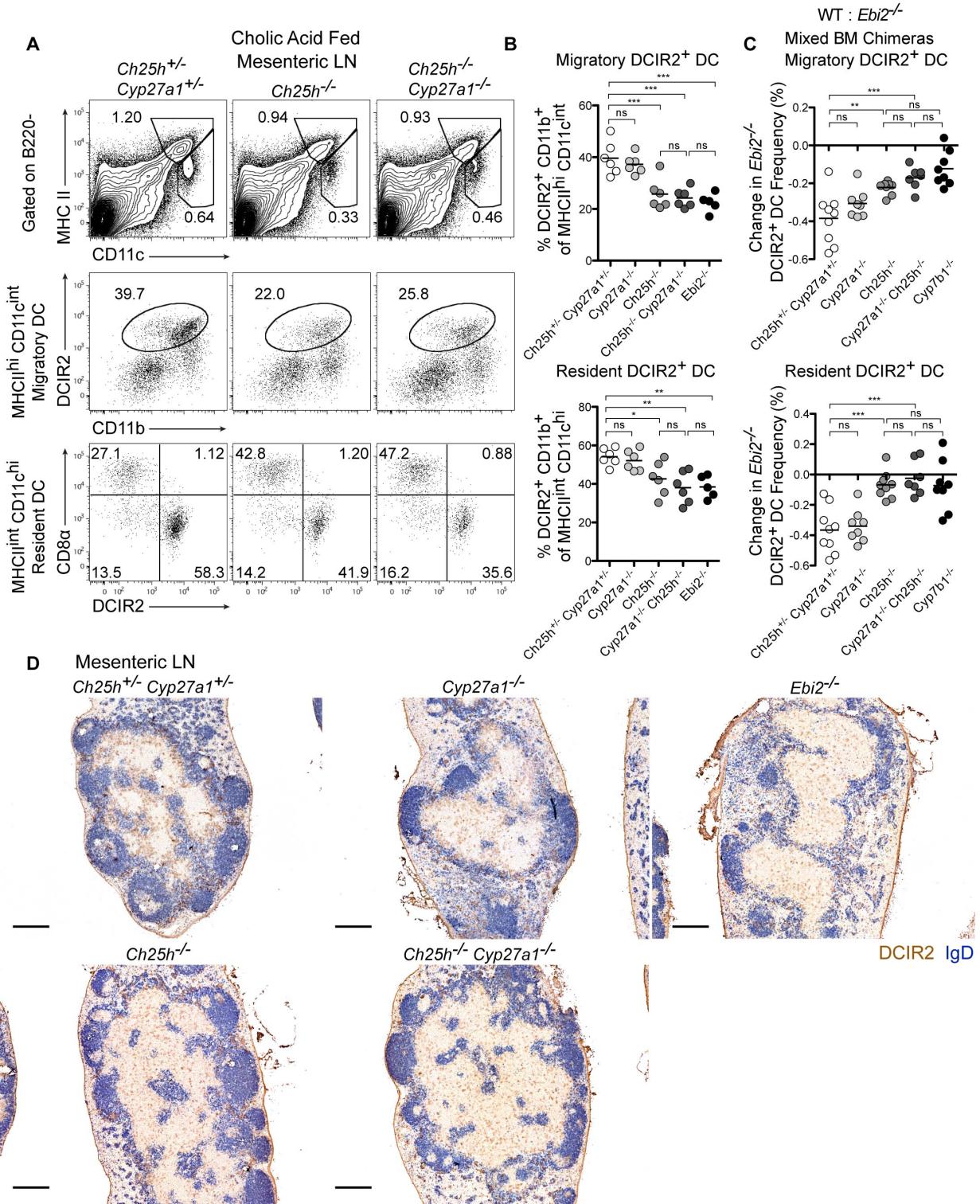


**Figure S4. Mesenteric LN DCIR2<sup>+</sup> DC homeostasis and positioning in Ch25h and Cyp27a1 single- and double-deficient mice.**

(A) Representative flow cytometry plots of mesenteric LN DC subsets in mice of the indicated genotype. (B) Summary data for migratory (top) and resident (bottom) DCIR2<sup>+</sup> DC frequencies

in mice of the indicated genotypes. **(C)** Percent change in frequency of *Ebi2*<sup>-/-</sup> DCIR2<sup>+</sup> migratory (top) or resident (bottom) DCs in the indicated host mice reconstituted with an equal mixture of WT and *Ebi2*<sup>-/-</sup> BM. Percent change was calculated by comparing the chimerism of DCIR2<sup>+</sup> DCs against resident CD8 $\alpha$ <sup>+</sup> DCs that are not affected by loss of EBI2. **(D)** Positioning of DCIR2<sup>+</sup> DCs (brown) and endogenous B cells (IgD, blue) in mesenteric LN sections from mice of the type in (B). Data are representative of two independent experiments with at least 3 mice per group (A, B, C) or of at least 3 mice per condition (D). Each dot in graphs indicates an individual mouse and horizontal lines indicate means. Scale bar, 200 $\mu$ m. \*p < 0.05, \*\*p < 0.01, \*\*\*p < 0.001, 'ns' p > 0.05 by one-way ANOVA with Bonferroni's post hoc test for the indicated comparisons.

in Cyp27a1-deficient mice (fig. S4D). Ch25h and Cyp27a1 DKO mice showed a similar disruption to that observed in Ch25h-deficient mice (fig. S4D). Thus, in contrast to the spleen, Cyp27a1 does not appear to be required for homeostasis of DCIR2<sup>+</sup> DCs in mesenteric LNs despite the relatively high Cyp27a1 mRNA expression level in this tissue (**Fig. 1E**).

### **Patterns of enzyme expression in the spleen**

To understand how Cyp27a1 and Ch25h might work together to control DC positioning and homeostasis, it was critical to determine the pattern of enzyme expression. Attempts to stain for Cyp27a1 using rabbit antisera or detect transcript distribution using standard in situ hybridization techniques were unsuccessful. We therefore turned to the RNAscope procedure that uses multiple tagged DNA oligonucleotides and a secondary hybridization procedure to amplify the signal to detect mRNA distribution (Wang et al., 2012). This approach revealed that Cyp27a1 mRNA was particularly abundant in splenic MZ bridging channels and was also present in the T cell zone and at lower levels in B cell follicles (**Fig. 3A**, boxed regions highlight example bridging channels; see also fig. S5A). Because Cyp27a1 is expressed in DCs (**Fig. 1E**), we also examined diphtheria toxin (DT)-treated Zbtb46-DT receptor (DTR) (zDC-DTR) BM chimeric mice that lack DCs (fig. S5B). DC-deficient mice showed a pattern of Cyp27a1 expression in MZ bridging channels similar to saline-treated zDC-DTR mice, with considerably less signal in the T cell zone (**Fig. 3B**). These data suggest that Cyp27a1 is expressed by stromal cells in the MZ bridging channels but is expressed by both DCs and stromal cells in the T cell zone. Using the same method, we found that Ch25h was abundantly expressed by cells in the outer follicle and within interfollicular regions, including in the MZ bridging channel (**Fig. 3A** and fig. S5A). Ch25h expression was conspicuously low within B cell follicles, in accord with earlier laser capture microscopy analysis (Yi et al., 2012), and was also low within the T

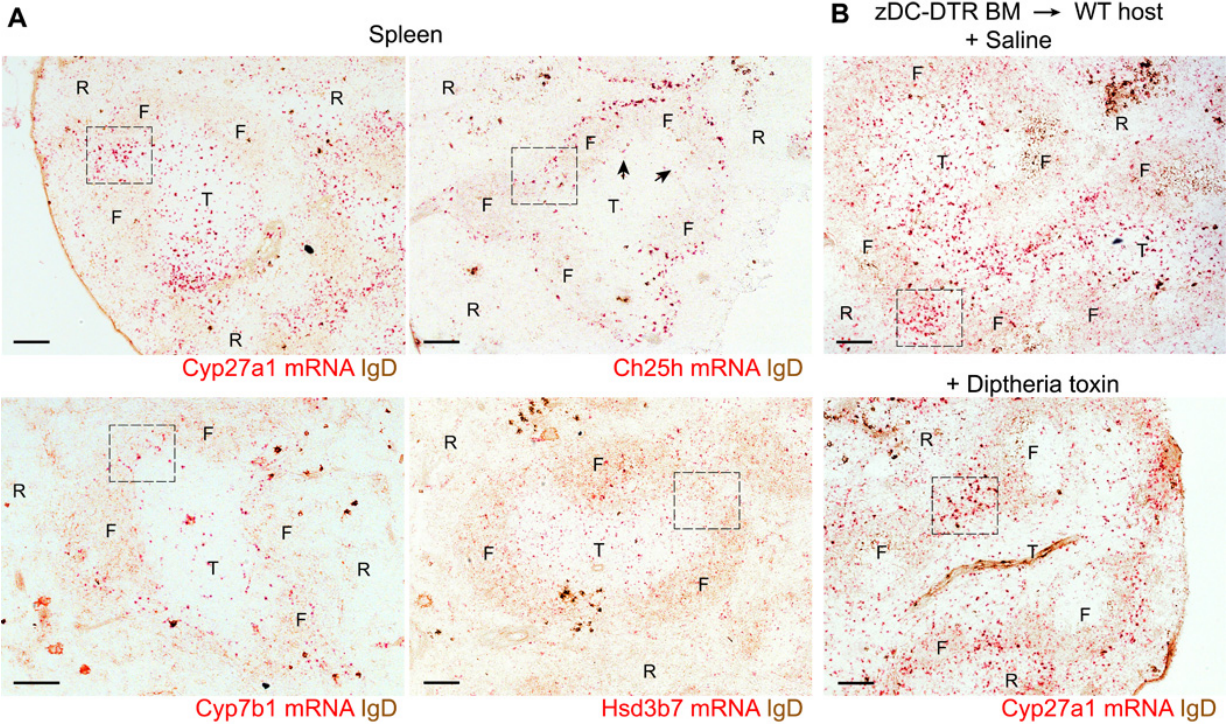


**Figure 3. Expression pattern of *Cyp27a1*, *Ch25h*, *Cyp7b1*, and *Hsd3b7* transcripts in the spleen determined using RNAscope.**

(A) Distribution of *Cyp27a1*, *Ch25h*, *Cyp7b1*, and *Hsd3b7* mRNA (red) in spleen sections co-stained for IgD (brown). Dashed box indicates staining within MZ bridging channel areas, and arrowheads highlight *Ch25h* signal at the B-T zone interface. T, T cell zone; F, follicle; R, red pulp. (B) Distribution of *Cyp27a1* mRNA in spleen sections of zDC-DTR chimeric mice treated with either saline (top) or DT (bottom). Images are representative of at least five (A) or three (B) mice per condition. Scale bars, 100  $\mu$ m.

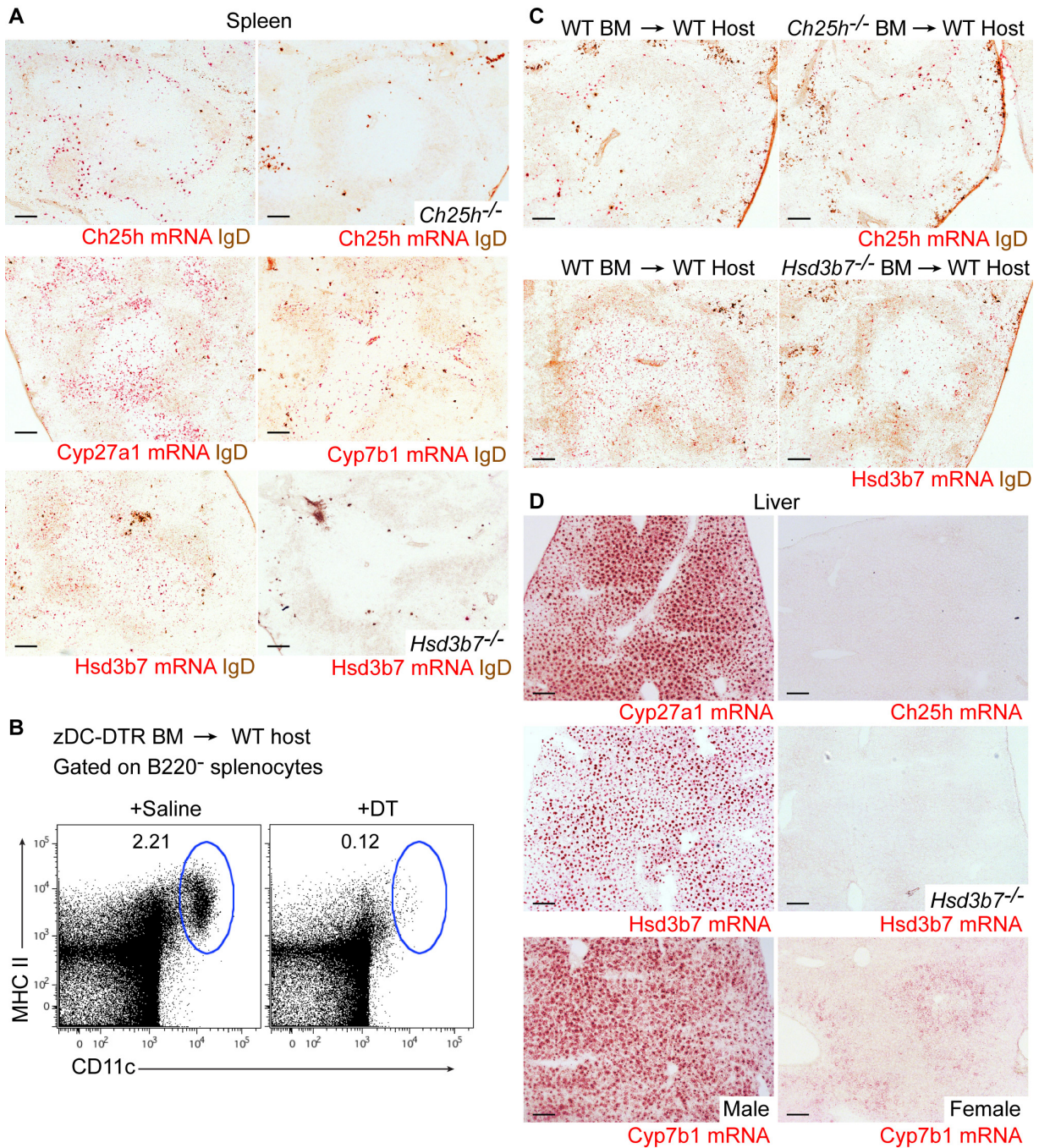


**Figure S5. RNAscope analysis of enzyme expression in spleen and liver, and efficiency of DC ablation.**

(A) Expression of the indicated enzyme transcripts in spleen sections of WT, Ch25h KO, and Hsd3b7 KO mice. (B) DC ablation efficiency in zDC-DTR BM chimeras treated with saline or DT. (C) Expression of *Ch25h* or *Hsd3b7* mRNA in irradiated WT mice reconstituted with either Ch25h KO (top row) or Hsd3b7 KO BM (bottom row). (D) Liver expression of transcripts for *Cyp27a1*, *Ch25h* and *Hsd3b7* in WT mice, *Hsd3b7* in KO mice, and comparison of *Cyp7b1* mRNA expression in male and female mice. Data are representative of at least 3 mice per condition, including mice of both sexes. Scale bar, 100 $\mu$ m.

cell zone, although expression could be detected at the B-T zone interface (**Fig. 3A**, arrows). The specificity of the Ch25h probe was confirmed using tissue from Ch25h KO mice [fig. S3A; this control was not possible with Cyp27a KO mice because they retain most of the coding region (Rosen et al., 1998) and express the mutated transcript]. The Ch25h mRNA detected by RNAscope was restricted to radiation-resistant cells because we observed no difference in the hybridization pattern in spleen tissue from mice reconstituted with Ch25h KO BM (fig. S5C). Cyp7b1 was more widely distributed than either Cyp27a1 or Ch25h, and expression could be detected in the MZ bridging channels, the T cell zone, and follicles (**Fig. 3A** and fig. S5A). The oxysterol-metabolizing enzyme, Hsd3b7, was particularly widely expressed (**Fig. 3A** and fig. S5A), and this included considerable expression by hematopoietic cells in the T cell zone (fig. S5C), most likely in DCs (Yi et al., 2012). RNAscope analysis of liver sections confirmed the very high expression of Cyp27a1, Cyp7b1, and Hsd3b7 and minimal expression of Ch25h in this bile-producing tissue (fig. S5D). The liver showed the expected sexual dimorphism in Cyp7b1 expression (Li-Hawkins et al., 2000), a difference that is not observed in lymphoid tissues (fig. S5D). The presence of both Cyp27a1 and Ch25h in MZ bridging channels is consistent with these enzymes acting cooperatively to generate EBI2 ligand in this region of the spleen.

### **EBI2 is required for positioning activated DCs in the outer T cell zone**

After activation, splenic DCIR2<sup>+</sup> DCs rapidly relocate from the MZ bridging channels, MZ, and RP and move into the T cell zone. In response to SRBC immunization and activation by missing self-recognition, the cells preferentially position in the outer T cell zone (Yi and Cyster, 2013; Yi et al., 2015). It seemed unlikely that EBI2 would have a role in this behavior, given its requirement for cell positioning in the bridging channels. However, studies in other contexts have shown that small shifts in responsiveness to competing cues can have major influences on

cell localization (Griffith et al., 2014). We therefore tested for changes in EBI2 expression in DCIR2<sup>+</sup> DCs after SRBC-induced activation. Within 6 hours of activation, the cells not only had strongly up-regulated CCR7 and CD86 but also had increased their surface EBI2 expression (**Fig. 4A**). Analysis of green fluorescent protein (GFP) levels in immunized EBI2-GFP reporter mice established that this reflected an increase in transcript abundance in the cells (**Fig. 4B**). To test whether EBI2 was required for outer T cell zone positioning while avoiding the effects of chronic EBI2 deficiency on DC numbers, we took advantage of a recently described EBI2 antagonist (Gessier et al., 2014). We first confirmed that the inhibitor was effective at inhibiting DC migration to EBI2 ligands in vitro while not affecting migration to control chemoattractants (fig. S6, A and B). Antagonist treatment resulted in a complete disruption in DCIR2<sup>+</sup> DC outer T cell zone preference (**Fig. 4C**), a defect that was confirmed by quantitating the fraction of DCIR2 staining in the outer T cell zone across multiple sections (**Fig. 4D** and fig. S6C). This observation led us to reanalyze the distribution of the DCs remaining in EBI2-deficient mice; in the cases where the T cell zone contained sufficient DCs for comparative analysis, the KO cells were uniformly distributed throughout the T cell zone (**Fig. 4E**). Activated DCIR2<sup>+</sup> DCs also showed little preference for the B-T zone interface in Ch25h-deficient mice, although, in this case, they were sometimes clustered within the T cell zone rather than being randomly dispersed (**Fig. 4E**). By contrast, in Cyp27a1-deficient mice, the activated DCs appeared to position normally to the B-T zone interface (**Fig. 4E**). In Cyp7b1- and Hsd3b7-deficient mice, the activated DCs were distributed uniformly throughout the T cell zone (**Fig. 4E**).

To determine whether EBI2 up-regulation on T cell zone tropic cells was sufficient to promote their positioning in the outer T cell zone, we examined the distribution of transferred T cells overexpressing EBI2. Flow cytometric analysis confirmed that EBI2 transduction led to

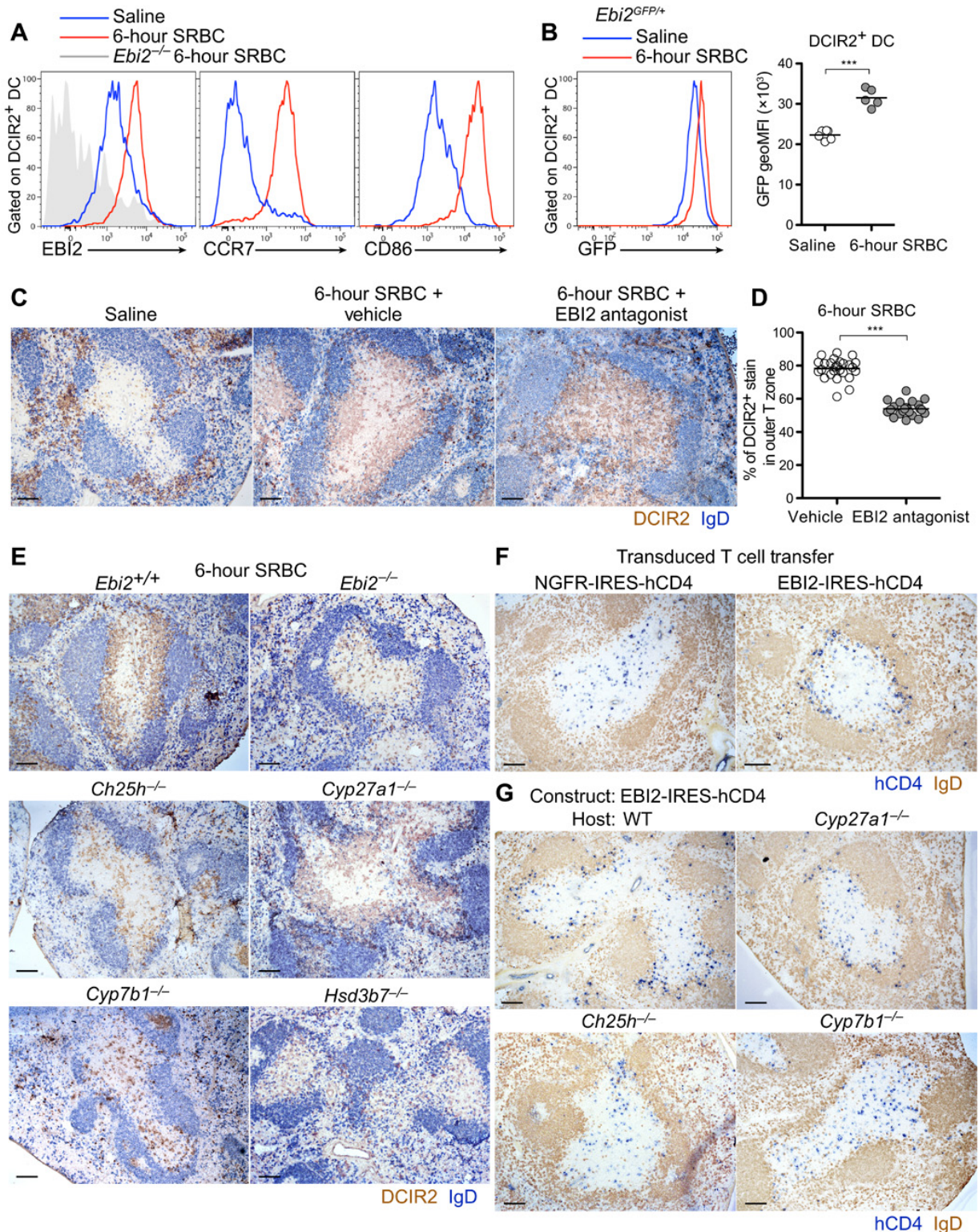


**Figure 4. Activated DCIR2<sup>+</sup> DCs up-regulate EBI2 and position at the B-T zone interface in an EBI2- and Ch25h-dependent manner.**

(A and B) Surface expression of EBI2, CCR7, and CD86 in DCIR2<sup>+</sup> DCs (A) and GFP expression in *Ebi2*<sup>GFP/+</sup> DCIR2<sup>+</sup> DCs (B) from mice 6 hours after intravenous immunization with

saline (blue) or SRBCs (red). geoMFI, geometric mean fluorescence intensity. **(C)** Positioning of DCIR2<sup>+</sup> DCs (brown) relative to B cells (blue) in mice 6 hours after treatment with saline, SRBCs plus vehicle (*N*-methyl-2-pyrrolidone), or SRBCs plus EBI2 antagonist (NIBR189). **(D)** Percentage of DCIR2<sup>+</sup> DC staining in the outer T cell zone in the spleens of the type in (C). Each point represents a white pulp cord. **(E)** Positioning of DCIR2<sup>+</sup> DCs in mice of the indicated genotypes 6 hours after SRBC immunization. **(F and G)** Positioning of activated T cells overexpressing EBI2 or a control receptor [truncated nerve growth factor receptor (NGFR)] 24 hours after transfer into WT mice (F) or mice of the indicated genotype (G). Sections were stained to detect transduced T cells (hCD4, blue) and B cells (IgD, brown). Data are representative of at least two independent experiments and at least four mice analyzed per condition. Scale bars, 100  $\mu$ m. \*\*\* $P < 0.001$  by unpaired Student's *t* test.

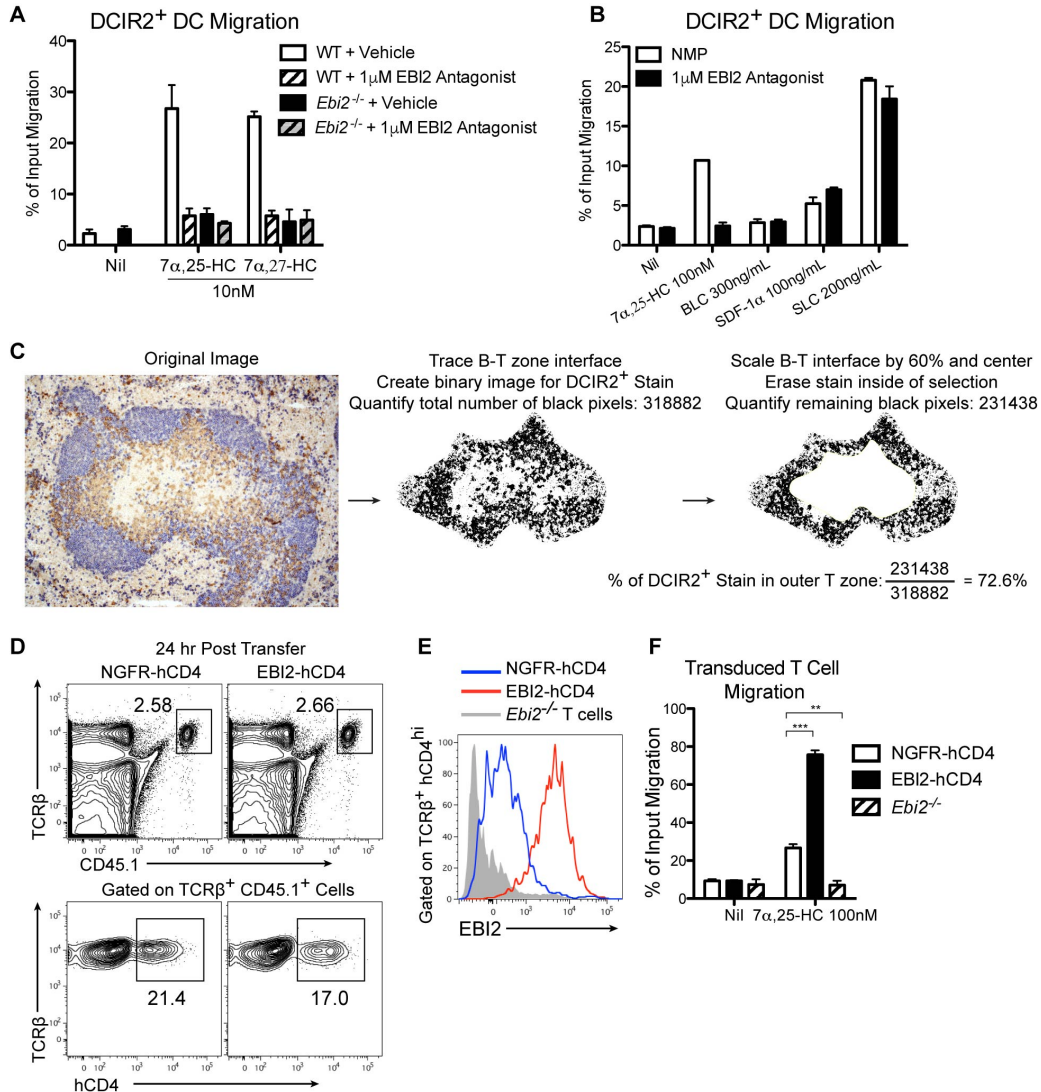


**Figure S6. EB12 antagonist specificity, method for quantifying DC distribution, and retroviral transduction efficiency of activated T cells.**

(A) Migration assay of WT or EB12 KO DCIR2<sup>+</sup> DCs towards indicated amounts of oxysterol. EB12 antagonist NIBR189 (1 $\mu$ M) or vehicle (NMP) was added to the bottom well along with oxysterol. WT or EB12 KO DCIR2<sup>+</sup> DC migration to Nil + 1 $\mu$ M EB12 antagonist was not performed in this experiment. (B) Migration assay of WT DCIR2<sup>+</sup> DCs towards Nil or the indicated chemoattractants with or without addition of EB12 antagonist (1 $\mu$ M) to the bottom well. (C) Example of quantitation method performed on an image of a white-pulp cord from a 6 hr SRBC immunized mouse. (D, E) Representative flow cytometry plots showing frequency of CD45.1<sup>+</sup> transduced T cells (D) and EB12 surface levels on the T cells (E) in the spleen 24hr after adoptive transfer. T cells were transduced with retroviral constructs encoding either NGFR-hCD4 or EB12-hCD4. Histogram in (E) is pre-gated on reporter (hCD4)-high cells. (F) Migration assay of T cells transduced with either NGFR-hCD4 or EB12-hCD4 towards the indicated amount of 7 $\alpha$ ,25-HC. \*\*p < 0.01, \*\*\*p < 0.001, by one-way ANOVA with Bonferroni's post hoc test for the indicated comparisons.

higher EBI2 expression on the reporter-expressing cells than on the matched vector-transduced cells, and the EBI2<sup>hi</sup> cells responded more robustly to 7 $\alpha$ ,25-HC (fig. S6, D to F). The EBI2<sup>hi</sup> T cells showed a preference to position in the outer T cell zone, whereas control vector-transduced cells were distributed throughout the T cell zone (**Fig. 4F**). Consistent with the findings for activated DCIR2<sup>+</sup> DCs, EBI2<sup>hi</sup> T cells continued to position in the outer T cell zone in Cyp27a1-deficient hosts but largely failed to do so in Ch25h-deficient hosts (**Fig. 4G**). In mice lacking Cyp7b1, the T cells were uniformly distributed throughout the T cell zone (**Fig. 4G**). These data indicate that Ch25h and Cyp7b1 contribute to EBI2 ligand production in the splenic outer T cell zone.

#### **DC outer T zone positioning enhances T follicular helper cell responses**

To test the importance of outer T cell zone positioning of DCs on the T cell response, we generated chimeric mice that had similar numbers of DCIR2<sup>+</sup> DCs but where the DCs were either EBI2 HET (control) or KO. This was achieved by reconstituting mice with either a 50:50 ratio of EBI2 HET and zDC-DTR BM or an 80:20 ratio of EBI2 KO and zDC-DTR BM (the higher ratio is needed to compensate for the deficiency in EBI2 KO DCs) and then treating mice with DT (**Fig. 5A** and fig. S7A). After DT treatment, the two types of chimeric mice were found to have well-matched numbers of DCs (**Fig. 5B**). Carboxyfluorescein diacetate succinimidyl ester (CFSE)-labeled OTII T cells were transferred into these mice, and the animals were immunized with SRBC-ovalbumin (OVA). Analysis after 12 hours confirmed that the control and EBI2 KO DCIR2<sup>+</sup> DCs became equally activated (fig. S7B). At this time point, WT DCIR2<sup>+</sup>DCs were colocalized with OTII cells in the outer T cell zone, whereas EBI2 KO DCIR2<sup>+</sup> DCs were only partly overlapping with OTII T cells because the DCs remained uniformly distributed in the T cell zone (**Fig. 5C**). After 3 days, the OTII T cells in hosts that had

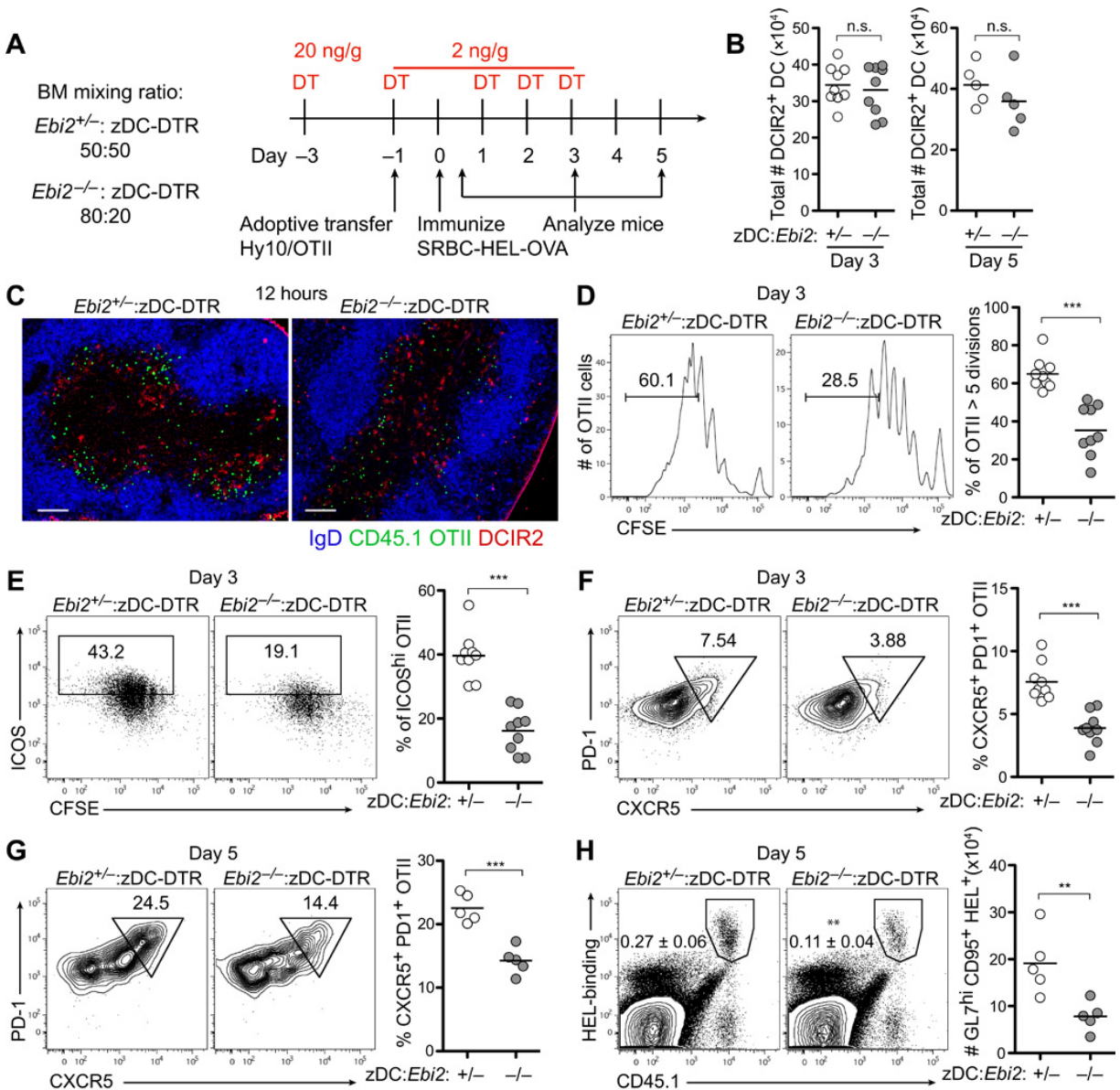


**Figure 5. EBI2-mediated DCIR2<sup>+</sup> DC positioning in the outer T cell zone augments induction of Tfh cells.**

(A) Time line of DT treatment, cell transfer, immunization, and analysis. OVA-specific OTII T cells were transferred alone (C to F) or together with HEL-specific Hy10 B cells (G and H) into mice containing matched frequencies of control (*Ebi2*<sup>+/-</sup>) or *Ebi2*<sup>-/-</sup> DCIR2<sup>+</sup> DCs (B) Total DCIR2<sup>+</sup> DC numbers in mice 3 or 5 days after immunization. (C) Immunofluorescence images of spleen sections showing distribution of CD45.1<sup>+</sup> OTII T cells (green), DCIR2<sup>+</sup> DCs (red), and B cells (IgD, blue) 12 hours after immunization. (D) Proliferation of OTII cells 3 days after immunization determined by CFSE dilution. (E and F) Up-regulation of ICOS (E) and acquisition of PD-1 and CXCR5 (F) by OTII cells 3 days after immunization. (G) Acquisition of PD-1 and CXCR5 by OTII cells after cotransfer with Hy10 B cells 5 days after immunization. (H) Frequency of total HEL-binding Hy10 cells (left plots) and total number of GL7<sup>hi</sup>Fas<sup>+</sup> HEL-

binding B cells (graph on right) from the mice in (G). Images in (C) are representative of three mice, and data in (B), (D), (E), and (F) are representative of two independent experiments with at least three mice per group. Data in (G) and (H) are obtained from one experiment with five mice per condition. Scale bars, 100  $\mu\text{m}$ . \*\* $P < 0.01$ ; \*\*\* $P < 0.001$ ; n.s., not significant ( $P > 0.05$ ) by unpaired Student's  $t$  test.

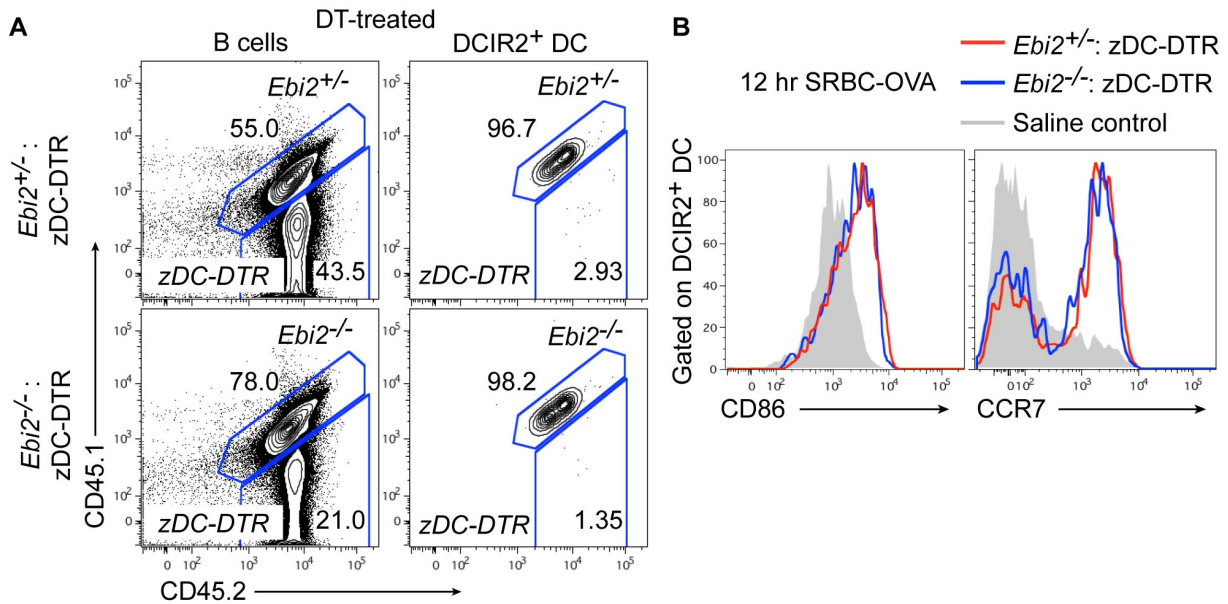


**Figure S7. Characterization of EBI2:zDC-DTR mixed chimeras.**

**(A)** Mixed chimeric mice were made using 50:50 ratio of EBI2 HET and zDC-DTR BM or an 80:20 ratio of EBI2 KO and zDC-DTR BM. Flow cytometry plots show ablation efficiency of DCs derived from zDC-DTR BM ( $\text{CD45.1}^- \text{CD45.2}^+$ ) compared to DCs derived from EBI2 HET or KO BM ( $\text{CD45.1}^+ \text{CD45.2}^+$ ) following DT treatment as in Fig. 5A, analyzed at day 3. B cells are shown as a control for the mixing ratio. **(B)** Upregulation of activation markers CCR7 and CD86 on DCIR2<sup>+</sup> DCs in mice of the type in (A), 12 hr after SRBC-OVA immunization. Data are representative of at least 5 mice per condition.

EBI2 KO DCs were deficient in proliferation, up-regulation of the activation marker inducible costimulator (ICOS), and acquisition of T follicular helper (Tfh) cell markers CXCR5 and programmed cell death protein 1 (PD-1) (**Fig. 5**, D to F). In an adoptive cotransfer experiment using hen egg lysozyme (HEL)-specific Hy10 B cells and OTII T cells and immunization with SRBC-HEL-OVA, Tfh cell induction was again defective (**Fig. 5G**) and Hy10 cells were less able to give rise to germinal center B cells in mice that lacked EBI2 on DCs (**Fig. 5H**). These data support the conclusion that EBI2-dependent positioning of DCIR2<sup>+</sup> DCs in the outer T cell zone augments their ability to support Tfh cell responses. The data do not exclude the possibility that EBI2 signaling in DCs may act in additional ways to promote Tfh cell responses.

#### **Type I IFN signaling overrides DC outer T cell zone positioning**

DCs also redistribute into the T cell zone after LPS or poly I:C treatment (De Becker et al., 2000; De Trez et al., 2005; Gunn et al., 1999; Idoyaga et al., 2009; Sousa and Germain, 1999), although whether these stimuli cause the cells to favor the outer T cell zone has been unclear. Analysis of EBI2 expression on DCIR2<sup>+</sup> DCs after exposure to these activating stimuli revealed that LPS induced similar expression to SRBCs, whereas poly I:C induced inferior expression of both EBI2 and CCR7, despite up-regulation of CD86 to similar levels (**Fig. 6**, A and B, and fig. S8A). In accord with the differences in EBI2 surface expression, LPS caused DCIR2<sup>+</sup> DCs to favor the B-T zone interface, whereas poly I:C did not (**Fig. 6C** and fig. S8B). In vitro migration assays confirmed that there was a close correspondence between the EBI2 surface levels and the ability of the DCIR2<sup>+</sup> DCs to respond to 7 $\alpha$ ,25-HC (**Fig. 6D**). These data led us to examine whether poly I:C could have a suppressing effect on EBI2 function in DCIR2<sup>+</sup> DCs. Analysis of mice treated with a mixture of SRBCs and poly I:C showed that, although DCIR2<sup>+</sup> DCs were able to up-regulate CCR7 and CD86 (fig. S8A), there was an

impaired surface expression of EB12 (**Fig. 6**, A and B) and the DCs failed to position at the B-T zone interface (**Fig. 6C** and fig. S8B). Analysis of EB12-GFP reporter expression showed that poly I:C did not suppress EB12 at the transcriptional level, suggesting that the receptor was being posttranscriptionally regulated (fig. S8C). This observation brought our attention to the type I IFN inducibility of Ch25h (Cyster et al., 2014). Ch25h transcripts were up-regulated in spleen tissue of poly I:C-treated mice (**Fig. 6E**), and there was a corresponding increase in EB12 ligand bioactivity (**Fig. 6F**). The increase in bioactivity after poly I:C treatment was lost in IFN- $\alpha$  receptor (IFNAR) KO mice (**Fig. 6F**), and the inhibition of EB12 surface expression and outer T cell zone positioning was rescued in these mice, establishing that these effects were mediated by type I IFN (**Fig. 6**, A to C, and fig. S8, A and B). Consistent with type I IFN-inducing Ch25h expression, induction of EB12 ligand bioactivity by poly I:C was lost in Ch25h KO mice (fig. S8D). Immunization of IFNAR KO $\rightarrow$ WT and WT $\rightarrow$ IFNAR KO BM chimeras showed that IFN was acting on both radiation-sensitive (hematopoietic) and radiation-resistant (stromal) cells to promote EB12 ligand production (**Fig. 6G**). In accord with this observation, IFNAR expression on either hematopoietic cells or stromal cells was sufficient to prevent DCIR2<sup>+</sup> DC positioning in the outer T zone (**Fig. 6H**). In contrast to the findings for EB12 ligand production, the modulating influence of poly I:C on surface EB12 levels was dependent on IFNAR expression in hematopoietic cells (fig. S8E), and mixed BM chimeras showed that this dependency reflected a DC-intrinsic effect (fig. S8F). Analysis of BM chimeric mice in which DCs were selectively IFNAR-deficient also showed the recovery in surface EB12 levels (fig. S8G). However, poly I:C treatment continued to cause dispersal of DCIR2<sup>+</sup> DCs throughout the T cell zone in these mice (fig. S8H). Spleen extract bioactivity analysis showed that poly I:C caused elevations in EB12 ligand levels in mice lacking IFNAR from DCs (fig. S8I). Together, these data indicate that type

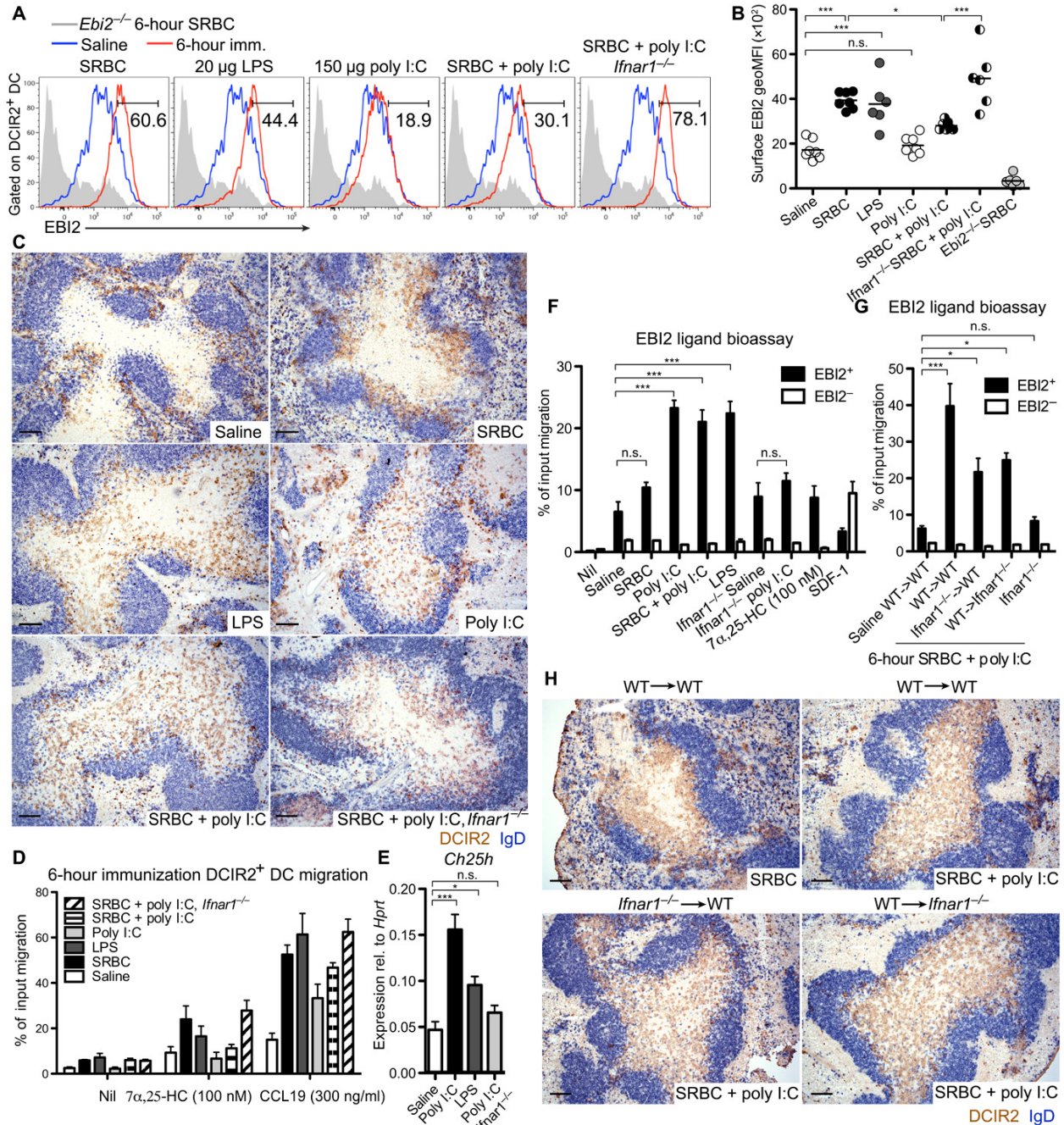


**Figure 6. Type I IFN suppresses EB12 up-regulation and disrupts outer T cell zone positioning of DCIR2<sup>+</sup> DCs.**

(A) Surface EB12 levels on DCIR2<sup>+</sup> DCs in WT or *Ifnar1*<sup>-/-</sup> mice 6 hours after treatment with the indicated stimuli (red), plotted alongside the same saline-treated (blue) or *Ebi2*<sup>-/-</sup> (gray) control. Numbers indicate gate for the immunized (imm.) condition. (B) Summary MFI data from data of the type in (A). (C) Distribution of DCIR2<sup>+</sup> DCs (brown) relative to B cells (blue) in the spleen of WT or *Ifnar1*<sup>-/-</sup> mice at 6 hours after immunization with the indicated stimuli. (D) Transwell migration of DCIR2<sup>+</sup> DCs from WT or *Ifnar1*<sup>-/-</sup> mice 6 hours after treatment with the indicated stimuli toward 7α,25-HC or CCL19. (E) Relative expression of *Ch25h* in total

spleen tissue 6 hours after the indicated immunization. **(F and G)** EBI2 ligand bioassay of spleen extracts from WT and *Ifnar1*<sup>-/-</sup> mice (F) or from WT→WT, *Ifnar1*<sup>-/-</sup>→WT, WT→*Ifnar1*<sup>-/-</sup> chimeric mice, and *Ifnar1*<sup>-/-</sup> nonchimeric mice (G) immunized as indicated. **(H)** Distribution of DCIR2<sup>+</sup> DCs (brown) in the spleens of mice in (G) 6 hours after immunization with the indicated stimuli. Data are representative of at least three mice per condition, and migration assay (D) contains data from two independent experiments. Scale bars, 100 μm. \**P* < 0.05; \*\*\**P* < 0.001; n.s., not significant (*P* > 0.05) by one-way ANOVA with Bonferroni's post hoc test for indicated comparisons.

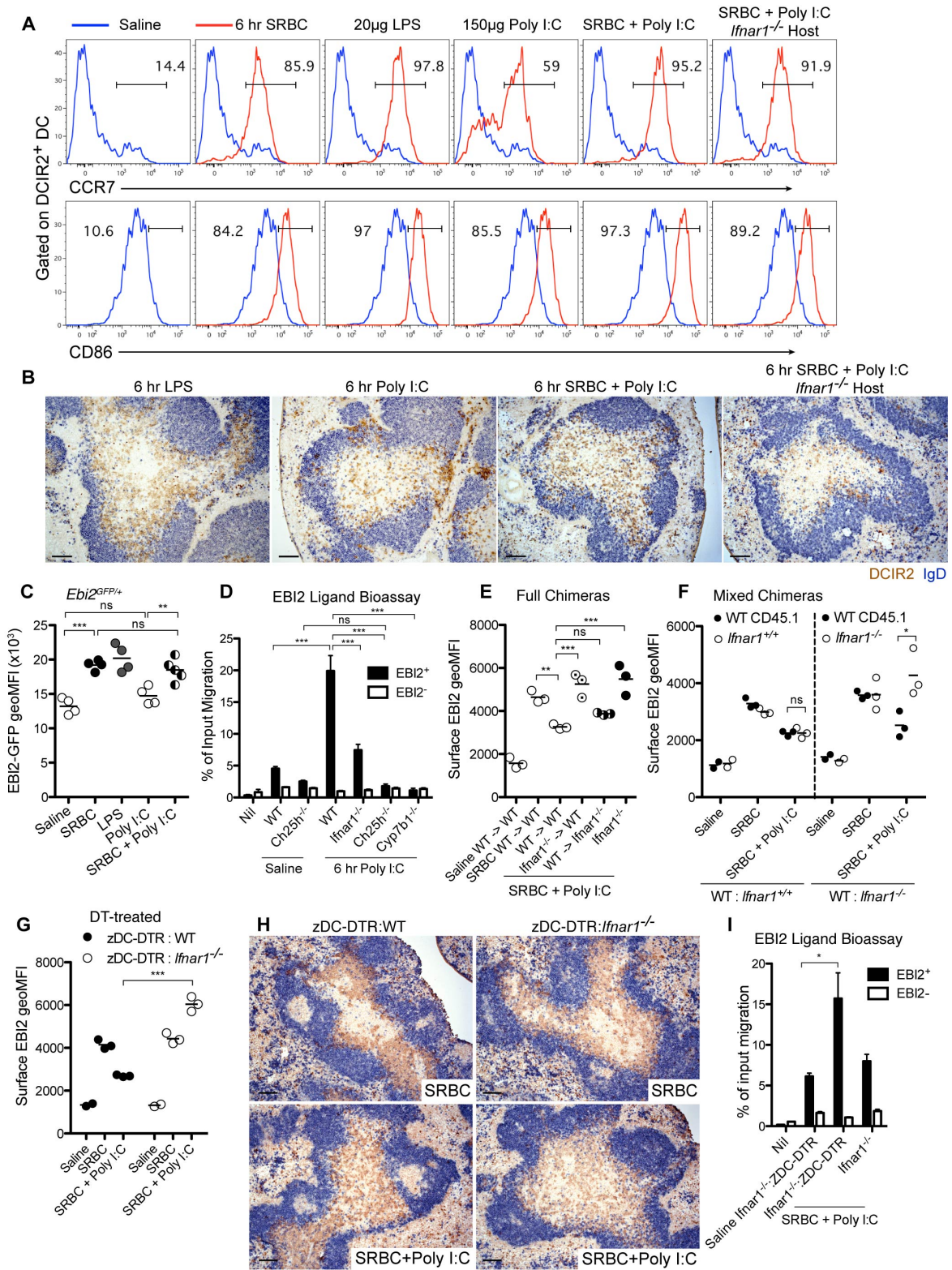


**Figure S8. Activation marker induction and positioning of DCIR2<sup>+</sup> DCs, and sites of type I IFN action in regulating EB12 expression and function.**

**(A)** CCR7 and CD86 expression on DCIR2<sup>+</sup> DCs 6 hr after immunization with the indicated stimuli. Each stimulus (red line) is plotted alongside the same saline condition (blue line) from the same experiment. Numbers in histograms represent % of cells in indicated gate for the immunized condition. **(B)** Additional examples of DCIR2<sup>+</sup> DC positioning 6 hr after LPS, poly I:C, SRBC plus poly I:C in WT mice, or SRBC plus poly I:C in IFNAR KO mice. **(C)** EBI2-GFP geometric MFI data on DCIR2<sup>+</sup> DCs from *Ebi2*<sup>gfp/+</sup> mice immunized as indicated for 6 hr. **(D)** EBI2 ligand bioassay of spleen extracts from WT, *Ifnar1*<sup>-/-</sup>, *Ch25h*<sup>-/-</sup>, or *Cyp7b1*<sup>-/-</sup> mice immunized as indicated for 6 hr. **(E-G)** EBI2 surface levels on DCIR2<sup>+</sup> DCs 6 hr after immunization with the indicated stimuli in full chimeric mice (E), mixed chimeric mice (F), or DT-ablated control (WT:zDC-DTR) or *Ifnar1*<sup>-/-</sup>:zDC-DTR mixed chimeric mice (G). **(H)** Distribution of DCIR2<sup>+</sup> DCs (brown) in the spleen of mice of the type in (G) at 6 hr after immunization with the indicated stimuli, relative to B cells (IgD, blue). **(I)** EBI2 ligand bioassay of spleen extracts from indicated mice of the type in E, 6 hr after immunization with SRBCs. Data are representative of 2 independent experiments (A-C) with at least 3 mice per group or of one experiment with at least 3 mice per condition (D-I), except for the saline condition (n=2) in (F, G). Each dot in graphs indicates an individual mouse and horizontal lines indicate means. Scale bar, 100μm. \*p < 0.05, \*\*p < 0.01, \*\*\*p < 0.001, 'ns' p > 0.05 by one-way ANOVA with Bonferroni's post hoc test for the indicated comparisons.

I IFN suppresses DCIR2<sup>+</sup> DC positioning in the outer T zone and suggest that this effect occurs, at least in part, because of disruption of EBI2 ligand gradients as a result of increased 7 $\alpha$ ,25-HC production by both hematopoietic and nonhematopoietic cells.

We note that LPS treatment caused a more diffuse distribution of DCIR2<sup>+</sup> DCs in the outer T cell zone than induction by SRBCs (**Fig. 6C** and fig. S8B). Similar to poly I:C, LPS caused an elevation of Ch25h mRNA and EBI2 ligand bioactivity in total spleen (**Fig. 6, E and F**). However, EBI2 surface levels appeared similar to those induced by SRBCs (**Fig. 6, A and B**). We rationalize that LPS treatment may lead to a smaller increase in EBI2 ligand abundance specifically in the T cell zone compared with that occurring after poly I:C treatment, and this only partially disrupts the EBI2-mediated navigation of activated DCs to this region.

#### **XCR1<sup>+</sup> DCs help establish EBI2 ligand gradients used by DCIR2<sup>+</sup> DCs**

During our characterization of DCIR2<sup>+</sup> DC positioning in response to the various stimuli, we observed that the T zone positioning of DCIR2<sup>+</sup> DCs correlated with a distinct positioning pattern of activated Batf3-dependent XCR1<sup>+</sup> DCs. XCR1 is expressed by ~85% of splenic CD8 $\alpha$ <sup>+</sup> DCs, and these cells are localized in the T cell zone, MZ, and RP in naïve mice (Alexandre et al., 2016; Bachem et al., 2012; Calabro et al., 2016; Dorner et al., 2009; Yamazaki et al., 2013). These DCs up-regulated CCR7 and CD86 but not EBI2 within 6 hours of SRBC immunization (**Fig. 7A** and fig. S9, A and B) and redistributed from MZ and RP locations into the central T cell zone (**Fig. 7B** and fig. S9C). In this location, the XCR1<sup>+</sup> DCs were surrounded by DCIR2<sup>+</sup>DCs in the outer T cell zone (**Fig. 7B** and fig. S9C). In vivo pulse labeling of blood-exposed cells by intravenous injection of phycoerythrin (PE)-labeled antibody (Cinamon et al., 2007) showed that SRBC immunization caused redistribution of many DCIR2<sup>+</sup> and XCR1<sup>+</sup> DCs from a highly blood-exposed location (likely corresponding to the RP, MZ, and bridging

channels) to a more secluded location, consistent with relocation into the white pulp (**Fig. 7C**). Redistribution of DCIR2<sup>+</sup> and XCR1<sup>+</sup> DCs into the white pulp could also be detected by in vivo CD45-PE labeling after immunization with LPS or poly I:C (fig. S9D).

The dichotomous relationship between XCR1<sup>+</sup> and DCIR2<sup>+</sup> DC positioning after activation, together with our earlier observation that CD8α<sup>+</sup> DCs highly express the oxysterol-metabolizing enzyme Hsd3b7 [confirmed here for cells from naïve and SRBC-immunized mice (fig. S9E)] (Yi et al., 2012), led us to test whether XCR1<sup>+</sup> DCs had a role in determining the distribution of DCIR2<sup>+</sup> DCs. SRBC immunization of Batf3 KO mice, which are deficient in XCR1<sup>+</sup> DCs (Durai and Murphy, 2016), resulted in the inability of DCIR2<sup>+</sup> DCs to position in the outer T cell zone (**Fig. 7D** and fig. S9F). Analysis of mice lacking Hsd3b7 specifically in hematopoietic cells revealed a defect in activated DCIR2<sup>+</sup> DC positioning in the outer T cell zone (**Fig. 7E**), consistent with a requirement for Hsd3b7 in DCs. To test whether this requirement was within Batf3-dependent cells, we examined BM chimeric mice where only the Batf3-dependent DCs were fully Hsd3b7-deficient and also observed that activated DCIR2<sup>+</sup> DCs failed to accumulate in the outer T cell zone (**Fig. 7F**). These observations provide evidence that XCR1<sup>+</sup> DCs can promote EBI2 ligand turnover and thereby help establish EBI2 ligand gradients needed for activated DCIR2<sup>+</sup> DC positioning. This property of XCR1<sup>+</sup> DCs may be modulated under some conditions because poly I:C treatment down-regulated *Hsd3b7* while up-regulating *Ch25h* and *Cyp7b1* in these cells (fig. S9E).

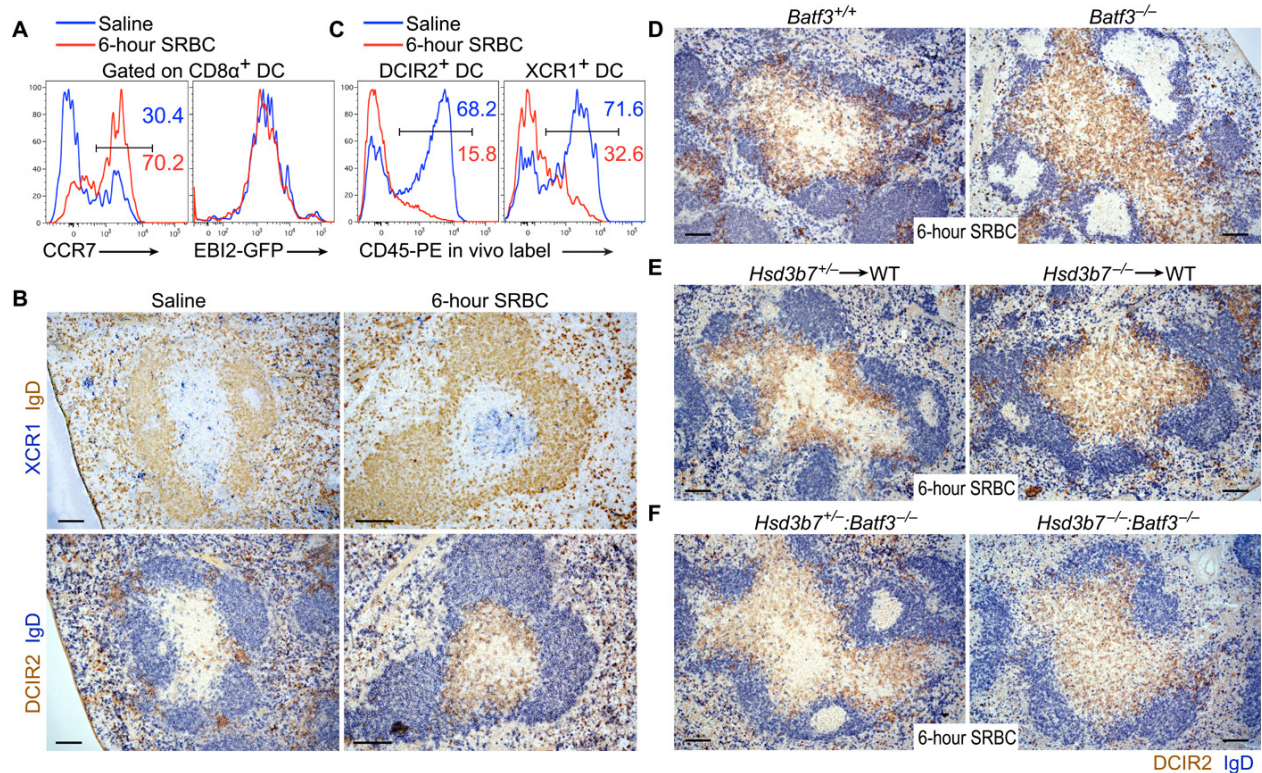


**Figure 7. Hsd3b7-expressing Batf3-dependent DCs are required for outer T cell zone positioning of activated DCIR2 $^+$  DCs.**

(A) CCR7 and EB12-GFP expression in CD8 $\alpha^+$  DCs 6 hours after intravenous immunization with saline or SRBCs. (B) Serial spleen sections from saline or 6-hour SRBC-treated mice stained for XCR1 (upper, blue) or DCIR2 (lower, brown) and IgD (upper, brown; lower, blue). (C) In vivo PE labeling on DCIR2 $^+$  (left) or XCR1 $^+$  (right) DCs in either saline-treated (blue line) or SRBC-treated (red line) mice injected with 1  $\mu$ g of anti-CD45-PE for 5 min. (D to F) Positioning of DCIR2 $^+$  DCs in *Batf3* $^{-/-}$  and control mice (D), in mice lacking Hsd3b7 in BM-derived cells versus controls (E), or in *Batf3* $^{-/-}$ :*Hsd3b7* $^{-/-}$  mixed BM chimeric mice lacking Hsd3b7 in Batf3-dependent DCs versus controls (*Batf3* $^{-/-}$ :*Hsd3b7* $^{+/-}$  mixed BM chimeras) (F). Histograms and images are representative of at least three mice analyzed per condition. Scale bars, 100  $\mu$ m.

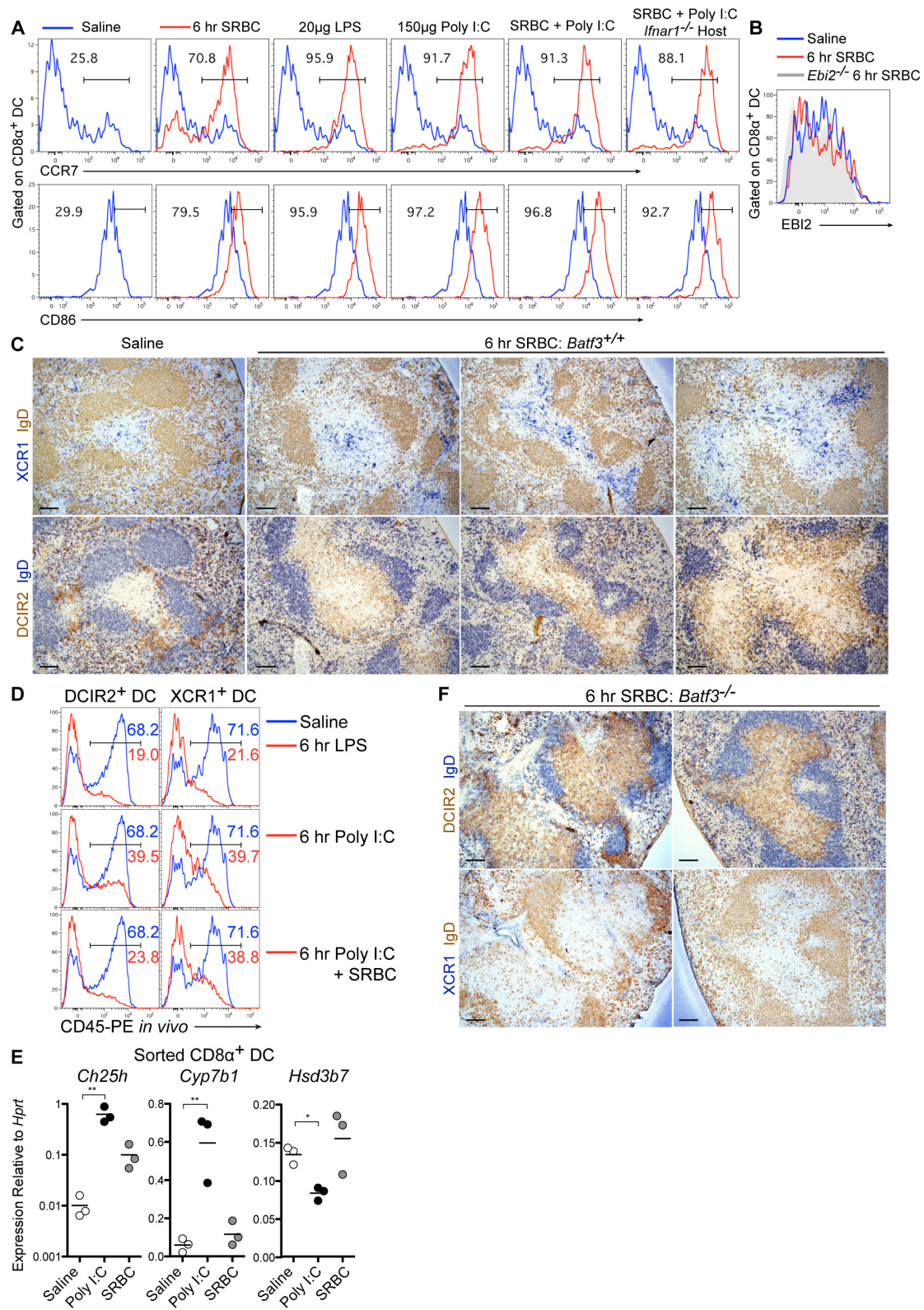


**Figure S9. Activation marker induction, positioning, *in vivo* PE labeling, and enzyme expression on XCR1<sup>+</sup> DCs.**

**(A)** CCR7 and CD86 expression on CD8 $\alpha$ <sup>+</sup> DCs 6 hr after immunization with the indicated stimuli. Each stimulus (red line) is plotted alongside the same saline condition (blue line) from the same experiment. Numbers in histograms represent % of cells in indicated gate for the immunized condition. **(B)** EBI2 surface staining on CD8 $\alpha$ <sup>+</sup> DCs after i.v. immunization with saline or SRBCs, plotted against EBI2 KO CD8 $\alpha$ <sup>+</sup> DCs as a staining control (grey fill). **(C)** Additional examples of XCR1<sup>+</sup> DC and DCIR2<sup>+</sup> DC positioning in serial sections 6 hr after saline or SRBC immunization of WT mice. Upper panels show positioning of DCIR2<sup>+</sup> DCs (brown) in spleen sections with respect to endogenous B cells (IgD, blue). Lower panels show positioning of XCR1<sup>+</sup> DCs (blue) in serial sections with respect to endogenous B cells (IgD, brown). **(D)** *In vivo* CD45-PE labeling of splenic DCIR2<sup>+</sup> DCs and XCR1<sup>+</sup> DCs 6 hr after immunization with indicated stimuli (red line). Each stimulus (red line) is plotted alongside the same saline condition (blue line) from the same experiment. This data was generated in the same experiment as shown in Figure 7C. Numbers in histograms represent percentage of cells in indicated gate. **(E)** Expression of *Ch25h*, *Cyp7b1*, and *Hsd3b7* by CD8 $\alpha$ <sup>+</sup> DCs 6 hr after the indicated immunization. **(F)** Serial sections of 6 hr immunized Batf3 KO mice stained as described in (C) for XCR1<sup>+</sup> DC and DCIR2<sup>+</sup> DC positioning. Data are representative of at least 3 mice per condition. Scale bar, 100 $\mu$ m. Each dot in graphs indicates an individual mouse and horizontal lines indicate means. \*p < 0.05, \*\*p < 0.01, 'ns' p > 0.05 by one-way ANOVA with Bonferroni's post hoc test for the indicated comparison (E).

## Discussion

This study identifies a role for Cyp27a1 in DC positioning and homeostasis and provides evidence that this activity occurs through synthesis of a second EBI2 ligand, 7 $\alpha$ ,27-HC. Cyp27a1 is expressed in lymphoid stromal cells, and we propose that the enzyme functions together with Ch25h to generate paired gradients of 7 $\alpha$ ,27-HC and 7 $\alpha$ ,25-HC that act combinatorially to control naïve (sentinel) cDC2 positioning (fig. S10). We further demonstrate that EBI2 is up-regulated along with CCR7 in activated cDC2s, and the associated increase in responsiveness to EBI2 ligands is necessary for DC positioning in the outer T cell zone to promote efficient induction of Tfh cells (fig. S10). Type I IFN negatively regulates DC outer T cell zone positioning, an influence that is likely to alter the types of T cell responses that are favored (fig. S11). Last, we provide evidence that Batf3-dependent DCs can act as an EBI2 ligand sink, an activity that appears necessary for correct localization of cDC2s under some activation conditions, revealing population-level coordination of cDC1 and cDC2 distribution in lymphoid tissues (fig. S11).

Cyp27a1 is expressed in the T cell zone and at lower levels in follicles, as well as in splenic MZ bridging channels. Several factors beyond Cyp27a1 expression are likely at play to shape the 7 $\alpha$ ,27-HC gradient. Cyp7b1 is required downstream of Cyp27a1 for 7 $\alpha$ ,27-HC synthesis, although our previous work suggests that the two enzymes would not need to be expressed in the same cells (Yi et al., 2012). A key factor in determining local 7 $\alpha$ ,27-HC concentrations may be the density of Cyp27a1- and Cyp7b1-coexpressing cells, or the proximity of cells expressing the individual enzymes. It is also possible that the amounts of Cyp27a1 and Cyp7b1 or their enzymatic activities are modulated posttranscriptionally. Tissue-wide

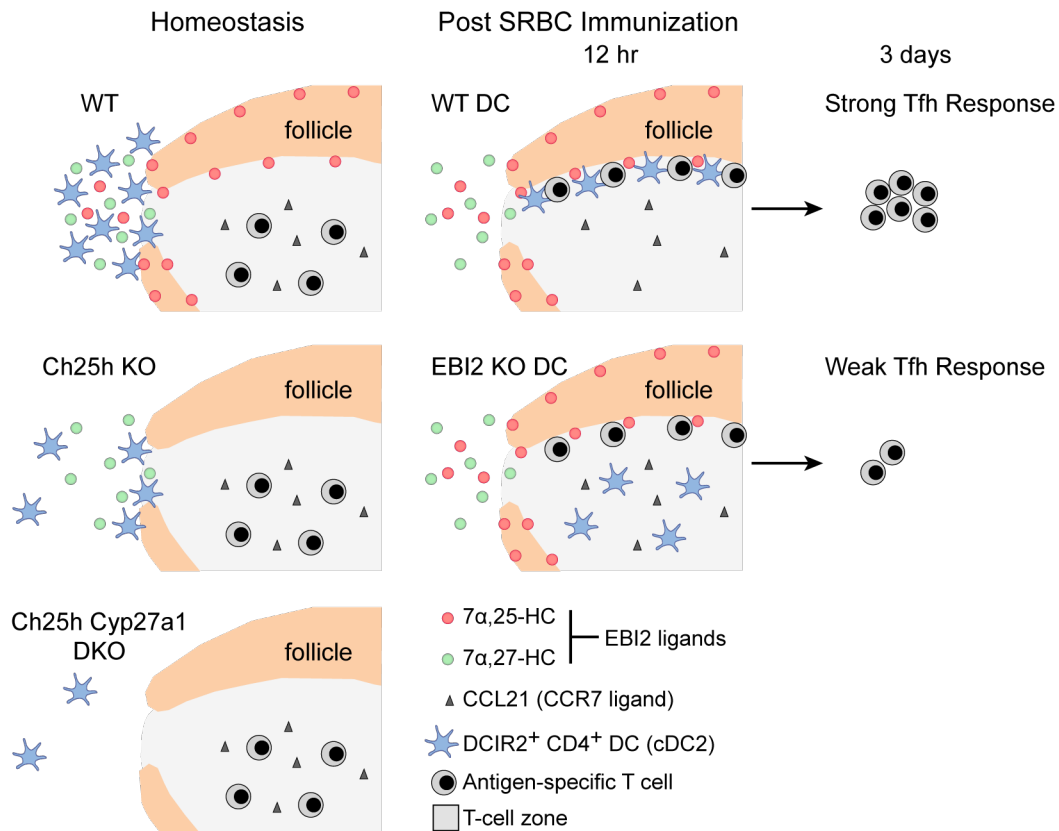


**Figure S10. Model for naïve and activated DCIR2<sup>+</sup> DC positioning.**

Under homeostatic conditions, DCIR2<sup>+</sup> DCs are localized primarily in marginal zone bridging channels. In these locations, *Ch25h* and *Cyp27a1* are expressed along with *Cyp7b1* to generate the oxysterols 7 $\alpha$ ,25-HC and 7 $\alpha$ ,27-HC, which act as ligands for EBI2 and attract DCIR2<sup>+</sup> DCs. In the absence of *Ch25h* and 7 $\alpha$ ,25-HC, 7 $\alpha$ ,27-HC is sufficient to promote positioning and homeostasis of some DCIR2<sup>+</sup> DCs. Mice lacking 7 $\alpha$ ,27-HC in addition to 7 $\alpha$ ,25-HC have a more severe DCIR2<sup>+</sup> DC deficiency, comparable to mice lacking EBI2.

After activation, DCIR2<sup>+</sup> DCs upregulate CCR7 to enter the CCL21-abundant T cell zone and require EBI2 and the oxysterol 7 $\alpha$ ,25-HC in order to position at the B-T zone interface. In the outer T cell zone, DCIR2<sup>+</sup> DCs can interact with early-activated T cells and promote Tfh cell differentiation. Disruption of EBI2-dependent outer T cell zone positioning of DCIR2<sup>+</sup> DCs results in impaired Tfh cell responses.

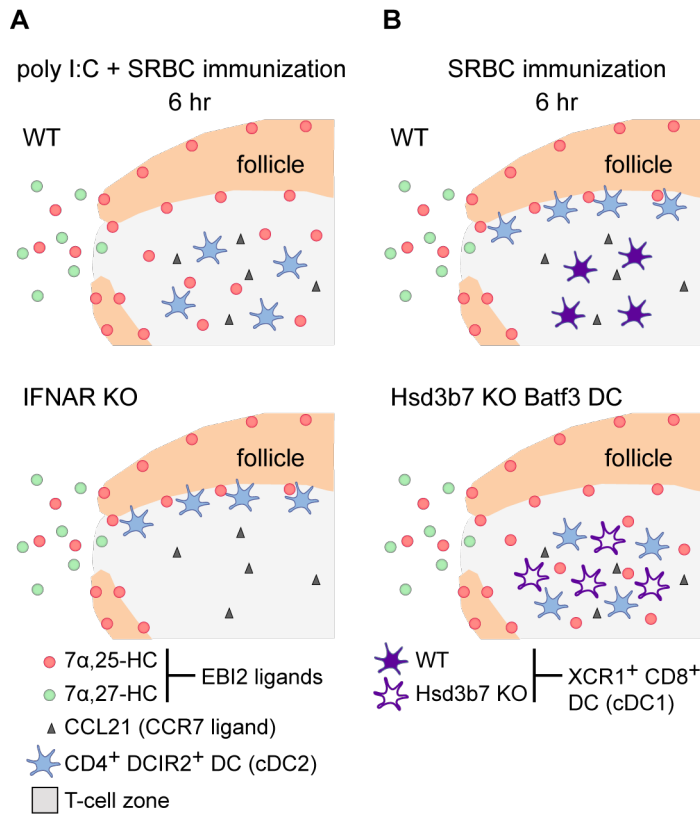


**Figure S11. Model for type I IFN and Batf3 DC effects on outer T-cell zone positioning of activated DCIR2<sup>+</sup> DCs.**

(A) Poly I:C increases  $7\alpha,25\text{-HC}$  production via induction of the enzyme Ch25h by type I IFN. Disruption of the EBI2 ligand gradient results in an inability of activated DCIR2<sup>+</sup> DCs to position preferentially in the outer T cell zone. IFNAR KO mice have an intact EBI2 ligand gradient after SRBC + poly I:C immunization and DCIR2<sup>+</sup> DCs can position in the outer T-cell zone in these mice. (B) *Hsd3b7*-expressing CD8 $\alpha^+$  DCs are necessary to promote outer T cell zone localization of DCIR2<sup>+</sup> DCs. Disruption of ligand gradient maintenance by removing *Hsd3b7* in CD8 $\alpha^+$  DCs results in loss of outer T cell zone positioning of DCIR2<sup>+</sup> DCs.

transcriptome analyses (e.g., **Biogps.org**) have shown that *Cyp27a1* and *Cyp7b1* are coexpressed in multiple tissues.  $7\alpha,27$ -HC may therefore be produced in a range of tissue types where the sterol could have actions, either together with or independently from  $7\alpha,25$ -HC, which influence the behavior of EBI2-expressing cells.

The expression pattern of *Ch25h* revealed by the RNAscope analyses agrees well with the distribution determined by less precise methods [laser capture microscopy and stromal cell sorting (Yi et al., 2012)] and demonstrates that this enzyme has a unique perifollicular expression pattern in the spleen. This pattern closely matches the established dependence of EBI2-mediated B cell positioning on *Ch25h* (Gatto and Brink, 2013; Yi et al., 2012) and is in accord with the EBI2 dependence of activated cDC2 positioning we describe here. The expression pattern in the outer follicle may correspond to marginal sinus–lining cells (Mueller and Germain, 2010), although definitive statements will require the development of procedures for combining RNAscope with markers specific for these cells. The stromal cells expressing *Ch25h* at the B-T zone interface do not match a well-defined subset and may represent an uncharacterized subtype of fibroblastic reticular cell.

Our finding that EBI2 is needed for controlling distinct positioning events of naïve and activated cDC2s represents a new example of cell positioning that is determined by cooperative or balanced responsiveness to multiple cues (Griffith et al., 2014). In naïve cDC2s where CCR7 expression is low, EBI2 likely guides the DCs to a position of high EBI2 ligand and low CCR7 ligand abundance (possibly cooperating with ligands for yet other receptors). In activated DCs, the increase in CCR7 makes the cells responsive to CCL21 and CCL19 that are abundant throughout the T cell zone, and EBI2 now cooperates with CCR7 to position the DCs in a zone where ligands for both receptors overlap, the outer T cell zone (fig. S10). The fact that

DCIR2<sup>+</sup>DC positioning in this location augments CD4<sup>+</sup> T cell responses is in agreement with the finding that activated CD4<sup>+</sup> T cells undergo extensive interactions with DCs, preferentially in this region (Li et al., 2016; Yi et al., 2015).

SRBCs have been shown to cause cDC2 activation because of missing self-CD47 recognition (Yi et al., 2015). The physiologically analogous mode of cDC2 activation has not yet been determined, but it is speculated that any circulating endogenous cells with reduced CD47 may engage this pathway. The similar cDC2 distribution after LPS treatment indicates that multiple modes of activation are likely to cause EBI2 up-regulation and outer T zone preference by cDC2s. However, pathogens that also strongly induce type I IFN (as modeled here using poly I:C) may disrupt DC EBI2 function in a cell-extrinsic manner, likely because of increased EBI2 ligand production (and possibly reduced degradation) by various cell types in the inner T cell zone. Our data also showed that type I IFN had a DC-intrinsic posttranscriptional effect on EBI2 surface levels. Although further work will be needed to determine whether this reflects effects on EBI2 translation, internalization, or turnover, the findings suggest that EBI2 surface levels cannot be taken as a simple correlate of extracellular EBI2 ligand abundance. Marked changes in the expression of homeostatic lymphoid tissue organizers (the chemokines CCL21, CCL19, and CXCL13) have been reported in various infection models (Mueller and Germain, 2010). It will be important in future studies to characterize how EBI2 expression and EBI2 ligand production are modulated in lymphoid tissues after various types of infection and to determine how this affects adaptive immune responses.

The finding that type I IFN antagonizes EBI2 function on activated cDC2s and favors their dispersal throughout the T cell zone raises questions about the different antigen-presenting roles of these DCs. Although they have been established to augment Tfh cell differentiation and

antibody responses (Durai and Murphy, 2016; Li et al., 2016; Shin et al., 2016), they also support IFN $\gamma$ -producing T cell responses (Neubert et al., 2014; Soares et al., 2007). Because type I IFN is most prominently induced during infections with intracellular pathogens, perhaps dispersal throughout the T cell zone allows the cDC2s to present antigen in a manner that more effectively induces a T helper 1 cell fate. In accord with this notion, cDC2s were shown to depend on interleukin-12 from cDC1s for induction of IFN $\gamma$ -producing cells (Soares et al., 2007). By up-regulating Ch25h expression, type I IFN increases not only EBI2 ligand but also 25-HC abundance (Cyster et al., 2014). Because 25-HC can have multiple actions on cells, including repression of cholesterol biosynthesis and antagonism of viral replication, it is possible that the actions of 7 $\alpha$ ,25-HC and 25-HC on DCs are coordinated to match the response to the type of invader.

Although some studies had suggested that CD8 $\alpha^+$  DCs may mostly be in the splenic T cell zone, other observations showed that they were more widely distributed (Idoyaga et al., 2009; McLellan et al., 2002; Qiu et al., 2009) and their presence in the RP and MZ, as well as in the T cell zone, was more clearly established using the XCR1 marker (Alexandre et al., 2016; Bachem et al., 2012; Calabro et al., 2016; Dorner et al., 2009; Yamazaki et al., 2013). These DCs move into the T cell zone after activation (Alexandre et al., 2016; Calabro et al., 2016; Qiu et al., 2009). Our finding that CD8 $\alpha^+$  DCs up-regulate CCR7 but not EBI2 under the activation conditions tested provides a possible explanation for why they were not enriched in the outer T cell zone. We establish that Batf3-dependent DCs help exclude EBI2<sup>hi</sup> DCIR2<sup>+</sup> DCs from the central T cell zone through their high expression of Hsd3b7 and presumed efficient metabolism of 7 $\alpha$ ,25-HC. We do not exclude the possibility that Hsd3b7-deficient Batf3-dependent DCs are altered in additional ways that affect T cell zone organization. Future work is also needed to

determine how much the cDC1 influence on cDC2 positioning affects T cell responses to various immunogens. The cross-talk between DC populations that we describe here likely represents an example of a broader set of population-level interplays that help fine-tune tissue reorganization events during the immune response.

## Materials and Methods

### Study design

The aim of this study was to characterize the oxysterol requirements for EB12-dependent positioning of naïve and activated DCs in lymphoid tissues and to assess how this positioning affects Tfh cell responses. Most of the experiments consisted of enumeration of population frequencies by flow cytometry, assessment of cell or enzyme distribution using immunohistochemistry, quantitation of EB12 ligand abundance using bioassay, and testing Tfh cell responses via adoptive transfer of antigen-specific T or B cells. Littermate comparisons were used for all mouse studies unless otherwise indicated. Control and experimental treatments were administered to age- and sex-matched mice. The investigators were not blinded. Experimental replication is indicated in the figure legends.

### Animals

C57BL/6NCr (code 556) and B6-Ly5.1/Cr (code 564) mice of 6 weeks of age were purchased from the National Cancer Institute (NCI) at Charles River (CRV). *Cyp27a1*<sup>-/-</sup>, *Batf3*<sup>-/-</sup>, *Ifnar1*<sup>-/-</sup>, Zbtb46-DTR (zDC-DTR) and OVA-specific OTII TCR-transgenic mice were purchased from Jackson Laboratories. *Ebi2*<sup>-/-</sup>, *Cyp7b1*<sup>-/-</sup>, *Ch25h*<sup>-/-</sup>, *Hsd3b7*<sup>-/-</sup>, and HEL-specific Hy10 knock-in mice have been described ((Pereira et al., 2009; Yi et al., 2012) and references therein). To generate BM chimeras, mice were lethally irradiated by exposure to 900-1100 rads of  $\gamma$ -irradiation in two doses 3 hr apart followed by injection of donor BM ( $5 \times 10^6$  cells). Chimeric mice were analyzed 6-10 weeks after reconstitution. Where indicated, adult mice or chimeric mice were fed rodent diet supplemented with 0.5% cholic acid (TD.04046, Envigo) for at least two weeks prior to analysis. Animals were housed in a pathogen-free environment in the Laboratory Animal Research Center at the University of California, San Francisco, and all

experiments conformed to ethical principles and guidelines approved by the Institutional Animal Care and Use Committee.

### **Immunizations and adoptive transfer**

For 6-hour immunizations,  $2 \times 10^8$  SRBCs (Colorado Serum Company), 20  $\mu\text{g}$  of LPS (0111:B4, Sigma), 150  $\mu\text{g}$  of poly I:C (GE Healthcare), or saline was injected retro-orbitally into mice. For immunization of mice with both SRBC and poly I:C, SRBCs were resuspended directly in corresponding doses of poly I:C.

For analysis of  $\text{CD4}^+$  T cell responses, pooled spleen and LN cells containing  $10^6 \text{CD45.1}^+ \text{CD4}^+ \text{V}\alpha 2^+$  OTII were adoptively transferred into mice. For analysis of B cell responses, spleen cells containing  $10^5$  HEL-binding Hy10 B cells and  $10^4$  OTII T cells were cotransferred. One day after cell transfer, recipients were immunized intraperitoneally with HEL-OVA conjugated to SRBCs (SRBC-HEL-OVA;  $2 \times 10^8$  cells).

### **RNAscope *in situ* hybridization**

RNA *in situ* hybridization was performed using the RNAscope RED 2.5HD manual assay kit (Advanced Cell Diagnostics) (Wang et al., 2012). Using this kit was necessary because we could not detect signal using digoxigenin-labeled probes and conventional *in situ* hybridization. The RNAscope probes used were: Ch25h (NM\_009890.1, targeting bp 115-1240), Cyp27a1 (NM\_024264.5, targeting bp 555-1440), Cyp7b1 (NM\_007825.4, targeting bp 179-1182), and Hsd3b7 (NM\_133943.2, targeting bp 330-1192). Tissues were frozen in OCT and stored at  $-80^\circ\text{C}$ . Within 24 hr of freezing, cryosections of 14  $\mu\text{m}$  were cut and slides were dried at  $-20^\circ\text{C}$  for 1 hr and at  $-80^\circ\text{C}$  for 30 min. Slides were fixed for 15 min with ice-cold 4% paraformaldehyde and washed in 50%, 70%, and 100% ethanol for 5 min each. After drying for

5 min, slides were treated with hydrogen peroxide (from kit) for 8 min and protease IV (from kit) for 15 min. Probes were allowed to hybridize in a humidified chamber at 40°C for 3.5 hr. The following incubation times for the amplification steps were used: Amp 1, 40 min; Amp 2, 25 min; Amp 3, 40 min; Amp 4, 25 min; Amp 5, 40 min; Amp 6, 25 min. Slides were then developed with FastRed (from kit) for 20 minutes, washed in PBS, and counterstained for IgD using goat anti-mouse IgD (Cedarlane Laboratories) and HRP-conjugated donkey anti-goat IgG (Jackson Immunoresearch).

### **Conjugation of HEL-OVA to SRBCs**

For SRBC-HEL-OVA conjugation, OVA protein (Sigma-Aldrich) was first cross-linked to HEL using glutaraldehyde. This HEL-OVA conjugate was further conjugated to SRBCs. 1 ml of SRBCs was washed with PBS three times and resuspended in 1mL of conjugation buffer (0.35 M mannitol & 0.01 M NaCl). 50µg of HEL-OVA was mixed with the SRBCs for 10 min and crosslinked using 100µL of 100 mg/ml EDCI (1-ethyl-3-(3-dimethylaminopropyl) carbodiimide, Fisher) for 30 minutes at 4°C while rocking. This was followed by three washes in PBS to remove free protein. Conjugation was confirmed by flow cytometry by staining the SRBCs with HyHEL9 mAb. This produces 8 doses of SRBC-conjugates and was scaled according to the number of mice requiring immunization. To visualize cell proliferation, OTII cells were labeled with 5µM CFSE (Invitrogen) for 10 min at 37°C in PBS with 1% FBS prior to transfer.

### **Dendritic Cell Ablation**

For DC ablation in zDC-DTR:EBI2 mixed BM chimeras, mice were injected i.v. with 20ng/g of diphtheria toxin (DT) (Sigma-Aldrich) 2 days before cell transfer of antigen specific B and/or T cells. These mice also received 2ng/g DT i.p. on the day of cell transfer as well as 1

day, 2 days, and 4 days after immunization to maintain ablation. DC ablation in zDC-DTR:IFNAR mixed chimeras and full zDC-DTR chimeras was performed using an initial injection of 20ng/g DT 4 days before analysis and a second injection of 4ng/g DT 2 days before analysis.

### **EBI2 Antagonist Treatment**

EBI2 antagonist (NIBR189, Avanti Polar Lipids (Gessier et al., 2014)) was administered retro-orbitally 30 min before and 3 hr after immunization with SRBCs (1.5mg/kg/dose). Mice were analyzed 6 hr after immunization for DC positioning. Each dose of antagonist was prepared by diluting a 10mg/mL stock solution into 50µl of saline. Control mice were given equivalent injections of vehicle (N-Methyl-2-pyrrolidone, NMP) diluted in 50µl of saline.

### ***In vivo* labeling of dendritic cells**

*In vivo* labeling of blood-exposed DCs was performed as described (Cinamon et al., 2007) with minor modifications. Mice were injected retro-orbitally with 1 µg PE-conjugated anti-CD45.2 (clone 104, Biolegend) diluted in 100µL of saline, 5 min before sacrifice. Spleens were digested for 10 minutes at 37°C, mashed through a 70µm filter and processed for flow cytometric analysis.

### **Flow cytometry and cell sorting**

For EBI2 surface staining, cells were incubated with 4% normal mouse serum (NMS) and 4% normal donkey serum (NDS) for 10 min on ice, a 1:20 dilution of goat polyclonal antibody against EBI2 (A-20, Santa Cruz Biotechnology) for 1 hr at RT, a 1:200 dilution of biotin-conjugated donkey anti-goat IgG (Jackson ImmunoResearch) for 30 min on ice, and a 1:200 dilution of PE-conjugated streptavidin (BD Biosciences) for 25 min on ice. Staining for CCR7

was performed using biotin-conjugated anti-CCR7 (4B12, Biolegend) at a dilution of 1:50 for 30 min at RT, followed by 1:200 PE-conjugated streptavidin. OTII-derived Tfh cell staining was performed using a 1:100 dilution of BV605-conjugated anti-CXCR5 (L138D7, Biolegend) for 1 hr at RT, followed by PE-conjugated anti-PD-1 (29F.1A12, Biolegend), PE-Cy7-conjugated anti-CD4 (RM4-5, Biolegend), Percp-Cy5.5-conjugated TCR V $\alpha$ 2 (B20.1, Biolegend), and APC-conjugated CD45.1 (A20, Biolegend) for 20 min on ice. Staining of Hy10-derived GCB cells was performed using HEL conjugated to A647, PE-Cy7-conjugated anti-CD95 (Jo2, BD Biosciences), Pacific Blue-conjugated anti-GL7 (GL7, Biolegend), Percp-Cy5.5-conjugated anti-B220 (RA3-6B2, Tonbo Biosciences), and BV605-conjugated CD45.1 (A20, Biolegend). Staining of DCs was performed using Alexa 647-conjugated anti-DCIR2 (33D1, Biolegend), PE-Cy7-conjugated anti-CD11c (N418, Tonbo Biosciences), FITC-conjugated anti-I-A<sup>b</sup> (AF6-120.1, BD Biosciences), Pacific Blue-conjugated anti-CD8 $\alpha$  (53-6.7, Biolegend), and PerCP-Cy5.5-conjugated anti-B220 (RA3-6B2, Tonbo Biosciences) to exclude B cells. Spleens (cut into 6-7 pieces) and mesenteric LNs were digested in RPMI 1640 media supplemented with 2% fetal bovine serum, 10mM HEPES, 1mg/mL collagenase type IV (Worthington Biochemical), and 20ug/mL DNase I (Sigma), for 15 min in a 37°C incubator while rotating. After digestion, cells were isolated by mashing through a 70  $\mu$ m cell strainer. DCs were stained in PBS containing 2% FBS and 0.1% sodium azide without EDTA. EDTA-free staining buffer is required since binding of anti-DCIR2 clone 33D1 is cation dependent. For sorting of DCs, DCs were first pre-enriched using anti-CD11c microbeads (Miltenyi Biotec) and sorted on a BD FACS Aria III. See Fig. S12 for sort gating strategy and purity. Flow cytometry data were analyzed using Flowjo (ver 9.7.6). Histograms for EBI2 and CCR7 surface levels were plotted using biexponential display.

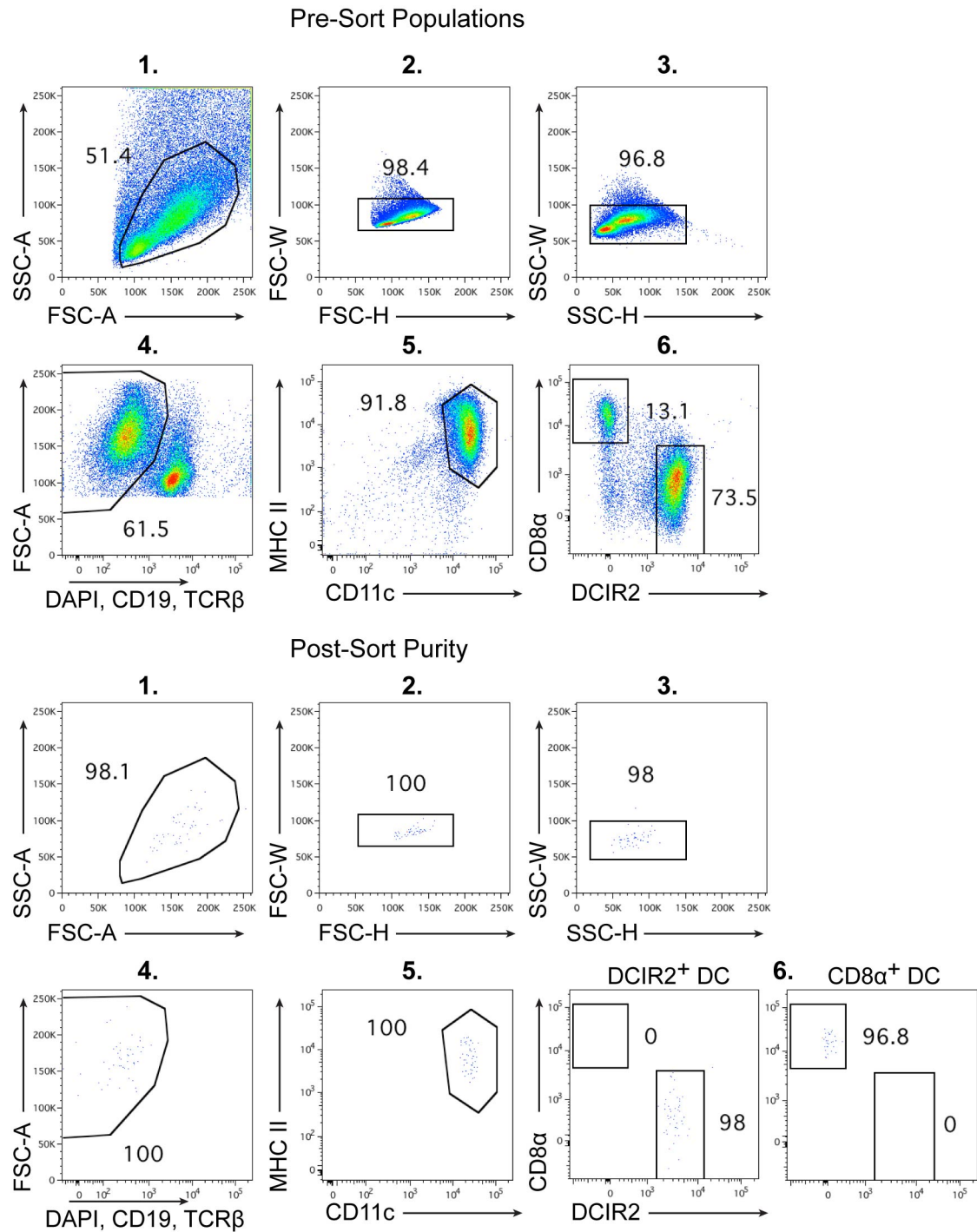


**Figure S12. Sort gating strategy and purity of sorted splenic DCs.**

Splenocytes were pre-enriched for DCs on a MACS LS column using anti-CD11c MACS beads and sorted for DCIR2<sup>+</sup> or CD8α<sup>+</sup> DCs using the indicated gating strategy. Consecutive gates are indicated by number. Representative example of post-sort purity for both DCIR2<sup>+</sup> and CD8α<sup>+</sup> DCs is shown in the lower panels.

## **Immunohistochemistry**

Tissues were frozen in OCT. Cryosections of 7 $\mu$ m were dried for 1 hr at -20°C, fixed in 4°C acetone for 10 min, and dried for 1 hr at RT. For staining of DCIR2<sup>+</sup> DCs, a 1:100 dilution of biotin-conjugated anti-DCIR2 (33D1, Biolegend) and a 1:100 dilution of goat anti-mouse IgD (GAM/IGD(FC)/7S, Cedarlane Laboratories) along with 1% NMS and NDS was incubated with the slides overnight at 4°C. Next, a tyramide signal amplification kit was used (TSA Biotin System; Perkin Elmer), in which the sections were first stained with streptavidin-HRP (1:100 dilution, Jackson Immunoresearch) for 45 min at RT, washed, then incubated with tyramide (1:50 dilution) for 4 min at RT. This was followed by staining with AP-conjugated donkey anti-goat IgG (1:100 dilution, Jackson Immunoresearch) and HRP-conjugated streptavidin (1:100 dilution, from TSA kit) for 2 hours at RT. Staining for XCR1 did not require signal amplification and was performed using biotin-conjugated anti-XCR1 (1:100 dilution, clone ZET) and AP-conjugated streptavidin (Jackson Immunoresearch). For immunofluorescence, slides were prepared for DCIR2<sup>+</sup> DC staining as described above with the addition of anti-mouse CD45.1-FITC (clone A20, biolegend), followed by AMCA-conjugated donkey anti-goat IgG (Jackson Immunoresearch), Alexa 488-conjugated donkey anti-FITC and Alexa 647-conjugated streptavidin (Invitrogen). Images were captured with a Zeiss AxioObserver Z1 microscope.

## **Quantification of IHC images**

Images of immunohistochemical stains of DCIR2<sup>+</sup> DC positioning were quantified using ImageJ (version 1.49). All images were captured at the same magnification using a Zeiss AxioObserver Z1 inverted microscope. Images were loaded into ImageJ and the freehand selection tool was used to outline the B-T zone interface. This selection was scaled to 60% of its size, centered, and saved in the ImageJ ROI manager. The outer T cell zone area was defined as

the area between this scaled selection and original B-T zone interface. The ImageJ IHC Image Analysis Toolbox was then used to isolate DCIR2<sup>+</sup> staining and create a binary black and white image (DCIR2<sup>+</sup> staining in black). The total amount of DCIR2<sup>+</sup> staining (total amount of black pixels) was quantified. Then, the previously defined selection from the ROI manager was applied to this binary image, and the black pixels within the selection (the “inner T-cell zone”) were erased. The total amount of remaining black pixels (in the “outer T-cell zone”) was quantified, and the proportion of DCIR2<sup>+</sup> staining in the outer T-cell zone was calculated. See Suppl. Fig. S6C for an example.

### **Transwell migration assay and M12 EBI2 ligand Bioassay**

For splenic DC migration assays, spleens were digested for 10 min in a 37°C incubator using 1mg/mL collagenase type IV (Worthington Biochemical; Lakewood, NJ) and 20µg/mL DNase I (Sigma) in migration media (RPMI 1640 containing 0.5% fatty acid free BSA and 10mM HEPES) and mashed through a 70µm filter. The cells were RBC-lysed, washed, and resensitized in migration assay media at 37°C for 20 min. 10<sup>6</sup> cells were placed into 5 µm transwell filters (Corning Costar), allowed to migrate for 3 hr at 37°C, and migrated cells were enumerated by flow cytometry. 7α,25-HC and 7α,27-HC was purchased from Avanti Polar Lipids and reconstituted as a 10mM solution in DMSO. For bioassays, spleen extracts were prepared by mashing spleens into migration media (1:10, weight by volume) through a 70µm filter and centrifuging at 500g and 4000g for 10 minutes to remove cells. Extracts were frozen at -80°C and re-centrifuged at 4000g prior to use. All extracts were further diluted 1:20 for use in transwell migration assays. EBI2-transduced M12 cells were grown to confluency in T75 flasks, washed three times in migration media, and resensitized for 20 min at 37°C in migration media prior to use in migration assays. 5x10<sup>5</sup> M12 cells were added to each transwell and allowed to

migrate for 3 hr towards spleen extracts. Data are shown as % of input cells that migrated. For spleen extract data, each mouse was plotted as a mean of technical duplicate.

### **EBI2 Receptor Internalization Assay**

Splenocytes were prepared as for migration assay. A titration of 7 $\alpha$ ,25-HC and 7 $\alpha$ ,27-HC in migration medium was prepared in a 96-well round bottom plate, with each well receiving 10  $\mu$ l of oxysterol. 90  $\mu$ l of cells (10<sup>6</sup> cells total) were added by multichannel to the 96-well plate and the plate was immediately placed in a 37°C incubator for 30 min. Afterwards, the plate was placed on ice and cells were washed three times before staining for EBI2 surface levels.

### **Retroviral transduction of T cells**

T cells were enriched from spleen and LNs of wild type mice using MACS manual cell separation LS columns (Miltenyi Biotec). Enrichment was performed by negative selection using biotin-conjugated anti-B220 and streptavidin-conjugated-MACS beads. T cells were cultured in 24 well plates (10<sup>6</sup> cells/2ml/well) and activated using a final concentration of 3 $\mu$ g/ml anti-CD3 $\epsilon$  (LEAF clone 2C11, Biolegend) and 1 $\mu$ g/ml anti-CD28 (LEAF clone 37.51, Biolegend) diluted in RPMI 1640 containing 10% FBS, 10mM HEPES, 55 $\mu$ M 2-mercaptoethanol, 2mM glutamine, and 50 IU penicillin/streptomycin. 24 hr after activation, the plate was centrifuged and the culture supernatant was saved. Retrovirus encoding a MSCV-EBI2-IRES-hCD4 plasmid (Pereira et al., 2009) or control plasmid (truncated nerve growth factor receptor, NGFR) was produced using the PLAT-E packaging cell line (Morita et al., 2000) and added to the activated T cells. The T cells were spininfected at 2400rpm for 2 hr at RT, the viral supernatant was aspirated, and the original culture supernatant was returned to the cells. This spininfection was repeated a second time 24 hr later. 24 hr after the second spininfection, cells were washed twice and adoptively

transferred into mice. Positioning of transduced T cells was analyzed 16-24 hr later in tissue sections by staining for hCD4.

### **Quantitative RT-PCR**

Total RNA from tissues or sorted cells was extracted using an RNeasy kit (Qiagen) and reverse-transcribed. Quantitative PCR was performed as described (Yi et al., 2012). Data were analyzed using the comparative CT ( $2^{-\Delta\Delta Ct}$ ) method using *Hprt* as the reference.

### **LC-MS/MS**

Spleen extracts were prepared as for the M12 bioassay. 10-12 spleen extracts from WT or *Cyp27a1*<sup>-/-</sup> mice were pooled per sample. *Hsd3b7*<sup>-/-</sup> spleen extracts were generated from single mice. The entire volume of spleen extract for each sample was extracted for LC-MS/MS analysis. 7 $\alpha$ ,27-HC was quantitated using a SCIEX API 5000 mass spectrometer coupled to a Shimadzu LC-20XR high performance liquid chromatograph as previously described (McDonald et al., 2012). The measured amount of 7 $\alpha$ ,27-HC for each sample was divided by the total mg of spleen tissue used to generate the extract in order to determine ng per mg of spleen tissue.

### **Statistical analysis**

Prism software (GraphPad, ver. 5.0a) was used for all statistical analyses. Two-tailed, unpaired Student's *t* tests were performed when comparing only two groups, and one-way analysis of variance (ANOVA) using Bonferroni's post hoc test for the indicated comparisons was performed when comparing one variable across multiple groups. *P* values less than 0.05 were considered significant. In summary graphs, points indicate individual mice, and horizontal lines indicate means. In bar graphs, bars indicate means, and error bars indicate SEM.

## Acknowledgments

We thank J. An and Y. Xu for expert technical assistance, B. M. Thompson and K. M. Eckert for technical assistance with LC-MS/MS, D. Russell for enzyme-deficient mice and Cyp27a1 antisera, T. Yi and J. Muppidi for helpful discussions, and L. Rodda and J. Wu for critical reading of the manuscript. **Funding:** E.L. was supported by the University of California San Francisco (UCSF) Biomedical Sciences Graduate Program and NSF grant 1144247. E.V.D. was supported by the UCSF Medical Scientist Training Program and NIH F30 grant F30AI120527. J.G.C. is an investigator of the Howard Hughes Medical Institute. This work was supported in part by NIH grant AI040098, and the mass spectrometry work was supported by grant HL20948. **Author contributions:** E.L. and J.G.C. designed the study, analyzed the data, and wrote the paper. E.L. performed the experiments. E.V.D. performed the initial experiments identifying the DC defect in Cyp27a1 single-KO mice on control diet and edited the paper. J.G.M. provided LC-MS/MS data for  $7\alpha,27$ -HC in pooled spleen extracts. E.L. performed the statistical analysis. **Competing interests:** The authors declare that they have no competing interests.

## **CHAPTER 3**

### **Conclusions and Discussion**

## **Distinct oxysterol gradients guide naïve and activated cDC2 positioning**

The work in this dissertation defines the oxysterol gradients required for EBI2-dependent positioning of naïve and activated dendritic cells in the spleen. We show that Cyp27a1 contributes to the production of a second EBI2 ligand, 7 $\alpha$ ,27-HC, and can support cDC2 positioning and homeostasis in mice lacking Ch25h. Under naïve conditions, we propose that a dual gradient of 7 $\alpha$ ,25-HC and 7 $\alpha$ ,27-HC operates to promote positioning of cDC2s in marginal zone bridging channel locations. We also identify the spatial expression pattern of oxysterol generating enzymes in the spleen, finding that Cyp27a1, Cyp7b1, and Ch25h are expressed by stromal cells in bridging channel locations. Cyp7b1 and Ch25h were also found to be expressed in peri-follicular locations and at the B-T interface.

Furthermore, we discover that EBI2 is rapidly upregulated by cDC2s following activation by SRBCs and LPS and promotes the positioning of these cells at the B-T interface in response to 7 $\alpha$ ,25-HC. Loss of EBI2 in cDC2s results in the inability of these cells to position at the B-T interface after activation, and also results in diminished Tfh cell and GC B cell responses. We find that different innate stimuli uniquely modulate EBI2 levels in cDC2s, and that type I IFN suppresses EBI2 upregulation and outer T zone positioning. We speculate that different innate stimuli lead to different T cell activating roles for DCs. Finally, we provide evidence that Batf3-dependent DCs promote outer T zone positioning of DCIR2<sup>+</sup> DCs by metabolizing oxysterols in the center of the T zone using Hsd3b7.

There are many future directions and questions that arise from this study, which I will discuss below.

## **Oxysterol gradients in peripheral tissues and lymph nodes**

EBI2 has been shown to play roles in tissues aside from the spleen, including lymph nodes (Li et al., 2016), bone marrow (Nevius et al., 2015), the thymus (Ki et al., 2017), and the gut (Chu et al., 2018; Emgård et al., 2018). Cells expressing high levels of EBI2 were also identified via histology in the pancreas, liver, kidney, and heart (Heinig et al., 2010). Defining the oxysterol gradients in lymph nodes and peripheral tissues will be important to understand how EBI2-dependent functions are supported in these locations.

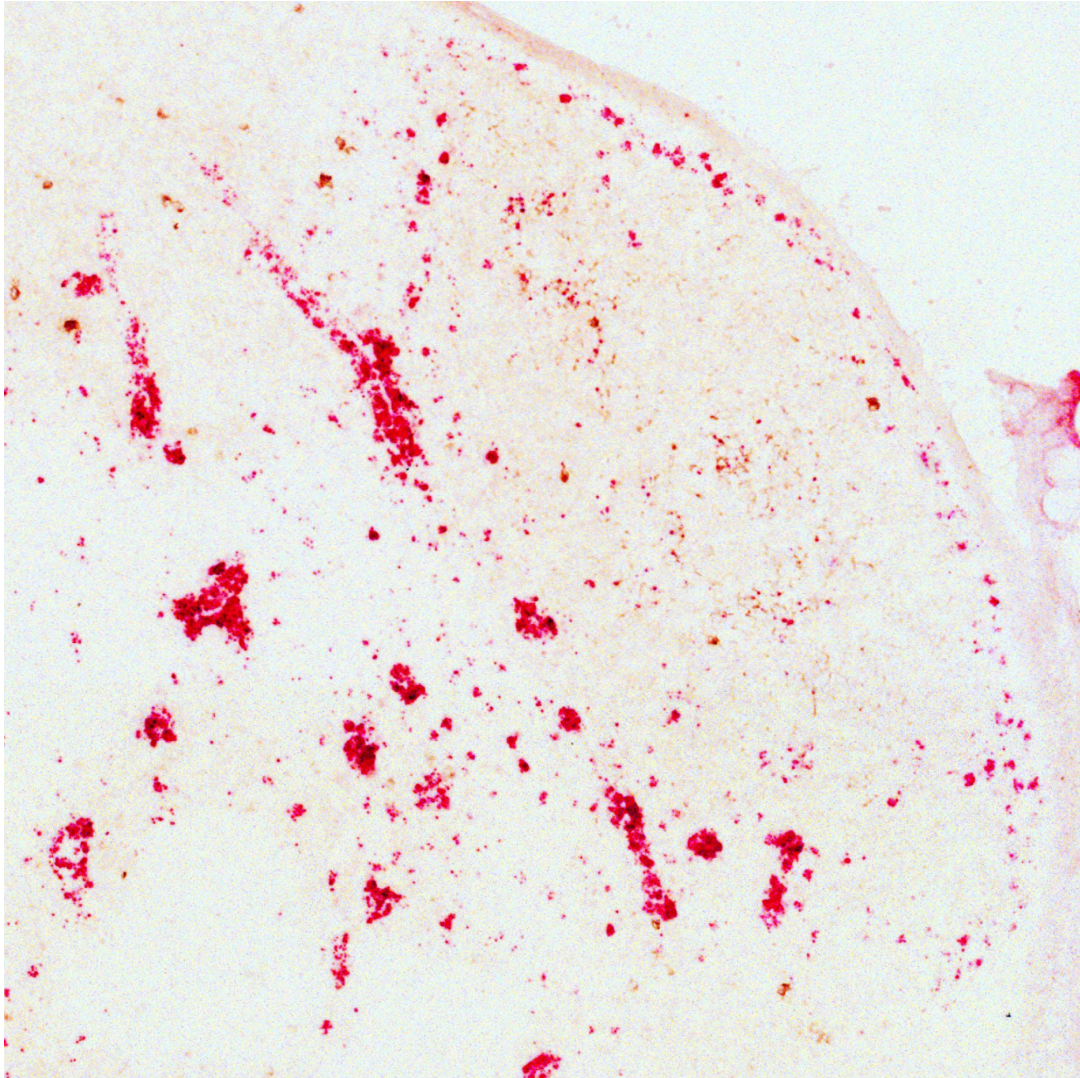
Two recent studies described a role for EBI2 in promoting ILC3 positioning and accumulation in cryptopatches in the gut, showing that EBI2 KO mice had fewer numbers of ILC3s in colonic tissue, impaired cryptopatch formation, and mispositioning of ILC3s in mesenteric LNs (Chu et al., 2018; Emgård et al., 2018). Interestingly, both studies show that the decrease in ILC3 numbers in colonic tissue of Ch25h knockout mice was less severe than in EBI2 knockout mice. This is similar to the incomplete splenic cDC2 deficiency we observe here in Ch25h knockout mice. This result suggests that Cyp27a1 and  $7\alpha,27$ -HC may be playing a role in supporting ILC3 positioning and homeostasis in colonic tissue in the absence of  $7\alpha,25$ -HC. These data also suggest that multiple tissue types in the body are able to support a dual  $7\alpha,25$ -HC and  $7\alpha,27$ -HC gradient system.

In lymph nodes, EBI2 has been shown to promote the positioning of early-activated CD4<sup>+</sup> T cells in the outer T cell zone (Li et al., 2016). Here we show that EBI2 also promotes mesenteric LN DCIR2<sup>+</sup> DC positioning in the outer T cell zone and inter-follicular regions. Ch25h KO mice exhibited similar defects compared to EBI2 KO mice, suggesting that Cyp27a1 does not play a role in this context. In a recent study, we identified the expression pattern of Ch25h in peripheral and mesenteric lymph nodes using RNAscope analysis (Rodda et al., 2018).

We found that Ch25h was expressed at the follicle perimeter, B-T zone interface, and inter-follicular regions (**Fig. 1**). Single-cell RNA sequencing identified subsets of lymph node stromal cells with enriched expression of Ch25h, including marginal reticular cells (MRCs) and CCL19<sup>lo</sup> T zone reticular cells (TRCs). The expression pattern around the follicle perimeter in LNs likely corresponds to MRCs (Katakai, 2012), and the expression of Ch25h in outer-follicular regions in the spleen likely corresponds to marginal sinus lining cells (Kraal and Mebius, 2006). CCL19<sup>lo</sup> TRCs represent a sub-type of T zone fibroblastic reticular cell that likely matches the cells expressing Ch25h at the B-T zone interface that we observe by RNAscope.

Expression of Cyp7b1, Cyp27a1, and Hsd3b7 were difficult to detect using single-cell RNA sequencing, due to issues with sequencing depth. Using RNAscope, Cyp7b1 expression was observed throughout the T zone and in outer- and inter-follicular regions, and Hsd3b7 expression was widespread throughout both the T zone and B cell follicles (unpublished data). These expression patterns are in accord with EBI2 promoting positioning of cells in the outer T zone area of lymph nodes. Co-staining of the RNAscope signals for these enzymes with markers specific for the stromal subsets described by Rodda et al. can be performed to determine which types of stromal cells express these enzymes. We also observed abundant Ch25h expression in high endothelial venules (HEVs). This is in accord with transcript data from purified cells (Lee et al., 2014), suggesting a possible role for oxysterol production in HEV function.

We note that the use of DCIR2 to track cDC2 positioning in mesenteric lymph nodes captures only a subset of the CD11b<sup>+</sup> DCs in this tissue, and that DCIR2 expression varies between the type of lymph node studied. Therefore, our conclusions are limited only to DCIR2<sup>+</sup> DCs in mesenteric lymph nodes and should not be generalized to cDC2 compartments in other lymph nodes. Notably, peripheral lymph nodes contain few DCIR2<sup>+</sup> DCs, and the majority of



IgD Ch25h

**Figure 1. RNAscope detection of Ch25h expression pattern in the mesenteric lymph node.**

Expression pattern of Ch25h in a section of the mesenteric lymph node identified using RNAscope and co-stained for IgD to label B cells. Note the equidistantly spaced red signals in the outer follicle near the subcapsular sinus, which may correspond to MRCs. The darker brown staining within the center of the follicle is due to non-specific capture of the goat anti-IgD antibody by FDCs. The intense red signal in below the follicle and in the T zone are HEVs. There are also equidistantly spaced red signals at the B-T interface, which may correspond to CCL19<sup>lo</sup> TRCs.

cDC2s in this location are DCIR2<sup>-</sup> CD11b<sup>+</sup>. Because these DCs have been shown to express high levels of EBI2 (Yi and Cyster, 2013), it will be interesting to explore whether EBI2 plays a role in the localization or function of these cells. However, tracking the positioning of this subset without observing contaminating DCIR2<sup>+</sup> CD11b<sup>+</sup> cells is difficult, and methods such as histocytometry will be needed. In mesenteric LNs, the corresponding subset of DCIR2<sup>-</sup> CD11b<sup>+</sup> migratory DCs was not significantly altered in EBI2 KO mice. This does not exclude that EBI2 could be playing a role in the function of these cells during different conditions. In addition to EBI2, other guidance receptors may be at play in promoting the positioning of cells at the B-T interface.

We speculate that the MLN DCIR2<sup>+</sup> DC deficiency in EBI2 knockout mice reflects reduced access to trophic signals such as LT $\alpha$ 1 $\beta$ 2 and Notch2 ligands at the B-T zone interface and inter-follicular regions. CD11b<sup>+</sup>CD103<sup>+</sup> MLN DCs have been shown to rely on IRF4 (Persson et al., 2013), LT $\beta$ R, and Notch2 signaling (Lewis et al., 2011; Satpathy et al., 2013), similar to splenic cDC2s. Due to lack of the DCIR2 marker in these studies, whether the decrease observed in IRF4 or LT $\beta$ R knockout mice was more severe in specifically the DCIR2<sup>+</sup> subset of CD11b<sup>+</sup>CD103<sup>+</sup> cells requires further investigation. ILC3s have recently been shown to utilize EBI2 to position in inter-follicular regions within mesenteric LNs (Chu et al., 2018), and it is possible that ILC3-derived LT $\alpha$ 1 $\beta$ 2 plays a role in supporting the homeostasis of DCIR2<sup>+</sup> DCs that also position in this region. A similar ILC3-cDC2 interplay has been described in Peyer's patches, in which CD11b<sup>+</sup> DC numbers were reduced in the Peyer's patches of ROR $\gamma$ t KO mice lacking ILC3s (Reboldi et al., 2016).

Furthermore, due to lack of a method to specifically ablate DCIR2<sup>+</sup> DCs, the types of T cell responses that they are able to support are not well studied. It will be interesting to examine

whether DCIR2<sup>+</sup> DCs play a specific role compared to their DCIR2<sup>-</sup> cDC2 counterpart. IRF4-dependent MLN DCs are involved in Th17 cell (Persson et al., 2013) and Th2 cell (Gao et al., 2013) responses, but how they support Tfh cell responses is less well defined.

### **How are EBI2 ligand gradients constructed in vivo?**

Although we show that Cyp27a1, Ch25h, and Cyp7b1 are co-expressed by stromal cells in marginal zone bridging channel locations, the mechanism by which these enzymes work together to produce 7 $\alpha$ ,27-HC and 7 $\alpha$ ,25-HC is still unclear. Our techniques are unable to discriminate whether the oxysterol-generating enzymes are expressed within the same cell, or within adjacent cells. One possibility is that the single-hydroxylated precursor oxysterols, 27-HC and 25-HC, are produced by one cell type and taken up and converted into their di-hydroxylated forms by a separate Cyp7b1-expressing cell. This mechanism has been shown to work in vitro, in which supernatants containing 25-HC were placed on Cyp7b1-expressing HEK293T cells to generate 7 $\alpha$ ,25-HC (Yi et al., 2012). Although these experiments support that such a mechanism is possible, we cannot be certain that the physiological concentrations of 25-HC present in the spleen are able to penetrate the appropriate Cyp7b1-expressing stromal cell. A second possibility is that a single cell type expresses both Ch25h and Cyp7b1 (or Cyp27a1 and Cyp7b1) to produce EBI2 ligands. This could be tested using dual-probe in situ hybridization immunofluorescence techniques along with defined markers of stromal cell subsets. Another cell type-dependent factor that may regulate the production of EBI2 ligands is the availability of the precursor, cholesterol, which may limit the amount of oxysterol produced.

The activity of the oxysterol-metabolizing enzyme, Hsd3b7, also plays an important role in shaping the EBI2 ligand gradient in vivo. Without a way to directly label 7 $\alpha$ ,25-HC and

7 $\alpha$ ,27-HC in vivo, it is unknown how local concentrations of oxysterols diffuse away from the cells they originate from. Although Hsd3b7 expression appears to be widely distributed throughout the splenic white pulp, it is possible that the abundance of the protein product or its level of activity differs between cell types.

Despite the issues stated above, the mRNA expression pattern for Ch25h in outer- and inter-follicular locations agrees well with the established EB12-dependent movement of activated B cells to these regions (Pereira et al., 2009; Yi et al., 2012). This supports using the mRNA expression pattern of oxysterol-generating enzymes to provide a sense of where EB12 ligands are most concentrated.

### **Effects of systemic cholesterol dysregulation on EB12 function**

Cyp27a1 knockout mice have greatly diminished bile acid production and impaired dietary cholesterol absorption. If their diets are not supplemented with cholic acid, they upregulate endogenous cholesterol biosynthetic pathways, resulting in hypercholesterolemia and accumulation of various sterol species in multiple tissues, including the spleen (Repa et al., 2000; Rosen et al., 1998). Here we show that EB12 ligands are also upregulated in spleen extracts from Cyp27a1 knockout mice that are fed diets without cholic acid supplementation, resulting in a DCIR2<sup>+</sup> DC deficiency comparable to EB12 knockout mice. This DC deficiency could be rescued by feeding the mice a diet supplemented with cholic acid, indicating that the phenotype was dependent on systemic regulation of cholesterol homeostasis. This is the first example of systemic cholesterol dysregulation having an impact on an EB12-dependent process in vivo. Due to the accumulation of sterols in multiple tissues, it is likely that other sites containing EB12-expressing cells will also be sensitive to changes in cholesterol homeostasis. These results also

suggest that oxysterol gradients may be disrupted in different mouse models of lipid dysregulation, such as mice that are fed diets high in fat or cholesterol. It is possible that some immune-related phenotypes observed in these mouse models may be influenced by defective EBI2 function.

In addition to expression in stromal cells, Cyp27a1 was highly expressed in both DCIR2<sup>+</sup> and CD8 $\alpha$ <sup>+</sup> DCs. However, expression of Cyp27a1 was not required intrinsically in these cells for their normal homeostatic maintenance. The direct product of Cyp27a1, 27-HC, is able to regulate cholesterol metabolism in cells and has also been shown to be an endogenous selective estrogen receptor modulator (Radhakrishnan et al., 2007; Umetani et al., 2007; 2014). We speculate that this enzyme has other undefined roles in DCs that may affect their function as antigen-presenting cells. We have not yet tested whether mice that lack Cyp27a1 in DCs are defective in their ability to promote Tfh cell responses. 7 $\alpha$ ,27-HC has been shown to promote Th17 cell differentiation (Soroosh et al., 2014), opening the possibility for paracrine secretion of 7 $\alpha$ ,27-HC by DCs to support this process.

### **Dynamics of EBI2-dependent cDC2 and CD4<sup>+</sup> T cell co-localization**

We show that EBI2 deficiency or antagonism results in dispersal of activated DCIR2<sup>+</sup> DCs uniformly throughout the T zone. Due to this uniform distribution, a fraction of DCs are still able to access the outer areas of the T zone, presumably through random, undirected movement. Although these cells are able to access the B-T interface, the duration they are able to dwell within this location without EBI2 function is unknown. It is likely that EBI2-deficient cells are unable to retain themselves in the outer T zone, resulting in insufficient or unstable contacts with

antigen-specific CD4<sup>+</sup> T cells. Cells expressing high levels of EBI2 are likely restricted in their movement back to the center of the T zone.

While cytokines secreted by DCs can act in a paracrine fashion, many signals require direct physical contact between the T cell and DC, most notably MHCII-TCR interactions. The probability of a T cell interacting with a DC presenting its cognate antigen can be increased by several mechanisms. One mechanism is where the activated DC secretes a chemokine that attracts T cells to promote the probability that a T cell will interact with it, such as the production of CCL22 (Tang and Cyster, 1999). Another mechanism is where both the activated T cell and DC express a common chemotactic receptor to bring them to the same ligand-enriched location. Our data would suggest that this second mechanism brings EBI2-expressing activated DCIR2<sup>+</sup> DC and CD4<sup>+</sup> T cells to the outer T cell zone. It is also likely that both of these mechanisms cooperate to increase the efficiency of cell-cell interactions. Here, we present only static images of what occurs in vivo as a dynamic process. Further work should be performed using 2-photon imaging to examine the dynamics of CD4<sup>+</sup> T cell and cDC2 interactions, and how they are affected by loss of EBI2. We hypothesize that EBI2 is needed for more prolonged interactions between CD4<sup>+</sup> T cells and DCIR2<sup>+</sup> DCs.

### **cDC2 positioning patterns and related T cell response outcomes**

CCR7 was uniformly upregulated by DCIR2<sup>+</sup> DCs after immunization with SRBCs, LPS, and poly I:C. However, we found that only a subset of these stimuli promoted EBI2 upregulation and outer T zone positioning. The outer T zone may contain special factors or cell types that support specific T cell-related outcomes. For example, T-regulatory cells have been shown to interact with self-reactive T cells in the outer T zone of lymph nodes in order to limit their

effector activity (Liu et al., 2015). Positioning at the B-T interface also allows for possible interactions with B cells or other follicular cell types, which may provide additional signals. While we show that SRBCs and LPS promote outer T zone positioning, it is likely that there are other types of stimuli that promote cDC2 positioning in this location. It will also be important to examine how physiological models of bacterial or viral infection affect EBI2 ligand generation and EBI2 function.

Poly I:C induces a strong type I IFN response and causes dispersal of DCIR2<sup>+</sup> DCs throughout the T zone. Given that early-activated CD4<sup>+</sup> T cells also require EBI2 to localize in the outer T zone, it is likely that these cells are also dispersed uniformly after poly I:C immunization. The dynamics of how these CD4<sup>+</sup> T cells interact with DCIR2<sup>+</sup> DCs in this context will be interesting to study. It is also unclear what the benefits are in preventing the accumulation of these cells in the outer T zone under conditions of elevated type I IFN. The disruption in outer T zone positioning can be attributed to both cell-extrinsic and cell-intrinsic factors. Extrinsic to the DC, type I IFN disrupts the oxysterol gradient within the T cell zone by inducing expression of Ch25h and increasing 7 $\alpha$ ,25-HC production. Intrinsic to the DC, IFNAR signaling prevents the upregulation of EBI2 surface levels, and further work will be needed to determine the mechanism by which this occurs. Our data shows that these two effects occur independently.

cDC2s have been shown to be able to promote multiple types of effector T cell responses, including Tfh (Chappell et al., 2012; Shin et al., 2015), Th2 (Gao et al., 2013), and Th1 responses (Neubert et al., 2014; Soares et al., 2007). These outcomes may be linked to cDC2 positioning strategies following immunization. By disabling EBI2 function, cDC2s may more efficiently interact with cDC1s. This DC-DC interaction was shown to be important in multiple

contexts. For example, cDC1-derived IL-12 was important for cDC2s to induce IFN $\gamma$ -producing cells (Soares et al., 2007). Antigen transfer between cDC2s and cDC1s has been shown to occur during viral infection, and is important for the CD8<sup>+</sup> T cell response (Eickhoff et al., 2015; Hor et al., 2015). Interactions between cDC2 and cDC1 may enhance antigen exchange between the cells, facilitating cross-presentation and CD8<sup>+</sup> T cell activation.

Because type I IFN upregulates expression of Ch25h, production of the oxysterol 25-HC is also increased in addition to the EBI2 ligand 7 $\alpha$ ,25-HC. 25-HC has been shown to suppress IL-1 $\beta$  production and inflammasome activation through inhibition of the SREBP-2 pathway in macrophages (Dang et al., 2017; Reboldi et al., 2014). It has also been shown to broadly inhibit viral entry through membrane modification, although these studies were performed using high concentrations of the oxysterol that are potentially not physiologically relevant. Cells that follow gradients of 7 $\alpha$ ,25-HC are likely to be exposed to higher levels of 25-HC. Whether there is any interplay between the effects of 25-HC and EBI2-directed migration remains unknown.

### **Positioning patterns of cDC1 following activation**

We observed that cDC1 and cDC2 activation vary based on the type of immunization administered. Notably, poly I:C activated cDC1s more extensively than cDC2s, inducing higher amounts of CCR7 and CD86 upregulation. The opposite was observed for SRBCs, which induced more activation in cDC2s compared to cDC1s. Explanations for these effects include the difference in expression of receptors on the DC subsets (in this case, TLR3 or SIRP $\alpha$ , respectively), or differences in exposure to the stimuli. While we have shown that cDC1s position in the center of the T zone following SRBC immunization, we have not assessed whether cDC1s position in other locations within the T zone in response to different stimuli. It is

possible that the dispersal of cDC2s we observe under conditions of elevated type I IFN could be influenced by changes in the positioning of cDC1s. It is also possible that cDC1 positioning is more important in these contexts, and that the cDC2 positioning effects we observe after poly I:C immunization are secondary to changes in cDC1 function.

There may also be specific guidance cues that allow cDC1s to accumulate in the center of the T cell zone after SRBC immunization. This cannot be fully explained by the lack of EBI2 expression, which we have shown results in uniform distribution throughout the T zone and not accumulation in the center. RNA sequencing could be used to assess which chemokine or chemoattractant receptors are modulated by CD8 $\alpha^+$  splenic DCs following SRBC immunization. Their exclusion from the outer T zone could also involve an undefined crosstalk between the DC subsets, with cDC1s avoiding regions with high cDC2 density. In this study, we show that this crosstalk allows cDC1s to metabolize EBI2 ligands in the center of the splenic T zone to support outer T zone positioning of cDC2s.

## REFERENCES

- Alexandre, Y.O., Ghilas, S., Sanchez, C., Le Bon, A., Crozat, K., and Dalod, M. (2016). XCR1+ dendritic cells promote memory CD8+ T cell recall upon secondary infections with *Listeria monocytogenes* or certain viruses. *Journal of Experimental Medicine* *213*, 75–92.
- Asselin-Paturel, C., Brizard, G., Chemin, K., Boonstra, A., O'Garra, A., Vicari, A., and Trinchieri, G. (2005). Type I interferon dependence of plasmacytoid dendritic cell activation and migration. *Journal of Experimental Medicine* *201*, 1157–1167.
- Bachem, A., Hartung, E., Guttler, S., Mora, A., Zhou, X., Hegemann, A., Plantinga, M., Mazzini, E., Stoitzner, P., Gurka, S., et al. (2012). Expression of XCR1 Characterizes the Batf3-Dependent Lineage of Dendritic Cells Capable of Antigen Cross-Presentation. *Front Immunol* *3*, 214.
- Baumjohann, D., Okada, T., and Ansel, K.M. (2011). Cutting Edge: Distinct waves of BCL6 expression during T follicular helper cell development. *The Journal of Immunology* *187*, 2089–2092.
- Birkenbach, M., Josefsen, K., Yalamanchili, R., Lenoir, G., and Kieff, E. (1993). Epstein-Barr virus-induced genes: first lymphocyte-specific G protein-coupled peptide receptors. *J. Virol.* *67*, 2209–2220.
- Björkhem, I., and Hansson, M. (2010). *Biochemical and Biophysical Research Communications*. *Biochemical and Biophysical Research Communications* *396*, 46–49.
- Calabro, S., Liu, D., Gallman, A., Nascimento, M.S.L., Yu, Z., Zhang, T.-T., Chen, P., Zhang, B., Xu, L., Gowthaman, U., et al. (2016). Differential Intrasplenic Migration of Dendritic Cell Subsets Tailors Adaptive Immunity. *Cell Reports* *16*, 2472–2485.
- Chappell, C.P., Draves, K.E., Giltiay, N.V., and Clark, E.A. (2012). Extrafollicular B cell activation by marginal zone dendritic cells drives T cell-dependent antibody responses. *Journal of Experimental Medicine* *209*, 1825–1840.
- Choi, Y.S., Kageyama, R., Eto, D., Escobar, T.C., Johnston, R.J., Monticelli, L., Lao, C., and Crotty, S. (2011). ICOS receptor instructs T follicular helper cell versus effector cell differentiation via induction of the transcriptional repressor Bcl6. *Immunity* *34*, 932–946.
- Chu, C., Moriyama, S., Li, Z., Zhou, L., Flamar, A.-L., Klose, C.S.N., Moeller, J.B., Putzel, G.G., Withers, D.R., Sonnenberg, G.F., et al. (2018). Anti-microbial Functions of Group 3 Innate Lymphoid Cells in Gut-Associated Lymphoid Tissues Are Regulated by G-Protein-Coupled Receptor 183. *Cell Reports* *23*, 3750–3758.
- Cinamon, G., Zachariah, M.A., Lam, O.M., Foss, F.W., and Cyster, J.G. (2007). Follicular shuttling of marginal zone B cells facilitates antigen transport. *Nature Immunology* *9*, 54–62.
- Crotty, S. (2014). T follicular helper cell differentiation, function, and roles in disease. *Immunity*

41, 529–542.

- Cucak, H., Yrlid, U., Reizis, B., Kalinke, U., and Johansson-Lindbom, B. (2009). Type I interferon signaling in dendritic cells stimulates the development of lymph-node-resident T follicular helper cells. *Immunity* 31, 491–501.
- Cyster, J.G., Dang, E.V., Reboldi, A., and Yi, T. (2014). 25-Hydroxycholesterols in innate and adaptive immunity. *Nat Rev Immunol* 14, 731–743.
- Czeloth, N., Schippers, A., Wagner, N., Muller, W., Kuster, B., Bernhardt, G., and Förster, R. (2007). Sphingosine-1 Phosphate Signaling Regulates Positioning of Dendritic Cells within the Spleen. *The Journal of Immunology* 179, 5855–5863.
- Dang, E.V., McDonald, J.G., Russell, D.W., and Cyster, J.G. (2017). Oxysterol Restraint of Cholesterol Synthesis Prevents AIM2 Inflammasome Activation. *Cell* 171, 1057–1071.e11.
- De Becker, G., Moulin, V., Pajak, B., Bruck, C., Francotte, M., Thiriart, C., Urbain, J., and Moser, M. (2000). The adjuvant monophosphoryl lipid A increases the function of antigen-presenting cells. *International Immunology* 12, 807–815.
- De Trez, C., Pajak, B., Brait, M., Glaichenhaus, N., Urbain, J., Moser, M., Lauvau, G., and Muraille, E. (2005). TLR4 and Toll-IL-1 Receptor Domain-Containing Adapter-Inducing IFN- $\gamma$ , but Not MyD88, Regulate Escherichia coli-Induced Dendritic Cell Maturation and Apoptosis In Vivo. *The Journal of Immunology* 175, 839–846.
- Dorner, B.G., Dorner, M.B., Zhou, X., Opitz, C., Mora, A., GÜttler, S., Hutloff, A., Mages, H.W., Ranke, K., Schaefer, M., et al. (2009). Selective expression of the chemokine receptor XCR1 on cross-presenting dendritic cells determines cooperation with CD8<sup>+</sup> T cells. *Immunity* 31, 823–833.
- Durai, V., and Murphy, K.M. (2016). Functions of Murine Dendritic Cells. *Immunity* 45, 719–736.
- Eickhoff, S., Brewitz, A., Gerner, M.Y., Klauschen, F., Komander, K., Hemmi, H., Garbi, N., Kaisho, T., Germain, R.N., and Kastenmüller, W. (2015). Robust Anti-viral Immunity Requires Multiple Distinct T Cell-Dendritic Cell Interactions. *Cell* 162, 1322–1337.
- Emgård, J., Kammoun, H., García-Cassani, B., Chesné, J., Parigi, S.M., Jacob, J.-M., Cheng, H.-W., Evren, E., Das, S., Czarnewski, P., et al. (2018). Oxysterol Sensing through the Receptor GPR183 Promotes the Lymphoid-Tissue-Inducing Function of Innate Lymphoid Cells and Colonic Inflammation. *Immunity* 48, 120–132.e128.
- Gao, Y., Nish, S.A., Jiang, R., Hou, L., Licona-Limón, P., Weinstein, J.S., Zhao, H., and Medzhitov, R. (2013). Control of T helper 2 responses by transcription factor IRF4-dependent dendritic cells. *Immunity* 39, 722–732.
- Garside, P., Ingulli, E., Merica, R.R., Johnson, J.G., Noelle, R.J., and Jenkins, M.K. (1998). Visualization of specific B and T lymphocyte interactions in the lymph node. *Science* 281,

96–99.

- Gatto, D., and Brink, R. (2013). B cell localization: regulation by EBI2 and its oxysterol ligand. *Trends in Immunology* *34*, 336–341.
- Gatto, D., Paus, D., Basten, A., Mackay, C.R., and Brink, R. (2009). Guidance of B cells by the orphan G protein-coupled receptor EBI2 shapes humoral immune responses. *Immunity* *31*, 259–269.
- Gatto, D., Wood, K., Caminschi, I., Murphy-Durland, D., Schofield, P., Christ, D., Karupiah, G., and Brink, R. (2013). The chemotactic receptor EBI2 regulates the homeostasis, localization and immunological function of splenic dendritic cells. *Nature Immunology* *14*, 446–453.
- Gerner, M.Y., Casey, K.A., Kastenmüller, W., and Germain, R.N. (2017). Dendritic cell and antigen dispersal landscapes regulate T cell immunity. *Journal of Experimental Medicine* *214*, 3105–3122.
- Gerner, M.Y., Kastenmüller, W., Ifrim, I., Kabat, J., and Germain, R.N. (2012). Histo-cytometry: a method for highly multiplex quantitative tissue imaging analysis applied to dendritic cell subset microanatomy in lymph nodes. *Immunity* *37*, 364–376.
- Gerner, M.Y., Torabi-Parizi, P., and Germain, R.N. (2015). Strategically localized dendritic cells promote rapid T cell responses to lymph-borne particulate antigens. *Immunity* *42*, 172–185.
- Gessier, F., Preuss, I., Yin, H., Rosenkilde, M.M., Laurent, S., Endres, R., Chen, Y.A., Marsilje, T.H., Seuwen, K., Nguyen, D.G., et al. (2014). Identification and characterization of small molecule modulators of the Epstein-Barr virus-induced gene 2 (EBI2) receptor. *J. Med. Chem.* *57*, 3358–3368.
- Griffith, J.W., Sokol, C.L., and Luster, A.D. (2014). Chemokines and Chemokine Receptors: Positioning Cells for Host Defense and Immunity. *Annu. Rev. Immunol.* *32*, 659–702.
- Guilliams, M., Ginhoux, F., Jakubzick, C., Naik, S.H., Onai, N., Schraml, B.U., Segura, E., Tussiwand, R., and Yona, S. (2014). PERSPECTIVES. *Nat Rev Immunol* *14*, 571–578.
- Gunn, M.D., Kyuwa, S., Tam, C., Kakiuchi, T., Matsuzawa, A., Williams, L.T., and Nakano, H. (1999). Mice lacking expression of secondary lymphoid organ chemokine have defects in lymphocyte homing and dendritic cell localization. *J. Exp. Med.* *189*, 451–460.
- Hannedouche, S., Zhang, J., Yi, T., Shen, W., Nguyen, D., Pereira, J.P., Guerini, D., Baumgarten, B.U., Roggo, S., Ben Wen, et al. (2011). Oxysterols direct immune cell migration via EBI2. *Nature* *475*, 524–527.
- Heinig, M., Petretto, E., Wallace, C., Bottolo, L., Rotival, M., Lu, H., Li, Y., Sarwar, R., Langley, S.R., Bauerfeind, A., et al. (2010). A trans-acting locus regulates an anti-viral expression network and type 1 diabetes risk. *Nature* *467*, 460–464.
- Hor, J.L., Whitney, P.G., Zaid, A., Brooks, A.G., Heath, W.R., and Mueller, S.N. (2015).

Spatiotemporally Distinct Interactions with Dendritic Cell Subsets Facilitates CD4+ and CD8+ T Cell Activation to Localized Viral Infection. *Immunity* 43, 554–565.

Idoyaga, J., Suda, N., Suda, K., Park, C.G., and Steinman, R.M. (2009). Antibody to Langerin/CD207 localizes large numbers of CD8alpha+ dendritic cells to the marginal zone of mouse spleen. *Proceedings of the National Academy of Sciences* 106, 1524–1529.

Kabashima, K., Banks, T.A., Ansel, K.M., Lu, T.T., Ware, C.F., and Cyster, J.G. (2005). Intrinsic lymphotoxin-beta receptor requirement for homeostasis of lymphoid tissue dendritic cells. *Immunity* 22, 439–450.

Katakai, T. (2012). Marginal reticular cells: a stromal subset directly descended from the lymphoid tissue organizer. *Front Immunol* 3, 200.

Kelly, L.M., Pereira, J.P., Yi, T., Xu, Y., and Cyster, J.G. (2011). EB12 Guides Serial Movements of Activated B Cells and Ligand Activity Is Detectable in Lymphoid and Nonlymphoid Tissues. *The Journal of Immunology* 187, 3026–3032.

Ki, S., Thyagarajan, H.M., Hu, Z., Lancaster, J.N., and Ehrlich, L.I.R. (2017). EB12 contributes to the induction of thymic central tolerance in mice by promoting rapid motility of medullary thymocytes. *Eur. J. Immunol.* 47, 1906–1917.

Kraal, G., and Mebius, R. (2006). New insights into the cell biology of the marginal zone of the spleen. *Int. Rev. Cytol.* 250, 175–215.

Krishnaswamy, J.K., Gowthaman, U., Zhang, B., Mattsson, J., Szeponik, L., Liu, D., Wu, R., White, T., Calabro, S., Xu, L., et al. (2017). Migratory CD11b+ conventional dendritic cells induce T follicular helper cell-dependent antibody responses. *Sci Immunol* 2.

Lee, M., Kiefel, H., LaJevic, M.D., Macauley, M.S., O'Hara, E., Pan, J., Paulson, J.C., and Butcher, E.C. (2014). Transcriptional programs of lymphoid tissue capillary and high endothelium reveal control mechanisms for lymphocyte homing. *Nature Immunology* 15, 982–995.

Lewis, K.L., Caton, M.L., Bogunovic, M., Greter, M., Grajkowska, L.T., Ng, D., Klinakis, A., Charo, I.F., Jung, S., Gommerman, J.L., et al. (2011). Notch2 receptor signaling controls functional differentiation of dendritic cells in the spleen and intestine. *Immunity* 35, 780–791.

Li, J., Lu, E., Yi, T., and Cyster, J.G. (2016). EB12 augments Tfh cell fate by promoting interaction with IL-2- quenching dendritic cells. *Nature* 533, 110–114.

Li-Hawkins, J., Lund, E.G., Turley, S.D., and Russell, D.W. (2000). Disruption of the Oxysterol 7 $\alpha$ -Hydroxylase Gene in Mice. *Journal of Biological Chemistry* 275, 16536–16542.

Liu, C., Yang, X.V., Wu, J., Kuei, C., Mani, N.S., Zhang, L., Yu, J., Sutton, S.W., Qin, N., Banie, H., et al. (2011). Oxysterols direct B-cell migration through EB12. *Nature* 475, 519–523.

- Liu, X., Yan, X., Zhong, B., Nurieva, R.I., Wang, A., Wang, X., Martin-Orozco, N., Wang, Y., Chang, S.H., Esplugues, E., et al. (2012). Bcl6 expression specifies the T follicular helper cell program in vivo. *Journal of Experimental Medicine* 209, 1841–1852.
- Liu, Z., Gerner, M.Y., Van Panhuys, N., Levine, A.G., Rudensky, A.Y., and Germain, R.N. (2015). Immune homeostasis enforced by co-localized effector and regulatory T cells. *Nature* 528, 225–230.
- Lu, E., Dang, E.V., McDonald, J.G., and Cyster, J.G. (2017). Distinct oxysterol requirements for positioning naïve and activated dendritic cells in the spleen. *Sci Immunol* 2.
- McDonald, J.G., Smith, D.D., Stiles, A.R., and Russell, D.W. (2012). A comprehensive method for extraction and quantitative analysis of sterols and secosteroids from human plasma. *J. Lipid Res.* 53, 1399–1409.
- McLellan, A.D., Kapp, M., Eggert, A., Linden, C., Bommhardt, U., Bröcker, E.-B., Kämmerer, U., and Kämpgen, E. (2002). Anatomic location and T-cell stimulatory functions of mouse dendritic cell subsets defined by CD4 and CD8 expression. *Blood* 99, 2084–2093.
- Merad, M., Sathe, P., Helft, J., Miller, J., and Mortha, A. (2013). The Dendritic Cell Lineage: Ontogeny and Function of Dendritic Cells and Their Subsets in the Steady State and the Inflamed Setting. *Annu. Rev. Immunol.* 31, 563–604.
- Morita, S., Kojima, T., and Kitamura, T. (2000). Plat-E: an efficient and stable system for transient packaging of retroviruses. *Gene Ther.* 7, 1063–1066.
- Mueller, S.N., and Germain, R.N. (2010). Stromal cell contributions to the homeostasis and functionality of the immune system. *Nat Rev Immunol.*
- Murphy, T.L., Grajales-Reyes, G.E., Wu, X., Tussiwand, R., Briseño, C.G., Iwata, A., Kretzer, N.M., Durai, V., and Murphy, K.M. (2015). Transcriptional Control of Dendritic Cell Development. *Annu. Rev. Immunol.*
- Neubert, K., Lehmann, C.H.K., Heger, L., Baranska, A., Staedtler, A.M., Buchholz, V.R., Yamazaki, S., Heidkamp, G.F., Eissing, N., Zebroski, H., et al. (2014). Antigen Delivery to CD11c+CD8- Dendritic Cells Induces Protective Immune Responses against Experimental Melanoma in Mice In Vivo. *The Journal of Immunology* 192, 5830–5838.
- Nevius, E., Pinho, F., Dhodapkar, M., Jin, H., Nadrah, K., Horowitz, M.C., Kikuta, J., Ishii, M., and Pereira, J.P. (2015). Oxysterols and EBI2 promote osteoclast precursor migration to bone surfaces and regulate bone mass homeostasis. *Journal of Experimental Medicine* 212, 1931–1946.
- Pereira, J.P., Kelly, L.M., Xu, Y., and Cyster, J.G. (2009). EBI2 mediates B cell segregation between the outer and centre follicle. *Nature* 460, 1122–1126.
- Persson, E.K., Uronen-Hansson, H., Semmrich, M., Rivollier, A., Hägerbrand, K., Marsal, J., Gudjonsson, S., Håkansson, U., Reizis, B., Kotarsky, K., et al. (2013). IRF4 transcription-

- factor-dependent CD103(+)CD11b(+) dendritic cells drive mucosal T helper 17 cell differentiation. *Immunity* *38*, 958–969.
- Qiu, C.H., Miyake, Y., Kaise, H., Kitamura, H., Ohara, O., and Tanaka, M. (2009). Novel Subset of CD8 + Dendritic Cells Localized in the Marginal Zone Is Responsible for Tolerance to Cell-Associated Antigens. *The Journal of Immunology* *182*, 4127–4136.
- Radhakrishnan, A., Ikeda, Y., Kwon, H.J., Brown, M.S., and Goldstein, J.L. (2007). Sterol-regulated transport of SREBPs from endoplasmic reticulum to Golgi: oxysterols block transport by binding to Insig. *Proc. Natl. Acad. Sci. U.S.A.* *104*, 6511–6518.
- Reboldi, A., Arnon, T.I., Rodda, L.B., Atakilit, A., Sheppard, D., and Cyster, J.G. (2016). IgA production requires B cell interaction with subepithelial dendritic cells in Peyer's patches. *Science* *352*, aaf4822–aaf4822.
- Reboldi, A., Dang, E.V., McDonald, J.G., Liang, G., Russell, D.W., and Cyster, J.G. (2014). Inflammation. 25-Hydroxycholesterol suppresses interleukin-1-driven inflammation downstream of type I interferon. *Science* *345*, 679–684.
- Repa, J.J., Lund, E.G., Horton, J.D., Leitersdorf, E., Russell, D.W., Dietschy, J.M., and Turley, S.D. (2000). Disruption of the Sterol 27-Hydroxylase Gene in Mice Results in Hepatomegaly and Hypertriglyceridemia. *Journal of Biological Chemistry* *275*, 39685–39692.
- Rodda, L.B., Lu, E., Bennett, M.L., Sokol, C.L., Wang, X., Luther, S.A., Barres, B.A., Luster, A.D., Ye, C.J., and Cyster, J.G. (2018). Single-Cell RNA Sequencing of Lymph Node Stromal Cells Reveals Niche-Associated Heterogeneity. *Immunity* *48*, 1014–1028.e1016.
- Rosen, H., Reshef, A., Maeda, N., Lippoldt, A., Shpizen, S., Triger, L., Eggertsen, G., Björkhem, I., and Leitersdorf, E. (1998). Markedly reduced bile acid synthesis but maintained levels of cholesterol and vitamin D metabolites in mice with disrupted sterol 27-hydroxylase gene. *J. Biol. Chem.* *273*, 14805–14812.
- Russell, D.W. (2003). The enzymes, regulation, and genetics of bile acid synthesis. *Annu. Rev. Biochem.* *72*, 137–174.
- Satpathy, A.T., Briseño, C.G., Lee, J.S., Ng, D., Manieri, N.A., KC, W., Wu, X., Thomas, S.R., Lee, W.-L., Turkoz, M., et al. (2013). Notch2-dependent classical dendritic cells orchestrate intestinal immunity to attaching-and-effacing bacterial pathogens. *Nature Immunology* *14*, 937–948.
- Shin, C., Han, J.-A., Choi, B., Cho, Y.-K., Do, Y., and Ryu, S. (2016). *Immunology Letters*. *Immunology Letters* *172*, 21–28.
- Shin, C., Han, J.-A., Koh, H., Choi, B., Cho, Y., Jeong, H., Ra, J.-S., Sung, P.S., Shin, E.-C., Ryu, S., et al. (2015). CD8 $\alpha$ (-) Dendritic Cells Induce Antigen-Specific T Follicular Helper Cells Generating Efficient Humoral Immune Responses. *Cell Reports* *11*, 1929–1940.
- Soares, H., Waechter, H., Glaichenhaus, N., Mougneau, E., Yagita, H., Mizenina, O., Dudziak,

- D., Nussenzweig, M.C., and Steinman, R.M. (2007). A subset of dendritic cells induces CD4<sup>+</sup>T cells to produce IFN- $\gamma$  by an IL-12-independent but CD70-dependent mechanism in vivo. *Journal of Experimental Medicine* 204, 1095–1106.
- Soroosh, P., Wu, J., Xue, X., Song, J., Sutton, S.W., Sablad, M., Yu, J., Nelen, M.I., Liu, X., Castro, G., et al. (2014). Oxysterols are agonist ligands of ROR t and drive Th17 cell differentiation. *Proceedings of the National Academy of Sciences*.
- Sousa, C.R.E., and Germain, R.N. (1999). Analysis of adjuvant function by direct visualization of antigen presentation in vivo: endotoxin promotes accumulation of antigen-bearing dendritic cells in the T cell ....
- Steinman, R.M., Pack, M., and Inaba, K. (1997). Dendritic cells in the T-cell areas of lymphoid organs. *Immunol. Rev.* 156, 25–37.
- Tang, H.L., and Cyster, J.G. (1999). Chemokine Up-regulation and activated T cell attraction by maturing dendritic cells. *Science* 284, 819–822.
- Umetani, M., Domoto, H., Gormley, A.K., Yuhanna, I.S., Cummins, C.L., Javitt, N.B., Korach, K.S., Shaul, P.W., and Mangelsdorf, D.J. (2007). 27-Hydroxycholesterol is an endogenous SERM that inhibits the cardiovascular effects of estrogen. *Nat Med* 13, 1185–1192.
- Umetani, M., Ghosh, P., Ishikawa, T., Umetani, J., Ahmed, M., Mineo, C., and Shaul, P.W. (2014). The Cholesterol Metabolite 27-Hydroxycholesterol Promotes Atherosclerosis via Proinflammatory Processes Mediated by Estrogen Receptor Alpha. *Cell Metabolism* 20, 172–182.
- Wang, F., Flanagan, J., Su, N., Wang, L.-C., Bui, S., Nielson, A., Wu, X., Vo, H.-T., Ma, X.-J., and Luo, Y. (2012). RNAscope: a novel in situ RNA analysis platform for formalin-fixed, paraffin-embedded tissues. *J Mol Diagn* 14, 22–29.
- Yamazaki, C., Sugiyama, M., Ohta, T., Hemmi, H., Hamada, E., Sasaki, I., Fukuda, Y., Yano, T., Nobuoka, M., Hirashima, T., et al. (2013). Critical Roles of a Dendritic Cell Subset Expressing a Chemokine Receptor, XCR1. *The Journal of Immunology* 190, 6071–6082.
- Yi, T., and Cyster, J.G. (2013). EBI2-mediated bridging channel positioning supports splenic dendritic cell homeostasis and particulate antigen capture. *eLife* 2, 309.
- Yi, T., Li, J., Chen, H., Wu, J., An, J., Xu, Y., Hu, Y., Lowell, C.A., and Cyster, J.G. (2015). Splenic Dendritic Cells Survey Red Blood Cells for Missing Self-CD47 to Trigger Adaptive Immune Responses. *Immunity* 43, 764–775.
- Yi, T., Wang, X., Kelly, L.M., An, J., Xu, Y., Sailer, A.W., Gustafsson, J.-A., Russell, D.W., and Cyster, J.G. (2012). Oxysterol Gradient Generation by Lymphoid Stromal Cells Guides Activated B Cell Movement during Humoral Responses. *Immunity* 37, 535–548.

**Publishing Agreement**

*It is the policy of the University to encourage the distribution of all theses, dissertations, and manuscripts. Copies of all UCSF theses, dissertations, and manuscripts will be routed to the library via the Graduate Division. The library will make all theses, dissertations, and manuscripts accessible to the public and will preserve these to the best of their abilities, in perpetuity.*

***Please sign the following statement:***

*I hereby grant permission to the Graduate Division of the University of California, San Francisco to release copies of my thesis, dissertation, or manuscript to the Campus Library to provide access and preservation, in whole or in part, in perpetuity.*



\_\_\_\_\_  
Author Signature

8/16/18

\_\_\_\_\_  
Date